IAEA-TECDOC-1706

Instrumentation for Digital Nuclear Spectroscopy

Proceedings of the IAEA Technical Meeting
Held in Vienna, Austria, 11–15 October 2010

IAEA
International Atomic Energy Agency

INSTRUMENTATION FOR DIGITAL NUCLEAR SPECTROSCOPY

The following States are Members of the International Atomic Energy Agency:

AFGHANISTAN
ALBANIA
ALGERIA
ANGOLA
ARGENTINA
ARMENIA
AUSTRALIA
AUSTRIA
AZERBAIJAN
BAHRAIN
BANGLADESH
BELARUS
BELGIUM
BELIZE
BENIN
BOLIVIA
BOSNIA AND HERZEGOVINA
BOTSWANA
BRAZIL
BULGARIA
BURKINA FASO
BURUNDI
CAMBODIA
CAMEROON
CANADA
CENTRAL AFRICAN REPUBLIC
CHAD
CHILE
CHINA
COLOMBIA
CONGO
COSTA RICA
CÔTE D'IVOIRE
CROATIA
CUBA
CYPRUS
CZECH REPUBLIC
DEMOCRATIC REPUBLIC OF THE CONGO
DENMARK
DOMINICA
DOMINICAN REPUBLIC
ECUADOR
EGYPT
EL SALVADOR
ERITREA
ESTONIA
ETHIOPIA
FIJI
FINLAND
FRANCE
GABON
GEORGIA
GERMANY
GHANA
GREECE
GUATEMALA
HAITI
HOLY SEE
HONDURAS
HUNGARY
ICELAND
INDIA
INDONESIA
IRAN, ISLAMIC REPUBLIC OF
IRAQ
IRELAND
ISRAEL
ITALY
JAMAICA
JAPAN
JORDAN
KAZAKHSTAN
KENYA
KOREA, REPUBLIC OF
KUWAIT
KYRGYZSTAN
LAO PEOPLE'S DEMOCRATIC REPUBLIC
LATVIA
LEBANON
LESOTHO
LIBERIA
LIBYA
LIECHTENSTEIN
LITHUANIA
LUXEMBOURG
MADAGASCAR
MALAWI
MALAYSIA
MALI
MALTA
MARSHALL ISLANDS
MAURITANIA
MAURITIUS
MEXICO
MONACO
MONGOLIA
MONTENEGRO
MOROCCO
MOZAMBIQUE
MYANMAR
NAMIBIA
NEPAL
NETHERLANDS
NEW ZEALAND
NICARAGUA
NIGER
NIGERIA
NORWAY
OMAN
PAKISTAN
PALAU
PANAMA
PAPUA NEW GUINEA
PARAGUAY
PERU
PHILIPPINES
POLAND
PORTUGAL
QATAR
REPUBLIC OF MOLDOVA
ROMANIA
RUSSIAN FEDERATION
RWANDA
SAUDI ARABIA
SENEGAL
SERBIA
SEYCHELLES
SIERRA LEONE
SINGAPORE
SLOVAKIA
SLOVENIA
SOUTH AFRICA
SPAIN
SRI LANKA
SUDAN
SWAZILAND
SWEDEN
SWITZERLAND
SYRIAN ARAB REPUBLIC
TAJIKISTAN
THAILAND
THE FORMER YUGOSLAV REPUBLIC OF MACEDONIA
TOGO
TRINIDAD AND TOBAGO
TUNISIA
TURKEY
UGANDA
UKRAINE
UNITED ARAB EMIRATES
UNITED KINGDOM OF GREAT BRITAIN AND NORTHERN IRELAND
UNITED REPUBLIC OF TANZANIA
UNITED STATES OF AMERICA
URUGUAY
UZBEKISTAN
VENEZUELA
VIETNAM
YEMEN
ZAMBIA
ZIMBABWE

The Agency's Statute was approved on 23 October 1956 by the Conference on the Statute of the IAEA held at United Nations Headquarters, New York; it entered into force on 29 July 1957. The Headquarters of the Agency are situated in Vienna. Its principal objective is "to accelerate and enlarge the contribution of atomic energy to peace, health and prosperity throughout the world''.

IAEA-TECDOC-1706

INSTRUMENTATION FOR DIGITAL NUCLEAR SPECTROSCOPY

PROCEEDINGS OF THE IAEA TECHNICAL MEETING HELD IN VIENNA, AUSTRIA, 11–15 OCTOBER 2010

INTERNATIONAL ATOMIC ENERGY AGENCY
VIENNA, 2013

COPYRIGHT NOTICE

For further information on this publication, please contact:

Physics Section
International Atomic Energy Agency
Vienna International Centre
PO Box 100
1400 Vienna, Austria
Email: Official.Mail@iaea.org

Printed by the IAEA in Austria
June 2013

IAEA Library Cataloguing in Publication Data

Instrumentation for digital nuclear spectroscopy : proceedings of the technical meeting held in Vienna, Austria, 11-15 October 2010. – Vienna : International Atomic Energy Agency, 2013.
p. ; 30 cm. – (IAEA-TECDOC series, ISSN 1011-4289 ; no. 1706)
ISBN 978-92-0-141310-9
Includes bibliographical references.

1. Nuclear engineering – Instruments. 2. Nuclear spectroscopy – Congresses. 3. Detectors – Design and construction. I. International Atomic Energy Agency. II. Series.

IAEAL 13-00816

FOREWORD

All nuclear facilities and institutions utilize radiation detectors to a certain extent as part of their operations, be it for research, monitoring or analytical purposes. Every radiation detector employed needs to have compatible nuclear electronics optimally matched to the detector's characteristics to achieve best possible system performance. Improvements in system performance are made possible in many cases by significant advances in digital electronics enabling new and enhanced methods to acquire and process signals from radiation detectors, and due to digital pulse rapidly replacing analog pulse processing in many nuclear spectrometry systems. This publication reviews the status, developments, and approaches in digital pulse processing in nuclear spectrometry, providing useful information for interested Member States to apply effectively and take advantage of new possibilities afforded by this technique.

The electronics attached to radiation detectors capture and process the electrical signals generated by the radiation detectors and produce, as a final output, a digital signature containing information about the radiation that activated the radiation detector. The design objective of the electronic circuitry is to obtain maximum information about the radiation detected, and information of the best possible quality, reliability and throughput.

Digital electronics and digital pulse processing methods have shown radiation spectrometry systems to be capable of accepting higher throughputs when compared with analog electronics. This opens up new opportunities in high resolution spectrometry at high count rates, an area of great interest to researchers using high intensity neutron beam and X ray beam facilities. Digital pulse processing technology has been proven to maintain system performance almost constant, independent of throughput, and with greater stability and resistance against temperature variations and noise sources. As a result, the quality, quantity and reliability of data delivered are increased and advances and new applications in handheld field instruments, and in remote and unattended nuclear spectrometry systems, are also enabled.

The objective of this technical meeting is to provide a forum for researchers and various industrial partners involved in the development of nuclear spectrometry to share best practices and practical experiences in the design, use and implementation of digital pulse processing in nuclear spectrometry. The meeting reviewed the state of the art and current trends in the field of digital pulse processing, the advantages and limitations, end user demands and future prospects. This publication summarizes the findings and conclusions arising from this technical meeting.

The IAEA wishes to express its appreciation to all those who contributed to the production of this publication and especially to N. Dytlewski, who revised and finalized the manuscript. The IAEA officer responsible for this publication was A. Zeman of the Division of Physical and Chemical Science.

EDITORIAL NOTE

This publication (including the figures, tables and references) has undergone only the minimum copy editing considered necessary for the reader's assistance.

The views expressed do not necessarily reflect those of the IAEA, the governments of the nominating Member States or the nominating organizations.

The use of particular designations of countries or territories does not imply any judgement by the publisher, the IAEA, as to the legal status of such countries or territories, of their authorities and institutions or of the delimitation of their boundaries.

The mention of names of specific companies or products (whether or not indicated as registered) does not imply any intention to infringe proprietary rights, nor should it be construed as an endorsement or recommendation on the part of the IAEA.

The authors are responsible for having obtained the necessary permission for the IAEA to reproduce, translate or use material from sources already protected by copyrights.

.

CONTENTS

1. INTRODUCTION

Digital technology is rapidly replacing analogue technology in many areas of nuclear instrumentation. This transition is enabling numerous benefits and opportunities in nuclear spectrometry that were previously not possible, or very difficult to implement using traditional analogue technology. Digital pulse processing (DPP), which replaces the traditional analogue pulse processing, provides technical improvements in spectroscopic performance and reliability, and instruments with small physical size, low weight and battery powered operations. These features deliver improvements in the quantity, quality and reliability of data for laboratory and research based nuclear spectroscopy systems, providing end users with data with a higher degree of accuracy and confidence to support their findings and conclusions, and the development and deployment of handheld instruments and field based instruments for remote and unattended operations.

Analogue and DPP energy spectroscopy systems have a common goal: to accurately determine the amplitude of the electrical voltage pulses produced by the radiation detector. These measurements are affected by various noise sources, both from the detector itself and the front end electronics which can degrade performance. Environmental factors such as temperature variations are an additional factor that can degrade performance. Digital pulse processing electronics have a number of advantages to overcome these performance degrading factors as will now be briefly illustrated.

A block diagram of an analogue nuclear spectrometry system is shown (Fig. 1). The radiation detector/preamplifier outputs electrical pulses which are input into an amplifier module which shapes and filters the electrical pulses for presentation to an analogue to digital converter (ADC), which measures the amplitude of the conditioned analogue voltage pulse. The output of the ADC is a digital number which is transferred to a multichannel analyser (MCA) which histograms the input data according to pulse height. The resultant histogram, or spectrum, is the energy distribution of radiations that stimulated the radiation detector.

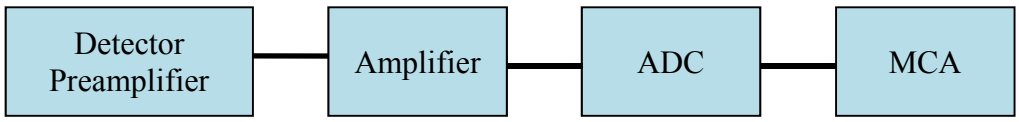

FIG. 1. Block diagram of an analogue nuclear spectrometry system.

The analogue output pulse from the preamplifier is diagrammatically shown (Fig. 2). The task of the amplifier and ADC is to accurately and reliably measure the amplitude V of the continuous voltage pulse which can be subject to various noise sources. Minimizing the noise component is achieved by filtering. Analogue filters typically apply a combination of differentiations and integrations of the voltage waveform to transform it into a Gaussian-like shape whose amplitude is proportional to the voltage V, and hence the energy of the radiation.

In a DPP system, the analogue amplifier and ADC units are replaced by a digitizer and digital filter units (Fig. 3).

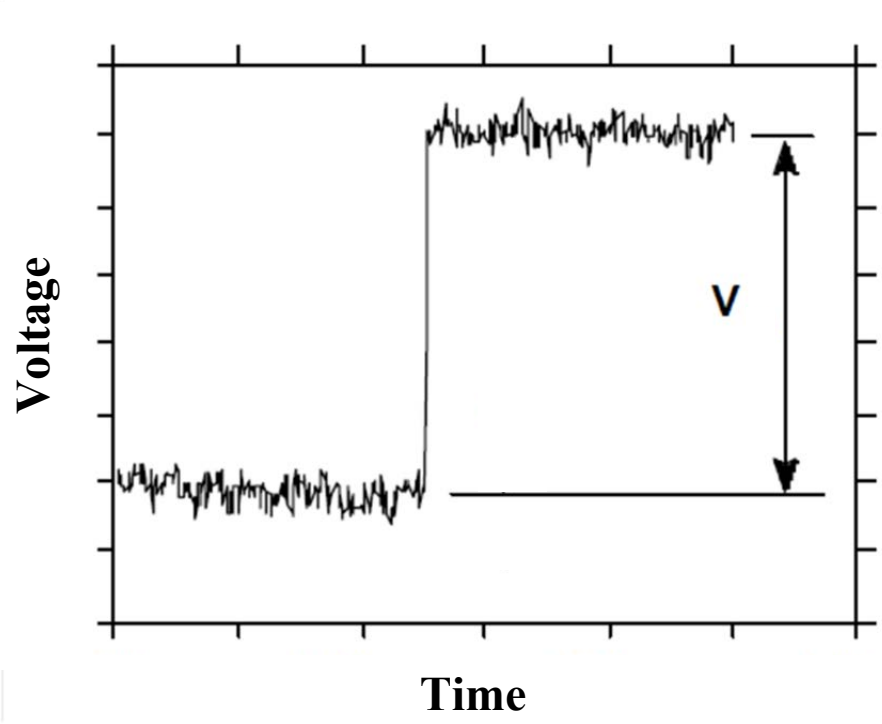

FIG. 2. Representation of the continuous output voltage from the charge sensitive preamplifier coupled to a radiation detector.

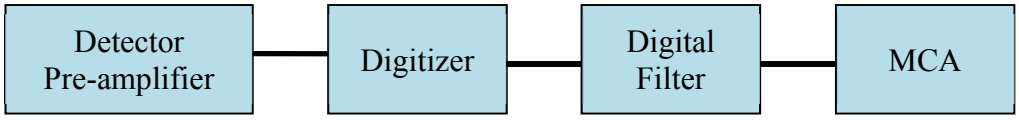

FIG. 3. Block diagram of a DPP nuclear spectrometry system.

The continuous output voltage from the preamplifier is sampled and digitized at a high frequency by the digitizer, producing a string of discrete digital values (Fig. 4). A mathematical filter is applied to this string of digital values to filter out the high frequency noise components to obtain the best signal to noise ratio, and to determine the voltage amplitude V.

Such an approach has significant advantages compared to the traditional analogue signal processing, in particular:

- Application of analysis with consideration of pulse by pulse differences
- Analysis of transient induced charge signals
- Improvement of dead time parameter
- Easy capturing of signals including implementation of complex analyses
- Signal processing with implemented coincidence based criteria (different detectors or different parts of the same detector)
- Effective application of data post-processing; pre-analysis of waveforms, pulse modelling and verification of pulse pile up deconvolution algorithms

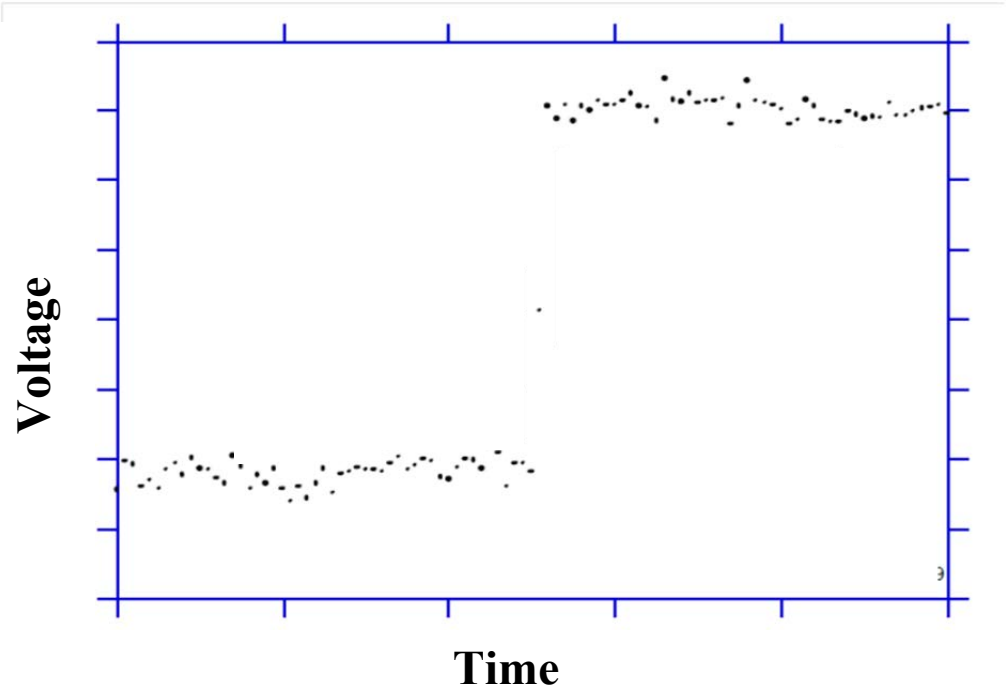

FIG. 4. Digitized output voltage in a DPP system from the charge sensitive preamplifier coupled to a radiation detector.

In both analogue and DPP systems, the common pulse shaping and processing goals are threefold:

- Noise suppression to achieve high energy resolution
- Reduction of dead time to optimize throughput
- Reduction of ballistic deficit to improve resolution and reduce peak distortion

Usually, the best performance for each of these goals cannot be achieved simultaneously and the end user must make compromises according to the required experimental outputs. High energy resolution typically requires adjustments to instrumentation settings that reduce the useable throughput and conversely, high throughputs require sacrificing some energy resolution. DPP systems have proved to provide superior performance to analogue systems in all three goals.

The theory of signal processing is well developed, both for analogue and DPP. An optimal filter can be designed whose output has the best signal to noise ratio, and which the amplitude is proportional to the measured physical value [1]. It is well known that cusp filtering is the optimal filter shape for exponential input signals which are produced by standard charge sensitive preamplifier with resistive elements in the feedback. The optimum filter shape to use depends on the nature of the noise source (e.g. white noise, 1/f noise, series or parallel noise) and the noise power spectral density. Optimum filters for various noise sources are given in referred publications [2–4]. The digital filter is a recursive mathematical algorithm, operating on the stream of digitized values (Fig. 4). The pseudo Gaussian [5] and triangular, trapezoidal, cusp and flat topped cusp [6] are some of the most commonly filter shapes synthesized. These optimum filters are generally not possible to implement with analogue circuitry.

The application of DPP systems leads to new possibilities in processing of measured data, development of automatic measurement set-ups, and offline data correction related to other measurement parameters like temperature or magnetic field influence. New software for processing of detector data can replace the task of analogue modules such as single channel analysers, constant fraction discriminators, time to amplitude converters and/or multichannel analysers. Another role is to add automatic measurement set-up capability and offline data filtering. A significant advantage of DPP is the possibility to use different approximation methods without the need to repeat measurements as in analogue systems. For example, small changes in channel window or in other parameters of analogue systems require repetitive measurements, whereas in a DPP system the same acquired data set can be used with the relevant software. From this point of view, the DPP approach is much more efficient and superior than analogue.

2. BENEFITS OF DIGITAL PULSE PROCESSING

Digital pulse processing for pulse height analysis (energy spectroscopy) is sufficiently well understood and the underlying technology is mature. Scientific publications over the last 2–3 years show a dramatic increase of DPP applications. It is evident from such publications that digital pulse processing is superior to the traditional analogue systems used in radiation spectroscopy.

DPP systems deliver important benefits of improved performance and reliability, increased versatility and new capabilities, all of which are helping to drive the transition from analogue technology to digital technology. These are discussed in the following sections.

2.1 Improved performance and reliability

Digital pulse processors provide superior performance compared to analogue systems in high resolution spectroscopy applications based on scintillation detectors, high purity germanium detectors (HPGe), Silicon detectors, proportional counters, CZT and other room temperature detectors. The spectroscopic performance of these detectors benefit from the ability of DPP to optimize the signal to noise ratio of the system, and to tailor and synthesize pulse shapes to accommodate the variations in the charge collection from the particular detector type. The optimization of the digital pulse shapes can be easily achieved via software reconfiguration without the need to modify the hardware as in the case of analogue systems.

Digital pulse processors provide extremely good stability and reliability since they only rely on a limited number of analogue components to provide gain and a simple prefiltering (e.g. differentiation) to make the input signal compatible with the dynamic range of the ADC. As the detector's output signal is digitized very early in the signal processing chain compared with analogue signal processing, drifts and instabilities are much reduced. With proper component selection, the overall temperature gain-stability of a DPP can be better than 25 ppm/°C.

The DPPs offer high throughput performance and better pile-up rejection. This is beneficial for dosimetry, radiometry, and high radioactivity isotope assay. DPPs allow high dose dosimetry in nuclear power plant environments which has been a challenging task for the traditional analogue spectroscopy set-ups. The DPP high counting rate capability and loss free counting are important for applications such as neutron activation analysis, synchrotron radiation material analysis, X ray fluorescent analysis and other, high throughput analytical applications.

2.2. Increased versatility

FPGA based DPPs are rich in digital logic resources allowing them to support multiple acquisition modes such as pulse height analysis, multichannel scaling, multispectrum scaling and time stamped list mode acquisition. They also offer very specialized functionality such as pulse shape discrimination/correction, pulse pile-up rejection, loss free counting and other measurement supporting features. Multiple DPPs can also be run with synchronized acquisition to allow for the timing correlation of events from multiple signal sources such as separate detectors or detector segments. In addition, the DPPs can be synchronized to external sample automation systems or source stimulating devices such as X ray or neutron generators.

DPPs offer flexible set-up and allow effortless replacement of analogue based equipment in a variety of high resolution spectroscopy applications. Flexibility and extended dynamic range of DPP make them suitable for nuclear power plant radiation environment monitoring, and their low power and small size makes them very suitable for field applications, portable dosimetry and radiation protection.

2.3. New capabilities

DDPs flexibility, remote control and environmental stability make them indispensable for remote and unattended applications such as environmental monitoring, and nuclear safety and security systems. DPPs afford self and remote diagnostic capabilities which assist in maintaining quality control without the need for operator intervention. High density, small size, and low power electronic components improve portability of nuclear spectroscopic systems for in situ applications such as space research, mining, and cultural heritage. Such instruments feature automatic or remote adjustment of critical parameters and require less experienced operators. They can be easily updated and upgraded.

DPPs can have the potential to download custom or possibly user created algorithms. This provides a high level of modularity. More modularity and functionality is possible using software configurations/modifications compared to the analogue systems that need hardware upgrade to change functionality. Adaptive measurements, non-linear LMS type adaptive algorithms and auto correlation methods can be developed.

Particle identification applications (e.g. neutron–gamma) are an area in which the digital algorithms offer performance and flexibility that are hard to achieve using traditional analogue systems.

3. MIGRATING FROM ANALOGUE TO DIGITAL PULSE PROCESSING

The migration from analogue techniques to digital pulse processing enables implementation of cheaper and more flexible solutions in nuclear instrumentation. However, there is still a deficiency in the understanding of the differences between analogue based spectroscopy and digital based spectroscopy, and how best to select and optimize digital filters. For many end users, a DPP is a “black box” provided by equipment manufacturers. These are inhibitors for many end users to adopt DPP in radiation spectroscopy. Training and education are seen as major priorities to promote greater use of DPP in radiation measurements and to fill the gap between the technology and applications.

There is typically less visibility to users into the processing of signals in DPPs due to the digitized nature of the information and which is contained within ICs, and the limited opportunities for test and inspection points as can be found in many analogue systems. This can be overcome by providing visualization to the user based on reconstruction circuits, digital oscilloscopes and logic analysers within the DPP. For the end user, digital spectroscopy set-ups are not as intuitive and easy as analogue set-ups, with many adjustable parameters available to the end user to optimize the experimental conditions. Determining the optimum values of the parameters can be time consuming and problematic using manual adjustments, however many commercial instruments afford automatic modes or recommendations which based on operational experiences, produce set-ups close to the optimal for general use.

Timing applications typically require expensive GHz digitizers and recorders which limits the proliferation of DPP in time measurements. Coincidence and timing measurements require clock synchronization between the channels which adds additional complexity. Commercial digital timing processors are non-existent, but would be useful for coincidence/ anticoincidence spectroscopy measurements. The area in which DPP has not matched the level of performance of analogue systems is the field of time pick-off and time measurements. This is likely due to limitations of sampling rates of available ADCs having insufficient number of bits.

Digital pulse processing systems are more difficult to service and repair than analogue systems since most of functional components are composed of many interconnecting ICs and containing custom embedded software programs. Due to their complexity, DPP systems are very difficult to repair in the field and if repairable, the cost is usually high and the repair time usually long. To mitigate, careful consideration must be given to procurement articles such as warranty and manufacturer support.

4. BRIEF SUMMARY OF CONTRIBUTIONS

Each of the contributions included in this document reports on the development and/or application of digital pulse processing. A short summary of each paper is given below.

In the first paper, Bogovac presents DPP hardware system designs and how FPGA design tools can be efficiently used in a process of developing a compact, reconfigurable and high performance data acquisition system for nuclear spectroscopy. This is followed by the contribution of Bryndziar who describes the optimization of digital filter parameters to achieve high throughputs in a high radiation field environment. Jordanov introduces a new concept of a digital pulser that can be readily incorporated into most digital spectroscopy systems, providing an important tool for the characterization, optimization and diagnostics of the detector front end electronics and the DPP system. A further description of DPP hardware design and implementation is presented by Messai, and the paper by Papp illustrates how the increased capabilities of a DPP system can record and store both accepted and rejected detector signals thus offering a quality assurance capability.

Moving on to applications, Petriska describes the implementation of a DPP system for Positron Annihilation Spectroscopy, and Rashid utilizes the DPP design concepts to develop replacement data acquisition hardware for obsolete and no longer available computer based instrumentation and control. The paper by Menaa tests and evaluates the performance of different digital filters for various types of commercially available radiation detectors. Zakrzewski provides a short history of the development of DPP and the technology improvements afforded by today's commercially available DPP systems. The final two papers by Zeynalova and Zeynalov describe the development and implementation of DPP techniques and algorithms for applications in nuclear fission research.

REFERENCES

[1] LOUDE, J.-F., "Energy Resolution in Nuclear Spectroscopy", internal report, Laboratory for High Energy Physics LPHE, Lausanne, Switzerland (2000).

[2] REDEKA, V., Optimum signal processing for pulse amplitude spectrometry in the presence of high rate effects and noise, IEEE Trans. Nucl. Sci. NS-15 (1968) 455.

[3] GATTI, E., SAMPIETRO, M., Optimum filters for detector charge measurements in presence of 1/f noise, Nucl. Instr. Meth. A287 (1990) 513.

[4] GATTI., E., et al., Optimum filter for current noise smoothed-to-white at low frequency, Nucl. Instr. Meth. A394 (1997) 268.

[5] YOUNG, I.T., VAN VLIET, L.J., Recursive implementation of the Gaussian filter, Signal Processing 44 (1995) 139.

[6] JORDANOV, V., KNOLL, G.H., Digital synthesis of pulse shapes in real time for high resolution radiation spectroscopy, Nucl. Instr. Meth. A345 (1994) 337.

DIGITAL PULSE PROCESSOR FOR ION BEAM MICROPROBE AND MICRO X RAY FLUORESCENCE 2-D AND 3-D IMAGING

M. BOGOVAC
Ruđer Bošković Institute,
Zagreb, Croatia
Email: Mladen.Bogovac@irb.hr

M. JAKSIC, D.WEGRZYNEK
Faculty of Physics and Applied Computer Science,
AGH University of Science and Technology,
Krakow, Poland

A. MARKOWICZ
IAEA Nuclear Science and Applications/Physics section
Seibersdorf, Austria

Abstract

For a long time, the implementation of optimal pulse processing in nuclear spectrometry was only possible with analogue electronic components. Following the development of fast analogue to digital converters, field programmable gate arrays, and digital signal processors, it became feasible to digitize pulses after a preamplifier or phototube and process them in a real time. Therefore, digital electronics, which were limited to data storage and control of the acquisition process, became feasible for signal processing as well. This brought numerous benefits, such as better energy resolution with higher data throughput, reduced size, easier upgrading, the ability to automate adjustment and control of the complete data acquisition process, and self-diagnostic capability. In the same time, evaluation of the Electronic Design Automation tools and Intellectual Property industry enables a System-On-a-Chip paradigm on high density reprogrammable devices and allows new approach for system level design. Such a design provides opportunity for small laboratories to develop a compact `all digital' customized instrumentation. In this work, we presented a design of FPGA IP core for high resolution, digital X ray, γ ray or particle spectrometry using high level FPGA design tool (Xilinx System Generator and Matlab — Simulink). The IP core has been used to build a simple low cost digital spectrometer (Spartan 3 FPGA based) and advance system for ion beam microprobe and X ray fluorescence 2-D and 3-D imaging. (Virtex 4 FPGA based).

1. INTRODUCTION

Historically, the implementation of optimal pulse processing in nuclear spectrometry was only possible with analogue electronic components. Following the development of fast analogue to digital converters (ADCs), field programmable gate arrays (FPGAs), and digital signal processors, it became feasible to digitize pulses directly after a preamplifier or phototube and process them in a real time. Thus, digital electronics, which were limited to data storage and control of the acquisition process, became feasible for signal processing as well. This brought numerous benefits, such as better energy resolution with higher data throughput, reduced physical size, easier upgrading, the ability to automate adjustment and control of the complete data acquisition process, and self-diagnostic capability.

At the same time, evaluation of the Electronic Design Automation tools and Intellectual Property (IP) industry enables a System-On-a-Chip paradigm on high density reprogrammable devices and allows new approach for system level design. Such a design provides opportunity for small laboratories to develop a compact `all digital' and customized instrumentation.

In this paper we presented a design of a FPGA IP core for high resolution, digital X ray, γ ray or particle spectrometry using high level FPGA design tool (Xilinx System Generator and Matlab — Simulink). The IP core has been used to build a simple, low cost digital spectrometer (Spartan 3 FPGA based) and advanced system for ion beam microprobe and X ray fluorescence 2-D and 3-D imaging (Virtex 4 FPGA based).

2. SYSTEMS OVERVIEW

In a typical ion beam microprobe system, an ion beam is focused to a submicrometre diameter and scanned over a sample area initiating different processes of interaction with the atoms of the target material. For each beam position x, y on the sample, the energy E of induced radiation (X or γ ray) or scattered/transmitted ions is measured. The measured energy usually gives elemental or density information, and so elemental or density distributions can easily be obtained.

The data acquisition system that is capable to collect the required data must simultaneously generate x and y positions and measure energy E from one or more detectors. The block schematics of the system are presented in this paper (Fig 1). The main component of the system is a commercial PCI board (Development Kit-IV User Guide, NT107–0272) that features two 105 MHz, 14-bit ADCs (AD6645), two 14-bit 160 MSPS DACs (AD9772), Virtex 4 FPGA (XC4SX35-10FF668) and SRAM memory (1M x 32-bits, 133 MHz). The signals (pulses) from the high resolution detector and charge sensitive preamplifier are first prepared for digitization by a simple analogue conditioner (performing high pass filtering, pole-zero correction and linear amplification), digitized using full ADC speed and processed inside the FPGA by using a newly developed IP core called Digital Pulse Processor (DPP). In parallel, the pair of x and y coordinates are generated and output to the two onboard DACs. The amplitudes of the pulses can be stored into onboard SRAM in correlation with x and y coordinates for fast 2-D real time imaging, or buffered and transferred to a PC together with position information. The acquisition is controlled using PC software. The software is capable of performing 2-D imaging and can synchronize sample rotation with acquisition enabling 3-D imaging.

The developed DPP core, which is suitable for high resolution spectroscopy, contains a digital equivalent of a modern spectroscopy amplifier, peak height detector and acquisition interface (to perform pulse-height analysis). It provides pulse shaping, pile-up rejection, base line restoration, peak detection, live time correction, pulse sorting by amplitude, and memory to store it. Implementation of these functions in a FPGA is demanding task and may additionally complicated by VHDL coding. Therefore, the Xilinx System Generator and Matlab/Simulink EDA tools are used for its development. These tools allow to use predefined and tested blocks (dual port memories, FIFO, math operations, etc.), script language for implementing control logic and finally to generate VHDL code. All this is done in a user friendly graphical environment.

The DPP core is implemented on a simple, low cost Spartan-3 based USB board (http://www.cesys.com/fpga/spartan/efm01_en.html), attached to a 14-bit ADC (LTC2248) at sampling rate of 48 MHz (Fig. 2).

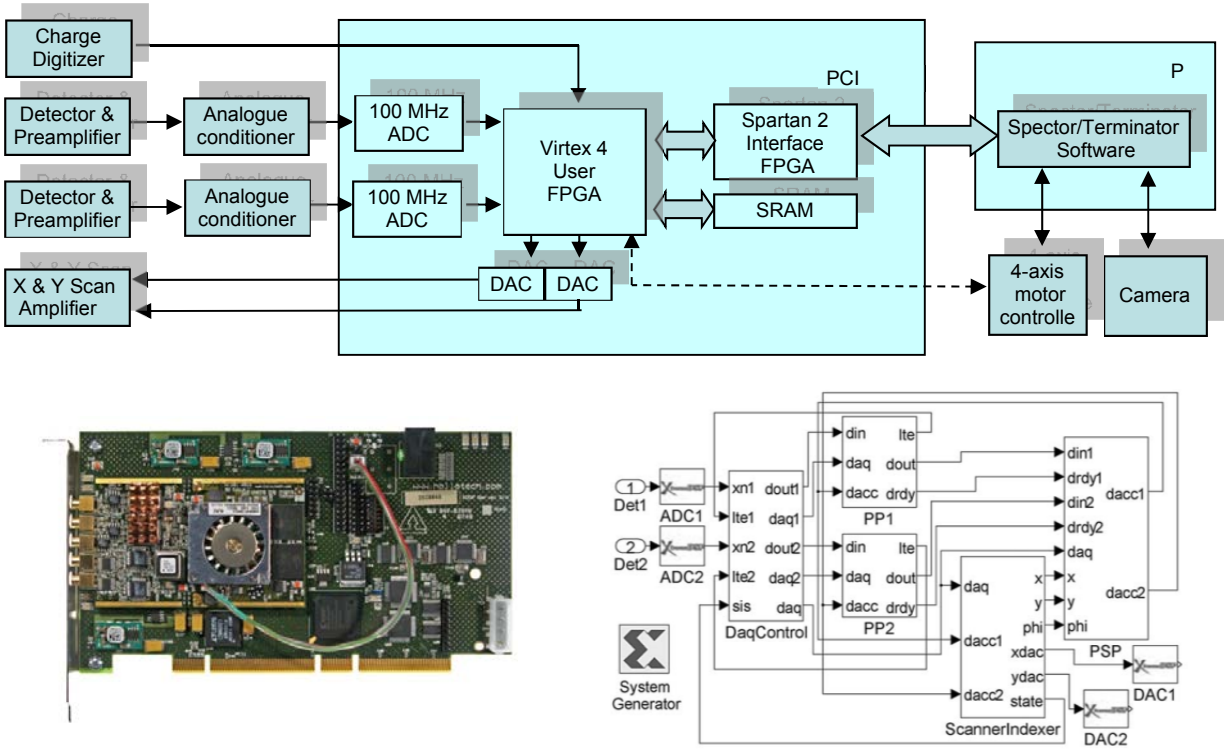

FIG. 1. Schematic block diagram of the system for ion beam imaging (top); FPGA design using state of the art tolls — Matlab/Simulink/Xilinx System generator (bottom right); Xilinx Virtex-4 PCI board (bottom left).

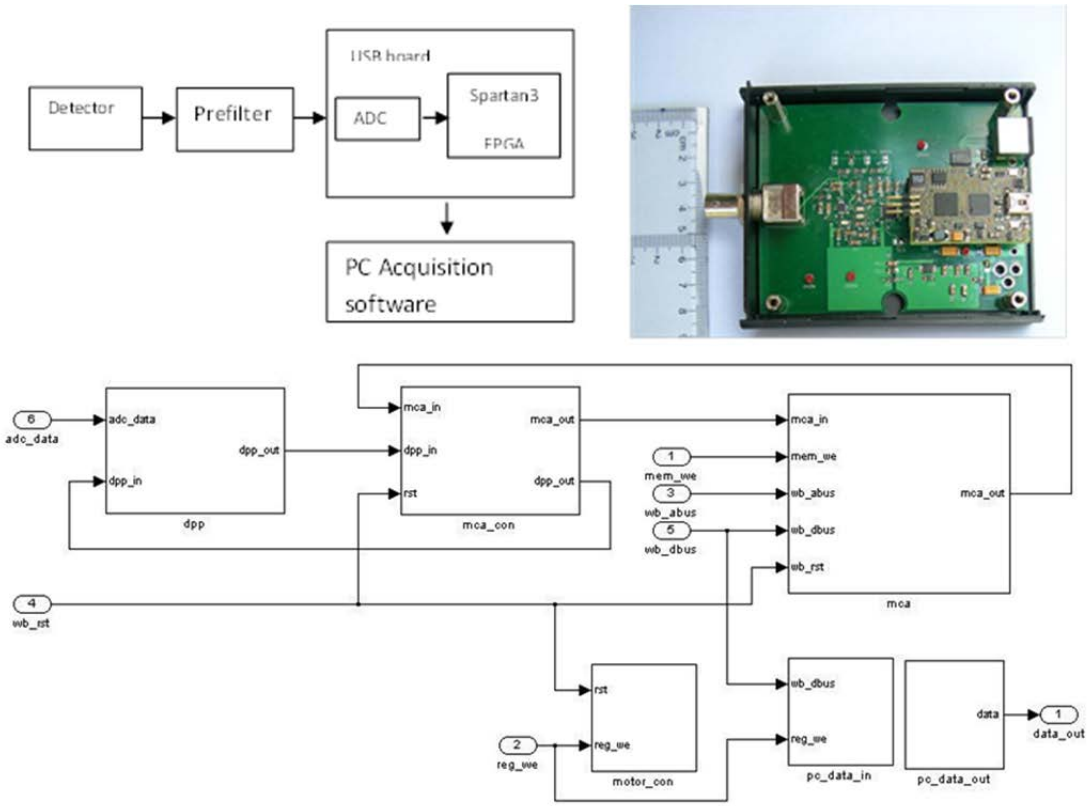

FIG 2. Schematic block diagram (top left) of the low cost, high resolution X ray spectrometer system based on the Spartan-3 USB board (top right) and its Simulink model (bottom).

3. DPP IP CORE

The DPP core, implemented as a Matlab/Simulink subsystem, is shown here (Fig. 3). The filled rectangles are Xilinx blocks and they contain either a Xilinx logic element (like memory. multiplier, accumulator, logic operators and/or/not, etc.) or a description of the logic in the form of a script language called M-Code. An empty rectangle is called subsystem and it may contain other subsystems and Xilinx blocks. The names in the rectangles represent input/output ports (floating point, integer or Boolean numbers). The lines show the flow of numbers. The numbers flow between ports in time intervals defined by the FPGA clock. This flow of numbers is also called signal. The Simulink model of the DPP core can be used to generate VHDL code or as a subsystem of a top-most system. The DPP core contains several subsystems. The logic and functions of each subsystem is explained in detail in the following sections. A brief description of the signal flows and subsystem function is given below.

The data is sampled by an external ADC and input at the port adc_data. They are a digital representation of the analogue signal that is connected to an external ADC (basically output from detector/preamplifier, more precisely output from prefilter that contains exponential pulses) The data stream (digital signal) is branched into two paths. In the first path, the signal is delayed and input into an EnergyFilter subsystem. In the second path, it is input into a FastFilter.

The energy filter transforms any stream that has a shape of exponential pulse into unipolar and bipolar triangular/trapezoidal pulses using optimal peaking time in order to get the best signal to noise ratio. The transformed unipolar signal feeds BLR subsystem that removes any DC offset from the signal on its input. The output from BLR subsystem feeds the PHP subsystem that calculates the amplitude of each pulse and forwards it out of the parent DPP subsystem to an external subsystem for storage.

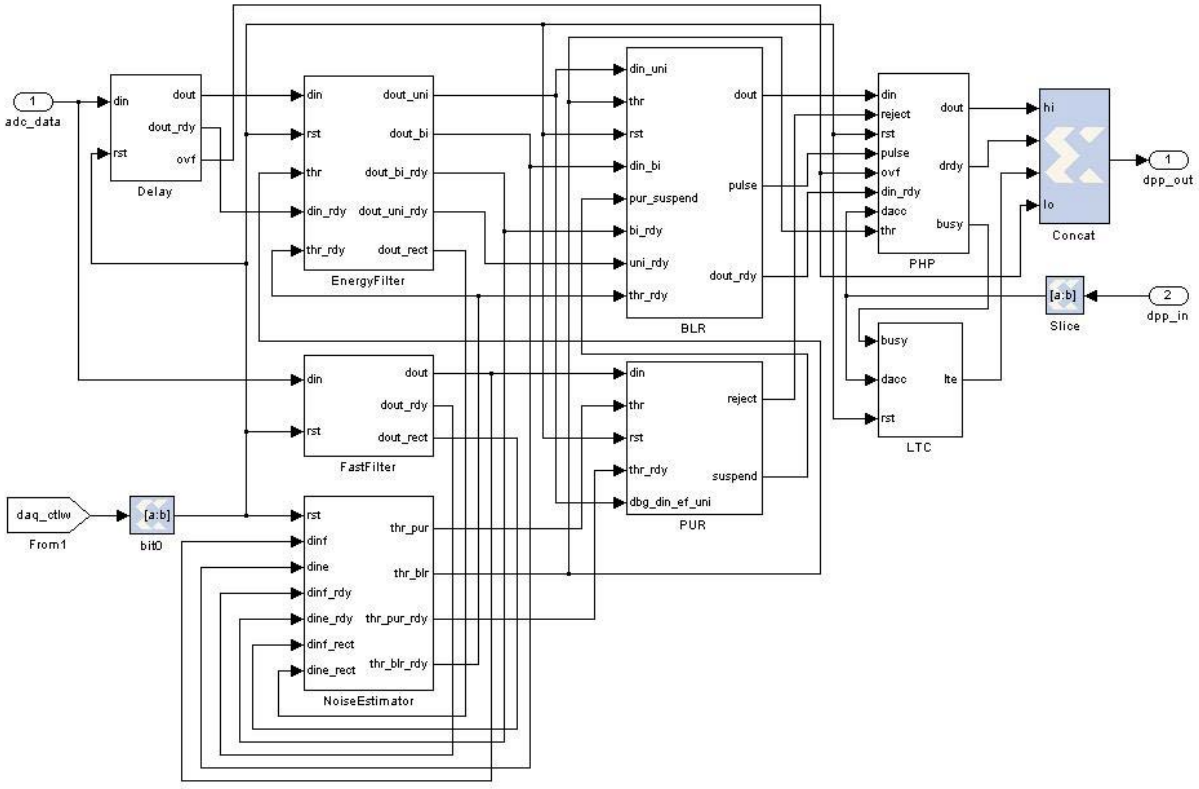

FIG. 3. The DPP subsystem performs data processing tasks.

The FastFilter performs a similar function as the Energy Filter but it uses very short peaking time. Its output is used by the PUR subsystem that detects any pile-up event. In the case of the pile-up, the PUR subsystem disables the PHP subsystem so it cannot forward data for storage. The presence of any pulse in the signals is detected using simple threshold discriminators. The threshold must be above the noise in the signal. The level of the noise is calculated by the Noise Estimator.

3.1. Energy filter subsystem

It is well known that trapezoidal pulse shaping of signals from semiconductor detectors used in high resolution spectroscopy gives signal to noise ratios close to optimal cusp shaping. If an exponential input signal x with amplitude A and fall time τ is digitized using a sampling period T, it should be converted into a symmetrical trapezoidal shape with peaking time kT and flat-top $(l-k)T$, where k,l are integers. The conversion is easily done in two steps.

First, the digitized input signal x_n (Eq. 1) is converted into the rectangular bipolar signal r_n by using Z-transforms $X(z) = Z\{x_n\} = \sum_n x_n z^{-n}$ as follows:

$$x_n = \begin{cases} 0 & n < 0 \\ Ae^{-\frac{T}{\tau}n} & n \geq 0 \end{cases} \tag{1}$$

$$r_n = A[(u_n - u_{n-k}) - (u_{n-l} - u_{n-l-k})] \quad \text{where } u_n = \begin{cases} 0 & n < 0 \\ 1 & n \geq 0 \end{cases} \tag{2}$$

$$\frac{Z\{r_n\}}{Z\{x_n\}} = \frac{Z\{A[(u_n - u_{n-k}) - (u_{n-l} - u_{n-l-k})]\}}{Z\{Ae^{-\frac{T}{\tau}n}\}} = \frac{[(1-z^{-k}) - (z^{-l} - z^{-(l+k)})](1-e^{-\frac{T}{\tau}}z^{-1})}{1-z^{-1}}, \tag{3}$$

$$(1-z^{-1})Z\{r_n\} = [(1-z^{-k}) - (z^{-l} - z^{-(l+k)})](1-e^{-\frac{T}{\tau}}z^{-1})Z\{x_n\} \tag{4}$$

Applying the well know Z-transform properties $Z\{y_{n-k}\} = z^{-k}Z\{y_n\}$ onto the Eq. 4 and then inverse Z-transform one can obtain recursive a relation given by Eq. 5.

$$r_n = r_{n-1} + d_n - e^{-\frac{T}{\tau}}d_{n-1}, \text{ where } d_n = (x_n - x_{n-k}) - (x_{n-l} - x_{n-l-k}) \tag{5}$$

Finally, a simple integrator (Eq. 6) converts the rectangular signal r_n with amplitude A into the trapezoidal s_n with amplitude kA (Fig. 6b).

$$s_n = s_{n-1} + r_n \tag{6}$$

The implementation of the transformation from exponential shape (Eq. 1, Fig. 6a) to trapezoidal shape (Eq. 6, Fig. 6c) in FPGA is shown in Fig. 4 and Fig. 5. It can be shown that above results are equivalent to those obtained in [1].

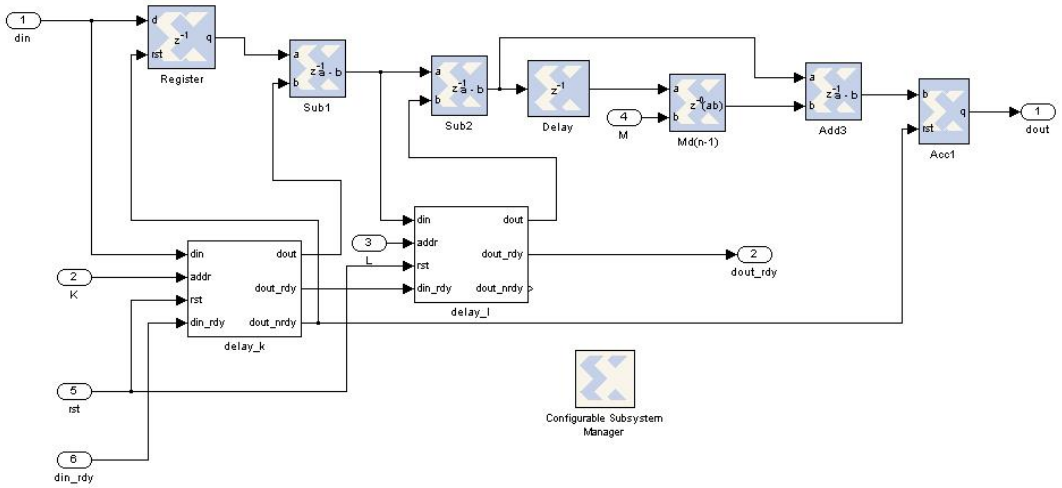

FIG. 4. The subsystem that transforms the exponential pulse into bipolar rectangular.

In the first step, the exponential signal is transformed to the rectangular (Eq. 5) by the subsystem ef (Fig. 5). The details of the subsystem *ef* is also shown (Fig 4). Note that multiplicator *M* in Fig. 4 is

$$M = e^{-\frac{T}{\tau}} \tag{7}$$

In the second step, the intermediate rectangular signal is transformed to triangular/trapezoidal by using accumulator *Acc2* in Fig. 5. The normalization factor *1/K* is applied by the multiplicator *Mult2*.

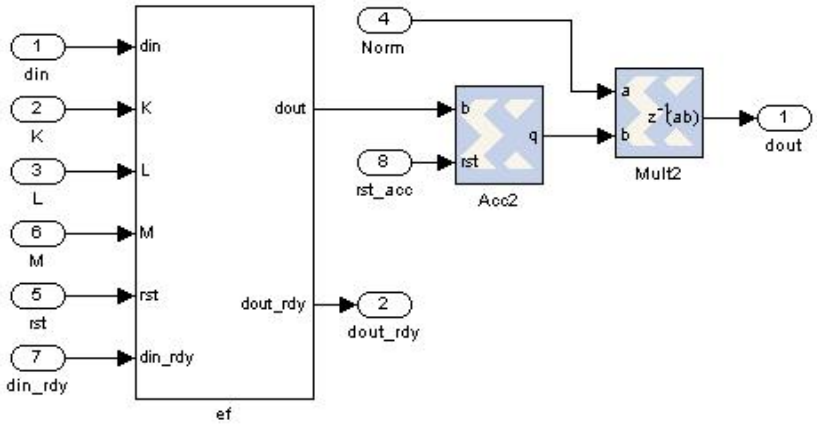

FIG. 5. The subsystem that transforms exponential pulse into triangular/trapezoidal.

It is seen that the signal to noise ratio (S/N) of the shaped unipolar (triangular/trapezoidal) signal is much better (larger) than of the intermediate rectangular and exponential as well (Fig. 6). On the other side, the rectangular signal is bipolar and it has an inherently stable base line. In difference, the shaped signal does not have stable base line. Due to Eq. 6, that is accumulator *Acc2*, any change in the base line will not be cancelled.

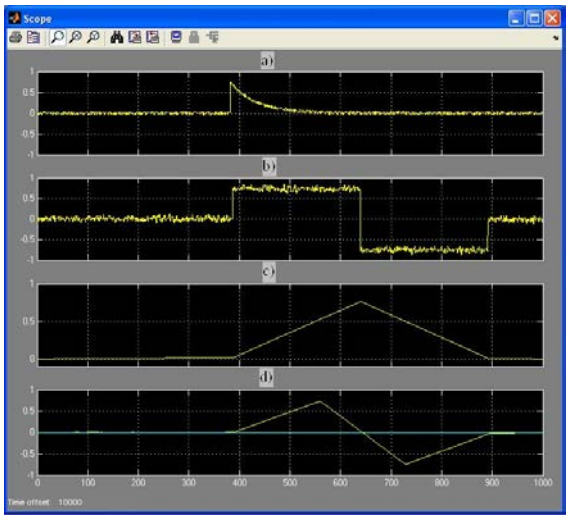

FIG. 6. The input exponential pulse (a) is first transformed into rectangular (b) and then into triangular (c) using Eq.'s 5 and 6 respectively.

Thus, it is convenient to generate a signal that has similar S/N ratio like triangular/trapezoidal, and a stable base line similar to the rectangular. Such a signal can be produced by averaging a rectangular signal. In order to get the same duration to the unipolar triangular/trapezoidal, first it is transformed to a rectangular signal with peaking time

$$k_r = l_r = \frac{k+l}{3} \tag{8}$$

and then averaged over the same peaking time k_r. This signal, called bipolar triangular, is shown on Fig. 6d. Finally, the Energy Filter outputs two main signals with equal duration and similar S/N ratios: energy unipolar that is used for amplitude calculation (after base line correction) and energy bipolar that is used in the Noise Estimator and BLR subsystems as a useful auxiliary signal which does not need any base line correction.

3.2. Fast filter subsystem

The Fast Filter subsystem produces a fast bipolar signal, similar to the energy bipolar, but with a much shorter peaking time (usually its peaking time is in order of 200 ns), which means that K = L = 10 [clock periods] for a 48 MHz clock. This value can be set by the user from the GUI. The base line of this signal does not need correction and it is used by the PUR subsystem in order to detect pile-up events.

3.3. PUR subsystem

The PUR subsystem outputs two signals *reject* and *suspend*. The reject is used to prevent PHP and MCA subsystems to store a pulse amplitude during pile-up event. The *suspend* prevents BLR to correct for baseline in the presence of the pulse.

The generation of *reject* signal is described as follows. First, the *pur_pkd* detects when the fast bipolar pulse at input *din* arrives. It is done by a simple level discriminator as follows: when the pulse excides threshold *thr* which is calculated by the Noise Estimator subsystem, the *pur_pkd* rises its *pkd* output. The *pkd* causes a state machine defined in the *pur_asrt* to

make transition from an idle state to a working state. In the working state it starts internal counter *Tcc* to count until it reaches *tc2*, (denoted *pur_tc2* in Fig. 7).

The *tc2* is called PUR window and it is defined as minimal time interval between two successive pulses that can be tolerated (does not produce pile-up). The *PUR* window can be expressed in the terms of peaking time *k* and *l* using rejection factor f_r which is usually greater than 1

$$TC_2 = l + (f_r - 1)k \tag{9}$$

If $f_r = 2$ then the second pulse arrives exactly when the first terminates. If $f_r = 1$ then the second pulse arrives when amplitude of the first starts falling. Normally, the maximum of the first pulse is detected when its amplitude *A* falls to $f_s A$. Therefore, in order to distinguish two pulses, the following condition must be satisfied

$$f_r > 1 + (1 - f_s) \tag{10}$$

In this design we put $f_s = 0.8$, therefore it must be $f_r > 1.2$.

If no new pulse comes before Tcc reaches *tc2*, then *pur asrt* state machine returns to its idle state and no *PUR* signal is generated. In the opposite, if the next pulse comes while Tcc is still counting (pile-up), the *pur_asrt* does the following: (1) starts new counter *Tcp* with the same preset time equal to *PUR* window (2) rises *PUR* flag (3) waits *Tcc* and *Tcp* to count-out (4) waits arrival of a new fast pulse. If the next pulse comes before *Tcp* counts-out then *Tcp* is restarted. Since the *Tcc* counter starts counting before the *Tcp* and both has the same preset value, the *Tcc* must count-out before *Tcp* does. When *Tcc* reaches its preset (PUR window) then *pur_asrt* asserts its pur output signal. The pur output is deasserted when *Tcp* counts-out. Since the energy signals are delayed for the duration of the *PUR* window, that is, for the value equal to the preset of both counters, it comes out that pur output starts when the first energy pulse starts arriving and terminates when the last pile-up ed signal starts arriving. This means that the pur output signal can prevent storage of all pile-up signals except the last one. For this reason, a *pur_make* module is constructed. It extends the pur output of the *pur_asrt* for the duration of the energy pulse and outputs a proper rejection signal. It should be noted that the duration of all energy signals is the same and equal to *k+l* in the FPGA clock units.

The suspend signal is generated by the *sus_make*. It is synchronized with unipolar energy signal and has the same width. If one or more energy signals overlap, and then suspend output is extended until the last overlapped unipolar signal terminates.

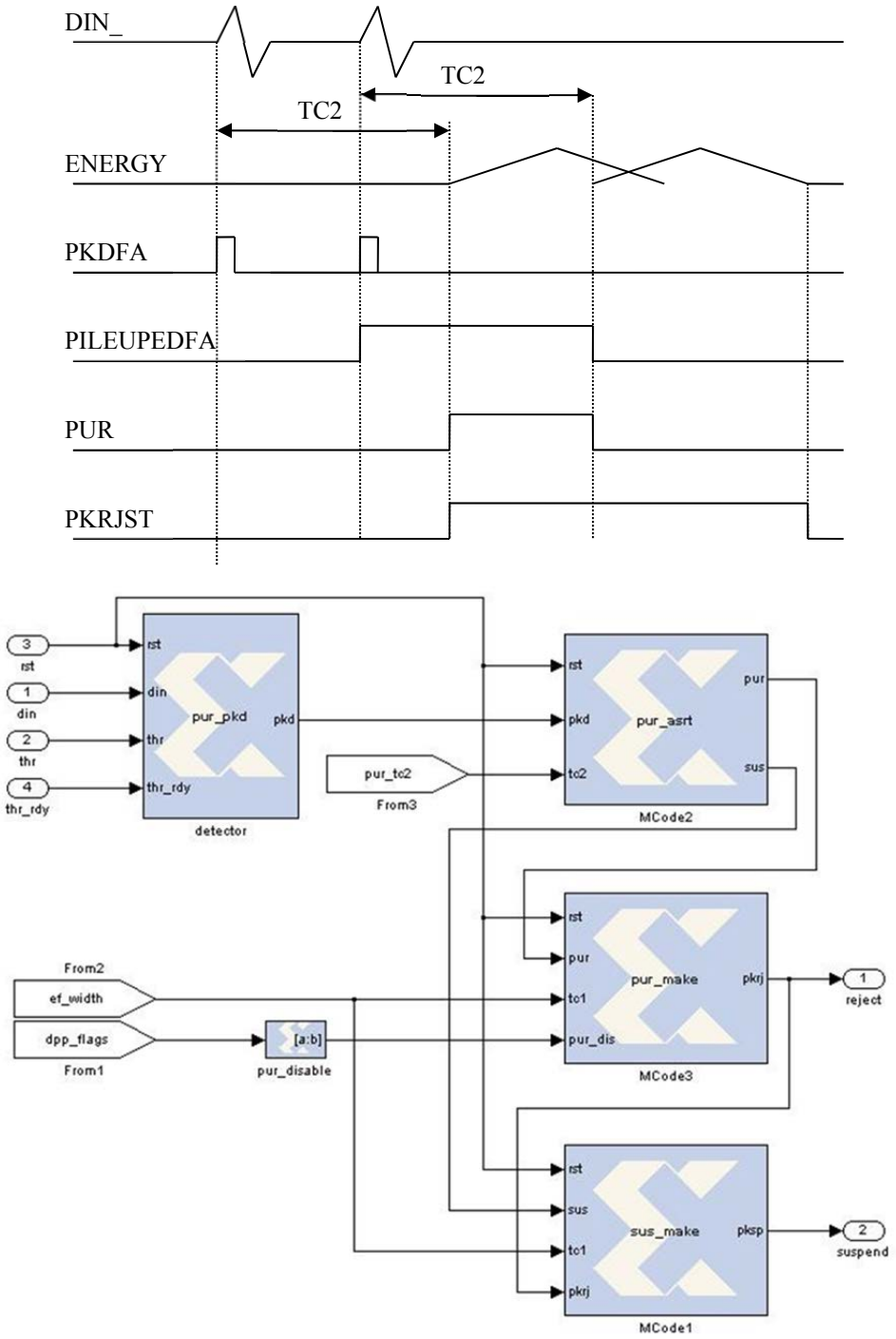

FIG. 7. The PUR subsystem (top) and timing relations of internal signals (bottom).

3.4. Noise estimator subsystem

The noise estimator monitors and outputs noise level in the energy and fast filter channels which is then used by other subsystems in order to discriminate signals from the noise. It comprises two structurally identical subsystems, the details of one of them is shown in Fig. 9.

The estimator is basically a moving average filter (Fig. 8). It calculates unweight mean $\bar{x}_n$ of the previous *k* samples.

$$\bar{x}_n = \frac{x_n + x_{n-1} + \ldots + x_{n-(k-1)}}{k} = \frac{S_{n,k}}{k} \tag{11}$$

This can be rewritten as

$$S_{n,k} = S_{n-1,k} + x_n - x_{n-k} \tag{12}$$

$$\bar{x}_n = \frac{S_{n,k}}{k} \tag{13}$$

If Eq. 11 is used for calculation, than the averaging requires *k-1* summing operations and one division, which makes latency of *k* clocks. If Eqs 12 and 13 is used, than only three operations are required: one summing, one subtraction and one division. It reduces latency to three clocks.

Since the mean value of the noise in the bipolar signal is zero, it is used absolute value of *x*, $|x|$ instead of *x* in the Eqs 11–13. Therefore, the average of the absolute values $|x|_n$ is equal to mean absolute deviation. In the case of white Gaussian noise the mean absolute deviation is related to the standard deviation σ_n as follows:

$$\overline{|x|_n} = \sqrt{\frac{2}{\pi}}\sigma_n = 0.8\sigma_n \tag{14}$$

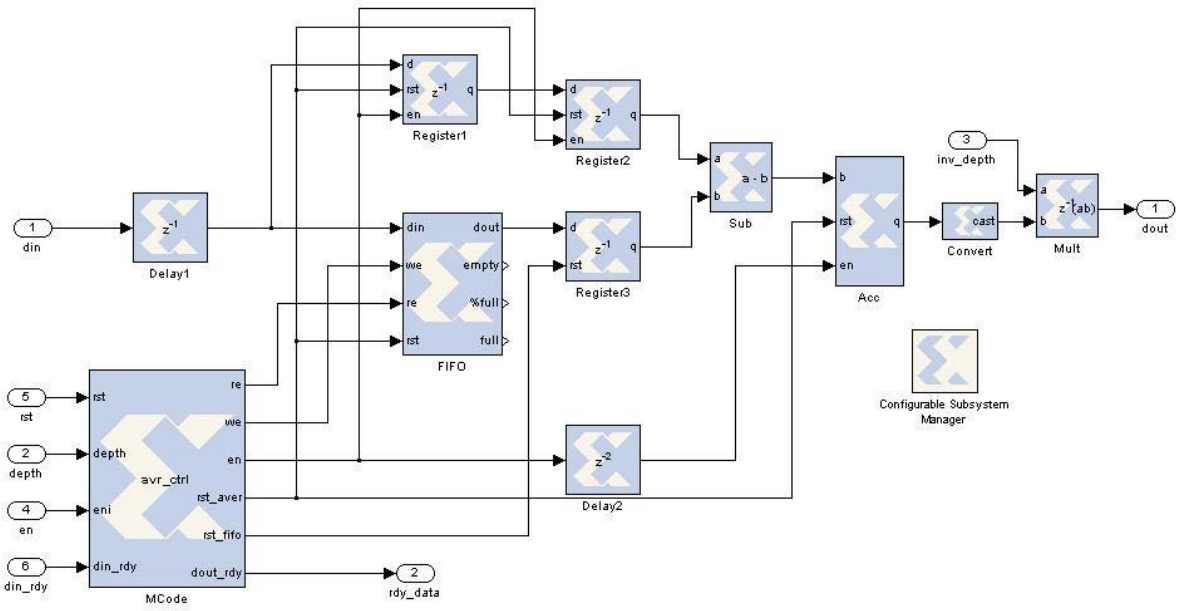

FIG. 8. The moving average subsystem.

It means that the moving average filter applied to the sampling signal in the absence of the any pulse, gives the output that is proportional to the standard deviation of the noise.

The implementation of the moving average filter in the FPGA is presented in this paper (Fig 8). The term x_{n-k} is provided by the FIFO (first in first out) memory blocks. The depth of the FIFO memory is set to k elements, which means that input appears at the output k clocks later. The term x_{n-k} is provided by Register1. The above two terms are subtracted by the Sub-block and result is added to the previously value by the accumulator *Acc* giving the sum $S_{n,k}$ The final result (Eq. 13) is obtained by multiplicator *Mult*. Note that division is replaced by multiplication with factor (*1/k*). The *avr_ctrl* block ensures proper initialization of all blocks including the calculation of initial value $S_{0,k}$.

The above moving average filter is used in the noise estimator subsystem (Fig. 8). It is encapsulated in the subsystem with name 'average noise'. The depth of its FIFO buffer is set to 1k, which means that the subsystem averages 1023 samples and it is done with a latency of only few clocks. The result would represent an average value of the input signal in the interval of time equal to 1023 FPGA clock periods, which is approximately 21 μs for a 48 MHz clock (1023/48 MHz). In order to increase this period, keeping the same depth of the FIFO buffer the decimation subsystem is introduced. It enables each *m-th* sample to be averaged. The decimation value *m* is set to 5, which means that averaging interval is around 100 μs. The *noise_ctr* block provides proper initialization, synchronization and absolute value of the samples. The initial value is obtained by using a predefined clamping level thr_0, and discarding all input samples din that exceed thr_0. Since the rectangular bipolar signal *din_rect* has faster rise time then din, it is also used in discarding condition. So the samples are discarding, that is averaging is suspended (en is false) if the following condition is satisfied:

$$|din\_rect| < thr_0 \quad AND \quad |din| < thr_0 \tag{15}$$

When all data are propagated through the delay line and stable value *pur_thr* of the noise level is established, the feedback is activated and clamping level thr_0 is replaced by already calculated *pur_thr*.

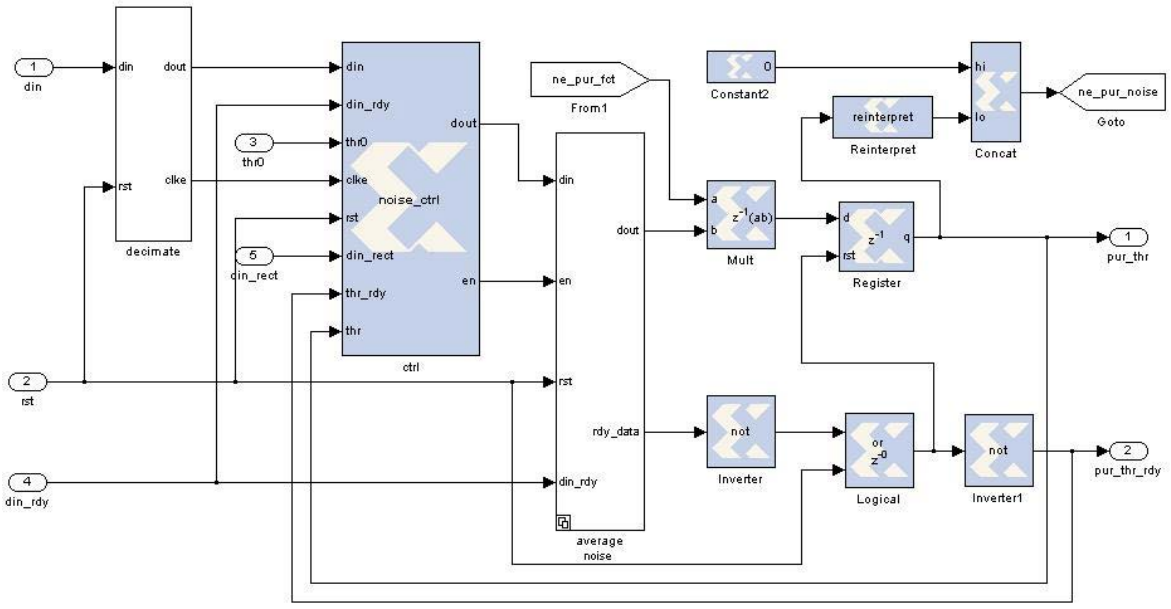

FIG. 9. The Noise Estimator subsystem – PUR section.

In order to establish a safe signal to noise discrimination level, the calculated noise threshold is multiplied by a factor called *ne_pur_fct*. This factor can be selected by the user from GUI

software. In the case of input signals with white noise and Gaussian distribution, a value slightly above 3 is reasonable.

3.5. BLR subsystem

The unipolar energy signal (Fig. 6c) does not have stable base line, which is DC offset, due to accumulator in Eq. 6. Therefore, its amplitude depends not only on the system noise, but also on the instantaneous value of the offset. It is reasonable to expect that the base line is constant in a certain period of time and that the instantaneous value for the base line is equal to the average value of the signal when no pulse is present. Therefore, in order to correct the signal for the base line, one should average the signal during a certain period and while pulse is absent in the signal and subtract the calculated average from the original signal. The implementation of the proposed method is shown in this paper (Fig. 10).

First, the DC offset of the uncorrected signal *din_uni* is calculated in the *blr_dc_offset* subsystem. Then, the calculated value is subtracted from the uncorrected signal by the subtractor Sub. The result is registered by the Register1 and output as dout.

In order to suspend calculation of the offset in the presence of the pulse, the *blr_sus* block is constructed. The presence of the pulse is checked using the bipolar energy signal *din_bi*. This signal has stable base line, it is synchronous with unipolar energy *din_uni* and has the same width. The *din_bi* pulse is detected using a simple threshold discriminator. The *blr_sus* is waiting for the pulse in the idle state and asserts the suspend signal only when a pulse is detected (crosses the threshold). The suspend remains asserted at least for the duration of the peak. The peak width is measured by an internal counter whose preset is equal to the *ef_width*. The suspend is disserted only when the counter counts-out and the *pur_suspend* is not active.

The DC offset is calculated by the *blr_dc_offset* subsystem which implementation is hereby presented (Fig. 11). It is similar to the Noise Estimator subsystem, but without using any feedback. The depth of the Moving Average block is fixed to 512, i.e. around 10 μs for 48 MHz clock (512/48 MHz). This defines minimal averaging period. The period can be extended by changing *blr_decimate* value, since the decimate block enables averaging each *blr_decimate* clocks.

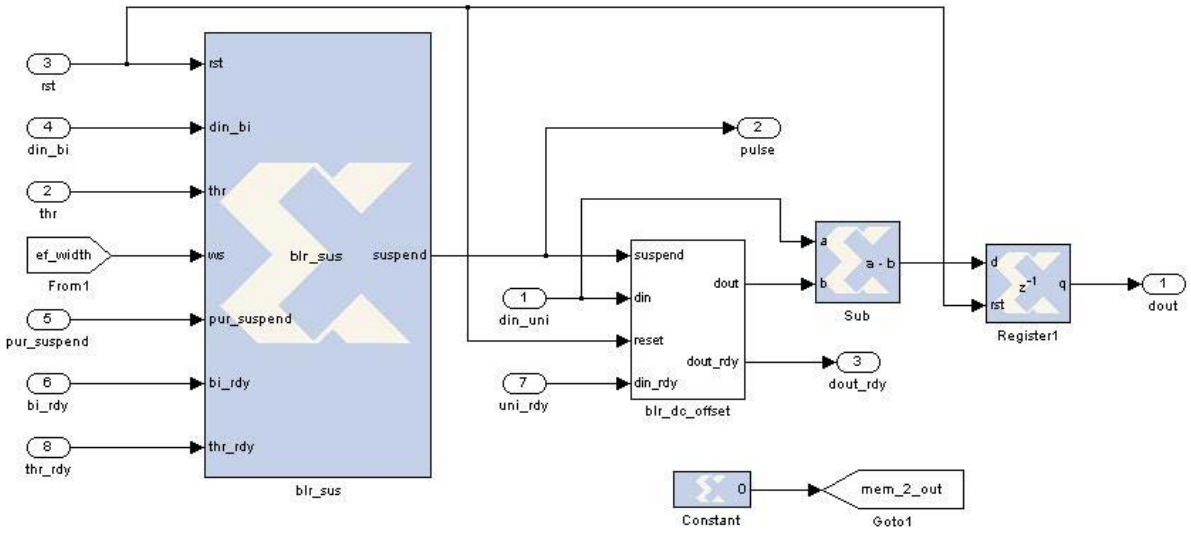

FIG. 10. The BLR subsystem

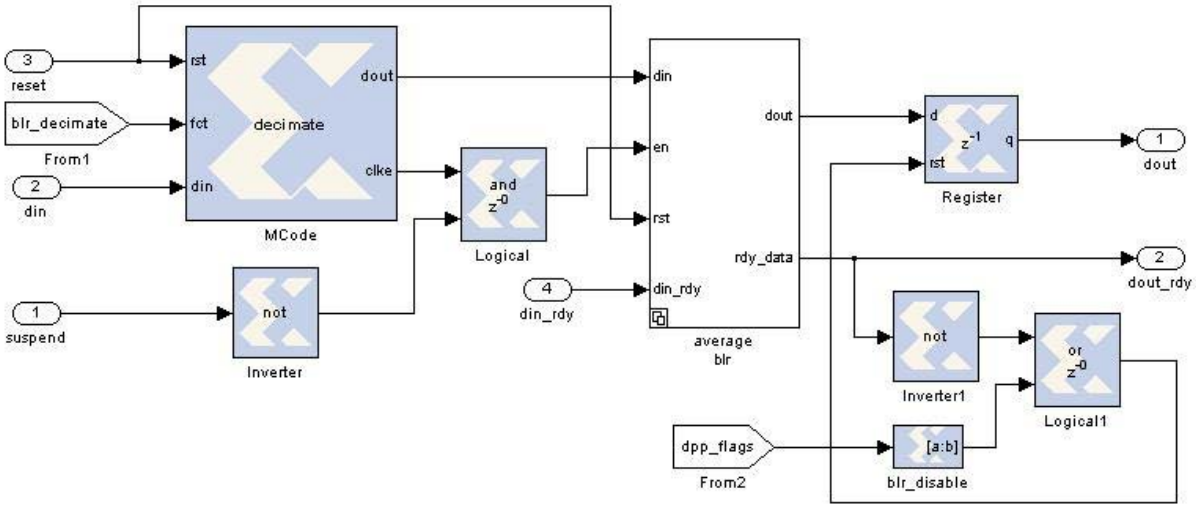

FIG. 11. The subsystem that calculates DC offset of the unipolar energy signal.

3.6. PHP subsystem

The Pulse Height Processor (PHP) subsystem is a peak detector implemented by the *php_pkd* block (Fig. 12). The block is normally in the idle state waiting for the input signal xn to exceed low level threshold *xt1*. When it happens, then *pha_busy* flag is asserted and block starts searching for a maximal value of the input signal. This is done by comparing current value with the temporary maximum. If the temporary maximum *xmax* is lower than current value *xn* then the temporary value is replaced by current value. This is applying while *xn* < *dxn*, where *dxn* is delayed input signal *xn.* The procedure can be symbolically written as follows:

$$\begin{aligned} &while(xn > dxn) \quad do \quad the \quad following \\ &\qquad\qquad if\,(xmax < xn) \quad then \quad xmax = xn \end{aligned} \tag{16}$$

The signal *dxn* is delayed for *dt*

$$dt = l - f_S k \tag{17}$$

where *k* is peaking time, *l-k* flat top time (width of the trapezoid on the top side, for a triangular pulse *l = k*) and f_s is a number, $0 < f_s < 1$ which meaning is explained as follows. Since the pulse shape is triangular or trapezoidal, it can be easily shown that after time $t = dt = l\text{-}f_s k$ measured from the start of the pulse, the pulse amplitude *A* drops to $f_s A$. In the current design it is defined $f_s = 0.8$. So, if the input signal *dxn* is delayed for $dt = l\text{-}f_s k$ respect to the *xn* then the while loop defined in the procedure (16) will be broken when amplitude falls to 80% of its maximal value and the *php_pkd* block makes transition to the next state. In the next state it asserts *data_rdy* signal and waits for data to be stored, but only if the following conditions are satisfied: *pur_rejected* is not active, *ovf_rejected* is not active and amplitude is lower than the upper level thresholds th2. The *pha_busy* is deasserted when amplitude is stored (*data_acc asserted*) or immediately if above conditions are not satisfied. In the both cases the block returns to the idle state when input signal drops below lower level threshold

th1 or the signal again starts rising (*xn* > *dxn*). The lower (*th1*) and upper (*th2*) threshold can be defined by user from GUI.

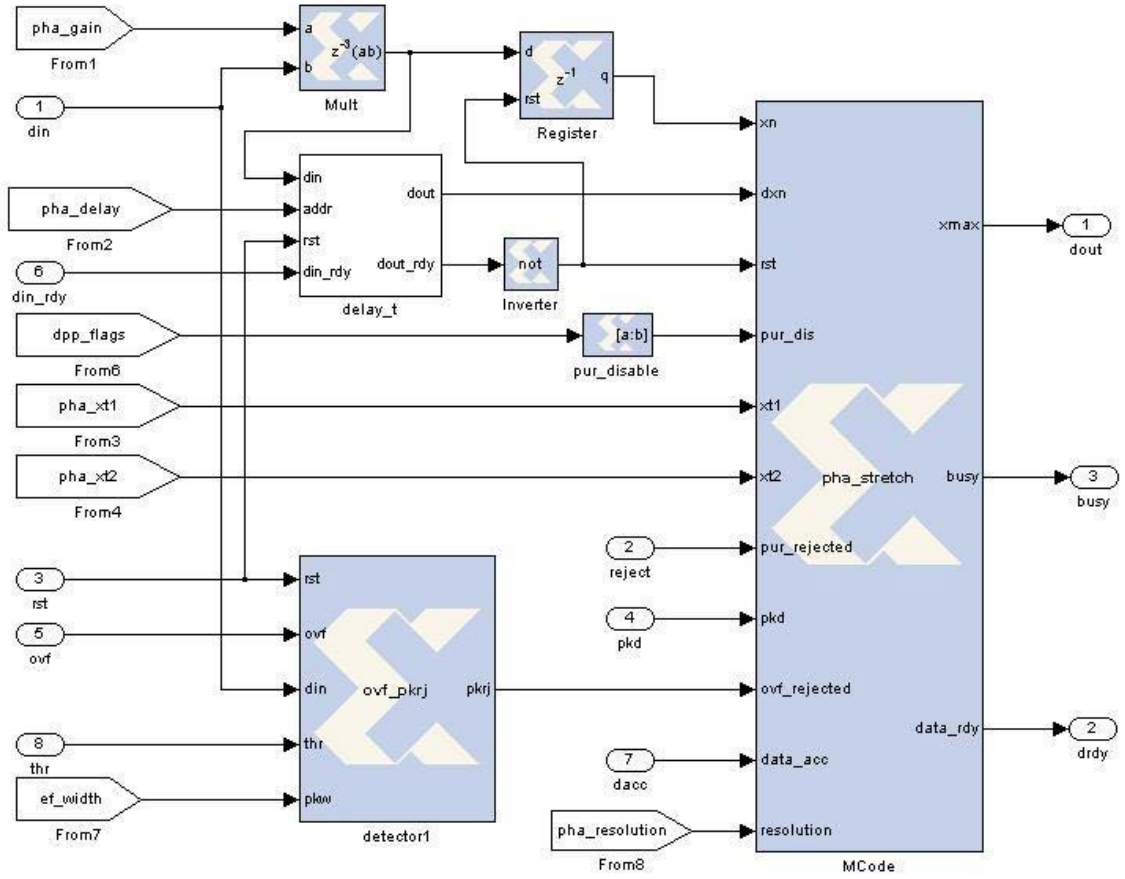

FIG. 12. The PHP subsystem.

3.7. LTC subsystem

The Live Time Correction (LTC) subsystem block corrects the real time for pulse processing time by gating the live time counter according to the live time correction method described in the Operators Manual, Canberra, Spectroscopy Amplifier Model 2020S. Several other are listed in literature [2] and can be utilized.

4. SYSTEM PERFORMANCE

The DPP core is used as a subsystem of the top-most models (Figs 1 and 2). The models are synthesized (VHDL files translated to gates and optimized for the target architecture) and implemented (mapped, placed, routed, final BIT file generated) using Xilinx XST and Xilinx ISE suit.

The performance of the DPP core has been tested in the terms of energy resolution and data throughput using Ketek's VITUS SDD-10 mm^2 detector and compared with an analogue and digital system. The analogue system was a Canberra spectroscopy amplifier model 2020 with semi-Gaussian pulse shaping, a fast ADC Canberra model 8715 and a fast MCA. The digital system was a Canberra Inspector 2000 model No. 1300.

The digital systems achieved best resolution with peaking time of around 3 μs and using triangular shaping, while the analogue system had the best performance for shaping times between 1 and 3 μs. Figure 13 shows a measurement with all three systems. Each spectrum was collected for 100 s using a high input counting rate of 40 kHz. Both digital systems were able to process around 30 kHz with resolution of 140 eV (Canberra) and 145 eV (this work). The analogue system could process only around 22 kHz by using 2 μs shaping time. It has comparable speed to the digital systems by using 1 μs shaping time. In both cases, resolution was 155 eV. At low counting rates, the resolution improved and it was 151 eV. The better resolution obtained with digital systems is due to the more efficient shaping of the triangular than semi-Gaussian shapers. The theoretical ratio, assuming fourth order semi-Gaussian is 1.165/1.075 which is close to the measured values.

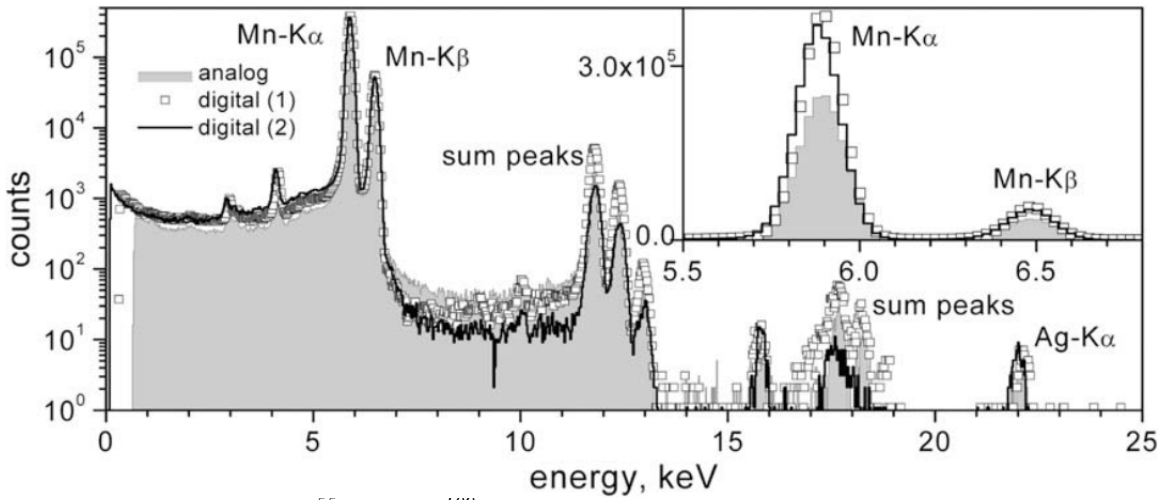

FIG. 13. Comparison of ^{55}Fe and ^{109}Cd X ray spectra collected with analogue and digital systems at a count rates of 40 kHz. The achieved energy resolution, FWHM, was 155 eV, 140 eV and 145 eV for the analogue, commercial digital (1) and developed digital (2) system, respectively.

Performances of the system in ion beam imaging applications were tested in terms of the speed as well. For this purpose an image of 1000 mesh Cu-grid were collected in transmission mode using 2 MeV proton beam over area of 100 um × 100 μm, 128 × 128 raster grid, different dwell times (50 μs, 100 μs and 200 μs). The beam is scanned magnetically using a pair of ferrite cored scan coils and OM40e dual scan amplifier. The amplifier is driven with two 14-bit 160 MSPS digital to analogue converters coupled to Virtex 4 FPGA (Fig. 1). The system was capable to produce x, y position, energy, time arrival and transfer it to the PC at counting rate over 20 kHz. The data is used to display real time image of the grid and make of line analysis (Fig 14). The time arrival information is used to produce a time interval distribution between two successive protons. It was found that distribution has expected exponential shape except for very short times due to pile-up effect. The calculated average interval time was ~50 μs which is in agreement with observed counting rate of approximately 20.000 protons/sec.

The images taken at different dwell times (Fig. 15) show clear distortion in the direction of the fast scan (x axis) at 50 μs dwell time (1.2 frames/sec), small distortion at 100 μs (0.6 frames/sec) and undistorted images above 200 μs (0.3 frames/sec). The distortions are due to hysteresis in the coils of the magnetic scanning system. It means that existing magnetic scanning system limits rapid imaging to only one frame per few seconds. In order to explore

the full speed of the developed acquisition system an electrostatic scanning system should be utilized.

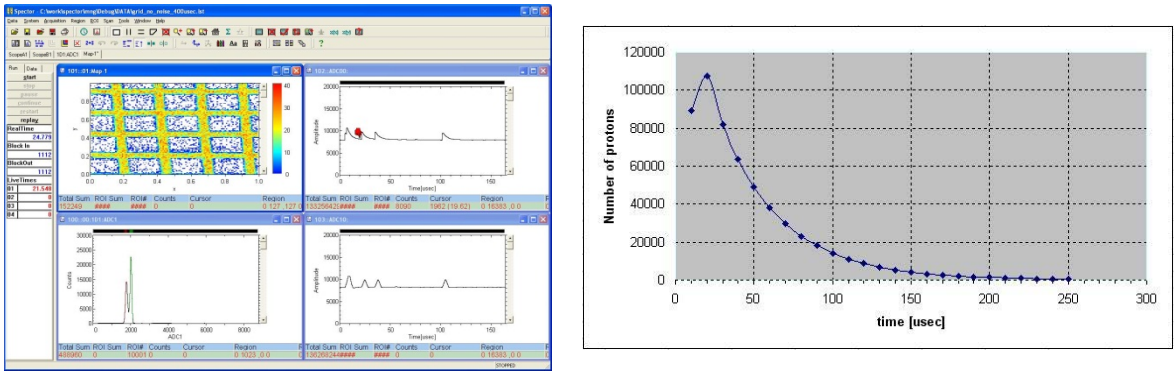

FIG. 14. Acquisition software real time output (top left) in ion beam imaging application. The data provided by the system can be used to extract additional information, for example time interval distribution between two successive protons (top right).

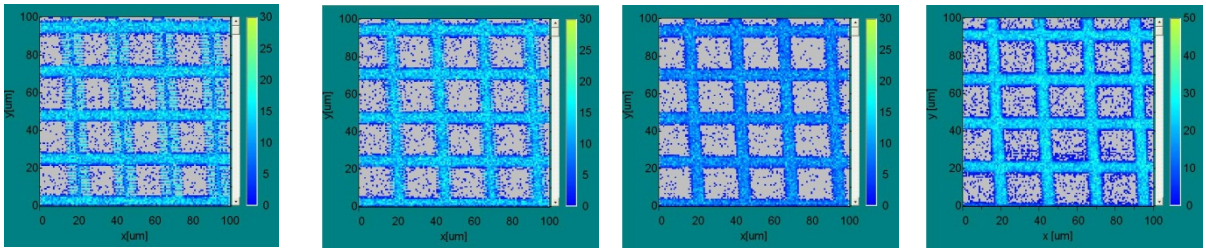

FIG 15. Ion beam images of the 1000 mesh grid with 2 MeV protons in the transmission mode with different dwell times (50,100,200,400 µs, left to right) shows that only magnetic scanning system limits rapid imaging.

5. CONCLUSIONS

In this work we have shown how an advanced hardware and FPGA design tools can be efficiently used in a process of developing a compact, reconfigurable and high performance data acquisition system for nuclear spectroscopy and particularly ion beam microprobe imaging. Such a system meets the high criteria for energy resolution while featuring higher speed and create potential for upgrading.

The comparison with a classical analogue system shows that both systems perform equally on lower counting rates, while the digital can better handle pile-up events on higher counting rates. In the ion beam application, the developed digital system proved to be suitable for fastest possible real time imaging with magnetic scan coils. In order to test its true potential a faster electrostatic scanning system should be used.

REFERENCES

[1] JORDANOV, V.T., KNOLL, G.F., HUBER, A.C., PANTAZIS, J.A., Digital Techniques for Real Time Pulse Shaping in Radiation Measurements, Nucl. Instr. Meth. A353 (1994) 261.

[2] PONIKVAR, D., JEGLIC, A., Dead time correction using a timer, Nucl. Instr. Meth. B88 (1994) 308.

SET-UP OF DIGITAL MCA WITH HPGE DETECTOR IN HIGH GAMMA FIELDS

P. BRYNDZIAR
Slovenské elektrárne, a.s.,
Nuclear Power Plant Mochovce,
Mochovce, Slovakia
Email: pavol.bryndziar@enel.com

Abstract

The processing time adjustability of a commercial portable spectroscopy workstation based on Digital Signal Processing technology was investigated in areas from highly contaminated (mSv/h dose rate) to high energies (up to 8 MeV) to throughput and resolution performance coaxial Germanium detector. Altering the rise/fall and flat top times of the trapezoidal filter, it was estimated the full width at half maximum at the following peaks: ^{54}Mn 834.8 keV, ^{60}Co 1332.5 keV, ^{16}O(n, p)^{16}N 6129.9 keV, ^{56}Fe(n, γ) 7631.1 keV and ^{56}Fe(n, γ) 7645.5 keV. First type measurement for ultra-high counting and throughput rates was performed at ionex filter which capture activation products (^{54}Mn, ^{60}Co) from primary cooling medium and second type measurement for highest resolution was carried out at pressure water reactor platform during nominal power level giving high energy gamma 6129.9 keV from interaction fast neutrons ^{16}O(n, p)^{16}N and 7631.1 keV, 7645.5 keV from radiation capturing thermal neutrons by ^{56}Fe(n, γ). To measure through energy range up to 8 MeV was reached setting coarse and fine gain to lower range and measuring at contaminated ionex filter by GBq activity was allowed using 50 mm cylindrical collimator by 30 mm diameter, without using this collimator was destroyed whole gamma spectrum despite altering rise/flat times. The results, which are presented, provide optimum performance for high throughput: FWHM 1.71 keV/834.8 keV (^{54}Mn) and 2.00 keV/1332.5 keV (^{60}Co) and best resolution: FWHM 4.49 keV/6129.9 keV (^{16}N), 4.97 keV/7631.1 keV/7645.5 keV (prompt gamma iron) setting 2.8 μs rise time and 0.6 μs flat top time. For 0.8/1.2 μs rise time and 0.2 μs flat top time occurred results with destroyed resolution broadening and peak shift at 6129.9 keV and 7631.1/7645.5 keV. For rise time above 8.8 μs and flat time above 0.8 μs were peaks at 834.8 keV and 1332.5 keV unusable for purpose peak analysis process.

1. INTRODUCTION

The measurements in the field of nuclear spectroscopy require the best digital spectrometer system with excellent resolution and throughput. The digital filter employed in this digital MCA has a trapezoidal weighting or shaping function. Further optimisation of the performance for the specific detector, spectral energy range and count range by selecting rise time and flat top, which determines trapezoidal pulse shape, was done.

2. PARAMETERS

2.1. Parameter descriptions

Beside the functions such as amplifier gain adjustment, baseline restoration, stabilization, and automatic pole-zero compensation, digital MCA also provides an advance shaping. The modelled pulse shape is a trapezoid whose sides and top may be adjusted. This shaping function is symmetrical. Two parameters that control the shape are rise time and flat top. These two parameters can be adjusted independent for each measurement to achieve the best results.

The rise time sets the noise filtering characteristics of the digital filter. The DSP rise time can be adjusted in the range from 0.8–36 μs. The fall time cannot be independently set; it always equals the rise time selection.

The flat top adjusts the width of the top of the trapezoid. Its width can be adjusted in range from 0.2 to 2.4 μs using the spin box. The flat top allows for the charge collection time of the particular detector. If the flat top is too short, it may result in low side spectral tailing and

degraded resolution. A larger width of the flat top makes the pulse shape wider, which may improve the resolution and decrease the throughput rate.

For high energies, an unshielded detector was located next to the reactor platform admittance (decking around the reactor platform). The measured spectrum indicated that the gamma field was mainly from ^{16}N photons with energy 6130 keV and photons emitted by thermal neutron interaction in iron (7631 keV and 7646 keV). The dose rate at the measurement point caused by neutrons was 220 μSv/h. The dose rate at the measurement point due to gamma photons was 10 μGy/h.

The energetic calibration for high energies was performed at 1173.21 keV, 1332.47 keV (^{60}Co), 6129.2 keV ($^{244}Cm/^{13}C$) energy levels including the escape peaks. An energy range spanning up to 8 MeV was reached by reducing the coarse and fine gain to about minimum level. In order to keep the counting at high energies within the peaks on statistically acceptable levels, the measurements took up to 1800 seconds. The measurements used a portable coaxial germanium characterized detector HPGe with a relative efficiency about 35%.

For ultra-high counting and throughput rates, a shielded detector was located next to a container that contains a homogeneous distributed activity (GBq). The dose rate at the measurement point due to gamma photons was 500 μGy/h. The distance between detector face and surface container was 1.5 m. In this case, the detector had to be shielded using a 50 mm cylindrical collimator by 30 mm diameter. Without this collimator the whole gamma spectrum was destroyed despite altering rise/flat times.

2.2. Parameter search and analysis

In order to optimize digital MCA usage with a germanium detector, one needs to find the best set of operating parameters for the detector in given conditions. The rise time values were varied from 0.8 to 36 μs. The flat top width values were changed from 0.2 to 2.4 μs. The sources used were highly contaminated ionex filters which capture activation products from the primary cooling medium and pressure water reactor during nominal power level giving high energy gamma rays [1]. For each data set, the full width at half maximum was calculated by gamma spectroscopy software (GenieTM 2000 Spectroscopy Software 9233653F V3.1 and 9233652F V3.1, respectively Customization Tools and Operations).

Tables 1 and 2 show the FWHMs and the corresponding rise and flat times obtained from the given measurements for high throughput/good resolution (good or equivalent Gaussian shaping resolution) and best resolution/lower throughput (equivalent Gaussian shaping processing time/throughput).

From Table 1, performance for high throughput, one can see that, for rise time above 8.8 μs and flat time 1.2 μs, the peaks at 834.8 keV and 1332.5 keV are unusable for peak analysis process. Lowest resolution 1.71 keV at 835 keV and 2.00 keV at 1333 keV was reached for setting rise time 2.8 μs and flat time 0.6 μs and for the same combination rise and fall time was achieved the best FWHM 4.49 keV at 6130 keV and 4.97 keV at 7631 keV. From Table 2, performance for best resolution, one can see that, for rise time above 12.0 μs and flat time 0.8 μs the peaks at 834.8 keV and 1332.5 keV are degraded. The best resolution 1.65 keV at 835 keV and 1.98 keV at 1333 keV was reached for setting rise time 5.6 μs and flat time 0.6 μs. For high energy, it reached the same FWHM as in the case performance for high throughput by setting rise time 2.8 μs and flat time 0.6 μs.

TABLE 1. FWHM FOR DIGITAL SIGNAL ANALYZER RISE TIMES AND FLAT-TOP SETTINGS THAT OPTIMIZE PERFORMANCE FOR HIGH THROUGHPUTS

			^{54}Mn	^{60}Co	^{16}O(n, p)^{16}N	^{56}Fe(n, γ)	^{56}Fe(n, γ)
Gaussian Shaping (μs)	Rise time (μs)	Flat time (μs)	835 keV FWHM (keV)	1333 keV FWHM (keV)	6130 keV FWHM (keV)	7631 keV FWHM (keV)	7646 keV FWHM (keV)
0.5	0.8	0.2	2.87	3.29	degrade	degrade	degrade
1.0	1.2	0.6	1.82	2.09	4.58	5.02	5.02
2.0	2.8	0.6	1.71	2.00	4.49	4.97	4.98
4.0	5.6	0.8	1.70	2.08	4.83	5.06	5.07
6.0	8.8	1.2	degrade	degrade	4.96	5.59	5.59
12.0	16.8	2.4	degrade	degrade	5.87	6.10	6.11

Degrade means that gamma spectrum was destroyed by broadening and peak shift.

TABLE 2. FWHM FOR DIGITAL SIGNAL ANALYZER RISE TIME AND FLAT-TOP SETTING WHICH OPTIMIZE PERFORMANCE FOR BEST RESOLUTION

			^{54}Mn	^{60}Co	^{16}O(n, p)^{16}N	^{56}Fe(n, γ)	^{56}Fe(n, γ)
Gaussian Shaping (μs)	Rise time (μs)	Flat time (μs)	835 keV FWHM (keV)	1333 keV FWHM (keV)	6130 keV FWHM (keV)	7631 keV FWHM (keV)	7646 keV FWHM (keV)
0.5	1.2	0.2	2.55	2.99	degrade	degrade	degrade
1.0	2.8	0.6	1.71	2.00	4.49	4.97	4.98
2.0	5.6	0.6	1.65	1.98	4.85	5.22	5.22
4.0	12.0	0.8	degrade	degrade	5.36	6.03	6.02
6.0	18.4	1.2	degrade	degrade	5.85	6.12	6.12
12.0	36.0	2.4	degrade	degrade	9.21	8.06	8.06

3. CONCLUSIONS

The processing time is set by rise time and flat top selections and is generally a compromise between optimizing throughput and resolution. Having the ability to independently set shaping parameters allows greater flexibility when optimizing the trapezoidal shaping for extreme measuring situations such as to estimate activity on-site characterized highly dose

rate due to gamma photons of the order mSv/h or for monitoring to obtain a qualitative analysis of high energy (up to 8 MeV) secondary gamma radiation sources accompanied by hard moderated neutrons. By this evaluated portable spectroscopy workstation based on digital signal processing, the best resolution 1.65 keV at 835 keV and 1.98 keV at 1333 keV was reached for setting rise time 5.6 μs and flat time 0.6 μs in gamma field with highly dose rate and the best resolution 4.49 keV at 6130 keV and 4.97 keV at 7631 keV was achieved for setting the rise time 2.8 μs and flat time 0.6 μs in high energy gamma field.

REFERENCE

[1] LONE, M.A., LEAVITT, R.A., HARRISON, D.A., Prompt gamma rays from thermal-neutron capture, Atom. Data Nucl. Data Tab. 26 (1981) 511–559.

DIGITAL PULSER FOR CHARACTERIZATION AND DIAGNOSTIC OF DIGITAL SPECTROMETERS

V.T. JORDANOV
Yantel, LLC,
Los Alamos, USA
Email: jordanov@ieee.org

Abstract

The concept and the realization of the digital pulser are presented. The digital pulser is implemented as a functional block of a digital spectrometer. The digital pulser provides noise free and distortion free measurement of the inherent electronic noise of the entire spectroscopy system. The digital pulser is introduced at the end of the signal processing chain and allows separate evaluation of the individual spectroscopy blocks. It offers the ability to characterize and diagnose problems of the digital pulse height analysers by grounding their inputs. The digital pulser does not interfere with the processing of the detector signals and does not contribute to the dead time and the pulse pile-up of the system. The digital pulser peaks are not affected by the presence of detector pulses and are stored in a separate histogram memory leaving the detector spectrum undistorted.

1. INTRODUCTION

Pulsers (test pulse generators) are used in radiation spectroscopy for estimation of the inherent electronic noise, correction of pile-up counting losses and dead time, calibration verification, gain stabilization and other characterizations of the spectroscopy systems [1–6]. Traditional pulsers are introduced at the beginning of the signal processing chain of the radiation spectrometers. They inject charge at the input of the detector preamplifier through a test capacitor or through the detector capacitance. Test capacitors increase the total input capacitance causing degradation of the noise performance of detector preamplifiers. Charge injection through the detector capacitance may create distortion and may require special high voltage circuitry. The analogue pulsers are subject to their own electronic noise, ground loops and other unwanted electromagnetic interferences. In addition, the amplitude of these pulsers may drift with time and temperature.

One of the major shortcomings of the traditional pulsers is the interference of the test pulses with the detector pulses. The preamplifier pulse shape from the pulser injected charge is bipolar and differs from the unipolar pulse shape from the detector charge collection. This may affect the operation of the shapers (analogue or digital), especially the base line restorers. As the test pulses are processed through the same signal chain as the detector pulses, the test pulses pile-up with the detector pulses and cause additional counting losses and distortion of the pulser and detector spectral peaks. The use of the traditional pulsers may be limited in portable system or in the field due to size requirements. Some detector configurations may not offer test input due to detector design, size or noise performance constraints.

With the introduction of digital pulse processing, some of the traditional uses of the pulsers have been replaced with new techniques. For example, the elimination of the ADC dead time and the employment of new digital shaping techniques allow estimation of the counting losses with much greater accuracy and the need to use pulsers for pile-up correction and dead time estimation diminishes. However, the use of pulsers to measure the inherent noise of the digital spectroscopy system remains important for optimal setting of the signal processing chain. This paper describes a digital pulser that allows for noiseless measurement of the electronic noise and evaluation of other characteristics of the digital spectrometers.

2. DIGITAL PULSER

In contrast to the traditional analogue pulser, the digital pulser is introduced at the end of the signal processing chain. Figure 1 depicts a simplified block diagram of a digital spectrometer utilizing a digital pulser. The digital pulser is fed by the output of the spectrometer's digital shaper. The digital pulser selectively processes sampled digital values. The digital pulser produces digital pulse heights with distribution that has variance equal to the variance of the digital shaper baseline distribution (inherent electronic noise). The mean of the baseline distribution, however, may be shifted by a digital offset generated by the digital pulser. The distribution of the digital pulse heights is recorded in a histogram memory.

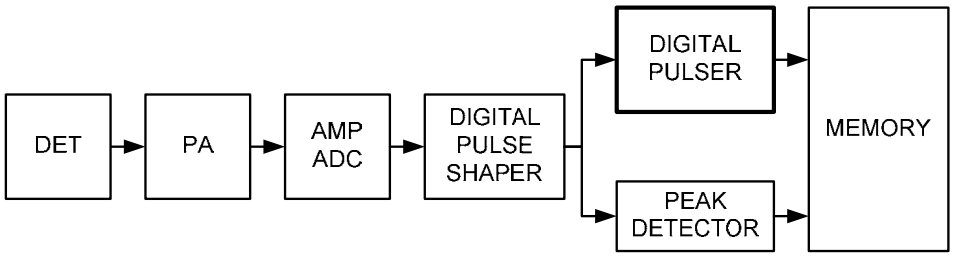

FIG. 1. Simplified block diagram of digital spectrometer using digital pulser.

The peak representing the distribution of the digital pulser output can be recorded independently from the detector spectrum. Therefore, the spectral interference between the detector spectrum and the pulser peak is eliminated without any additional means as in the case of the traditional analogue pulsers [5, 6]. It is clear that the digital pulser cannot be used for calibration verification or gain stabilization because of its position at the end of the signal processing chain.

Figure 2 shows a simplified block diagram of the digital pulser. *Pulser Strobe* is a digital pulse signal with width equal to the width of one cycle of the digital shaper clock. These short pulses may be generated randomly, or at fixed frequency. The digital signal from the digital shaper (*Digital Shaper*) is added to a fixed *Digital Offset*. The result from the addition feeds the input of a data register (REG) which captures the adder's digital value at each *Pulser Strobe*. The captured digital value is held by the register until the next *Pulser Strobe*.

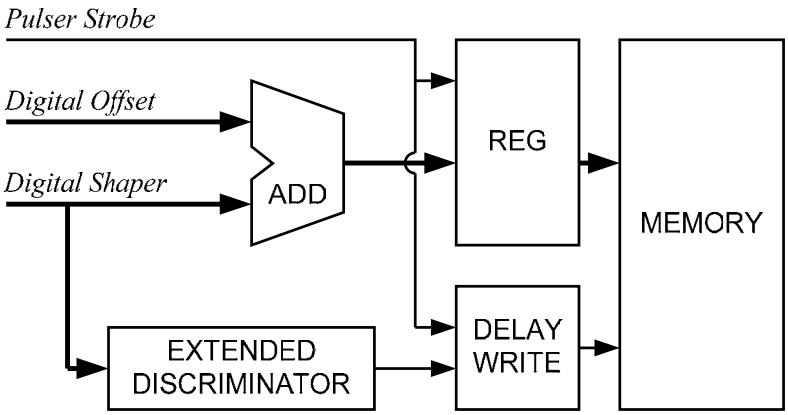

FIG. 2. Block diagram of digital pulser.

The *Digital Shaper* signal drives a discriminator with threshold set just above the noise envelope of the base line (EXTENDED DISCRIMINATOR). The discriminator pulse is extended in order to prevent capturing digital samples that represent superposition of the falling edge of the digitally shaped detector signal and the shaper's base line. A delay write technique is used to prevent memory storage of samples that are superposition of the leading edge of the shaped detector signal and the baseline. The delay write is triggered by the *Pulser Strobe* only when the extended slow discriminator is inactive. The delay write is aborted if the extended slow discriminator becomes active during the delay period.

To illustrate the operation of the digital pulser, a timing diagram is presented (Fig. 3). The *Digital Shaper* signal represents the baseline signal (electronic noise) and a single detector pulse with amplitude exceeding the *Noise Threshold*. When the detector pulse exceeds the *Noise Threshold* the *Discriminator* becomes active. The *Discriminator* signal is extended by an *Extension* resulting in the *Extended Discriminator* signal. When active, the *Extended Discriminator* prevents the *Pulse Strobe* to trigger the *Write Delay*, thus preventing capturing baseline samples that may be contaminated by the detector signal. When the *Extended Discriminator* is inactive each *Pulse Strobe* pulse triggers the *Write Delay*. In this particular case the *Write Delay* is just a fixed extension of the *Pulser Strobe*.

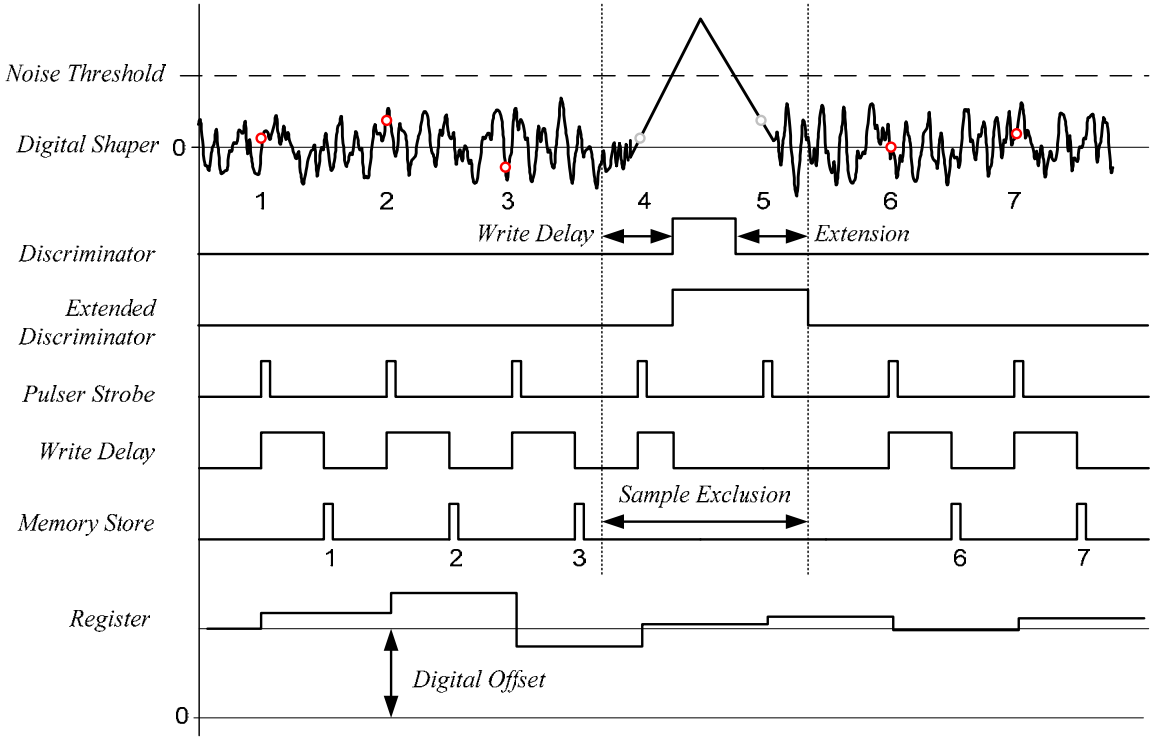

FIG. 3. Timing diagram illustrating the digital pulser operation.

At the falling edge of the *Write Delay,* a *Memory Store* signal is generated which initiates the memory histogram function using the captured *Register* data. The *Write Delay* is terminated and no *Memory Store* is generated when the *Extended Discriminator* becomes active. Using this functionality, *Digital Shaper* samples that may be contaminated by the detector signal are excluded from capturing by the digital pulser. For example, only samples 1, 2, 3, 6, 7 (red dots) will be recorded in the digital pulser peak. Samples 4 and 5 (grey dots) will be excluded from the digital pulser peak (Fig. 3).

Other realizations of the digital pulser are possible but they all should prevent capturing of data that may be contaminated by the detector signal. The *Pulser Strobe* may be generated at

frequencies up to few MHz. However, for efficient capture of the samples, more sophisticated registers may be used, e.g. FIFO register or circular buffer. As in the case of the traditional pulser, the digital pulser data is histogramed and stored in the memory. Therefore, the output of the digital pulser is a spectral peak and can be used for detailed analysis by existing spectral data processing software programs.

3. EXPERIMENTAL TESTS

In the following examples a digital pulser is used that is a part of a Digital Pulse Processor "*labZY-X"* developed by Yantel, LLC. This processor is optimized for processing signals from silicon drift detectors. Figure 4 shows a Fe-55 spectrum and the digital pulser peak obtained simultaneously using thermoelectrically cooled silicon drift detector with resolution of 162 eV @ 5.9 keV. Figure 4a shows the X ray spectrum undisturbed by the digital pulser. The digital pulser is stored in a separate memory group depicted in Fig. 4b and shows no signs of the X ray spectrum. As illustrated in Fig. 4c, the digital pulser peak can be added to the detector spectrum if desired. This addition, however, will cause peak distortion if the digital pulser peak is added to a spectrum area with a significant number of counts. In the case of Fig. 4c, the pulser peak is added to a part of the spectrum with few background counts. The FWHM of the digital pulser is 109 eV and is direct measure of the system electronic noise.

One of the major applications of the digital pulser is to estimate precisely the electronic noise of the digital spectroscopy system in a very short time. To optimize the performance and the settings of the digital pulse shaper, a noise profile of the entire signal processing chain was measured. The FWHM of the pulser peaks were recorded for different rise times of the digitally shaped triangular pulses. The digital pulser operated at frequencies between 1 MHz and 20 kHz depending on the rise time of the triangular pulses. More than one million counts were recorded in each pulser peak. The intrinsic electronic noise is measured as FWHM of the recorded digital pulser peak. Figure 5 shows the electronic noise dependence from the rise time of the digitally shaped triangular pulse. All data shown in Fig. 5 were taken manually in less than 5 minutes. The process can be automated and will allow "noise optimization" of the system in less than one minute.

The digital pulser is also a powerful diagnostic tool. As stated earlier, the digital pulser is connected at the end of the signal processing chain. This allows diagnostic of the individual modules comprising the spectroscopy system. For example, the preamplifier response can be eliminated by disconnecting the preamplifier and grounding the input of the amplifier that follows the preamplifier. This connection is shown in Fig. 6.

The digital pulser allows to diagnose some hard to find problems in this "grounded configuration". Figure 7 shows an example digital pulser peak indicating amplifier oscillation or pick-up of external sinusoidal signals. The split peak results from the convolution of the sinusoidal signal and the electronic random noise of the system. If the preamplifier is connected, its noise dominates all other noise sources and the split peak disappears. The sinusoidal oscillation case of Fig. 7 was simulated by introducing a 200 kHz signal at one of the components of the main amplifier.

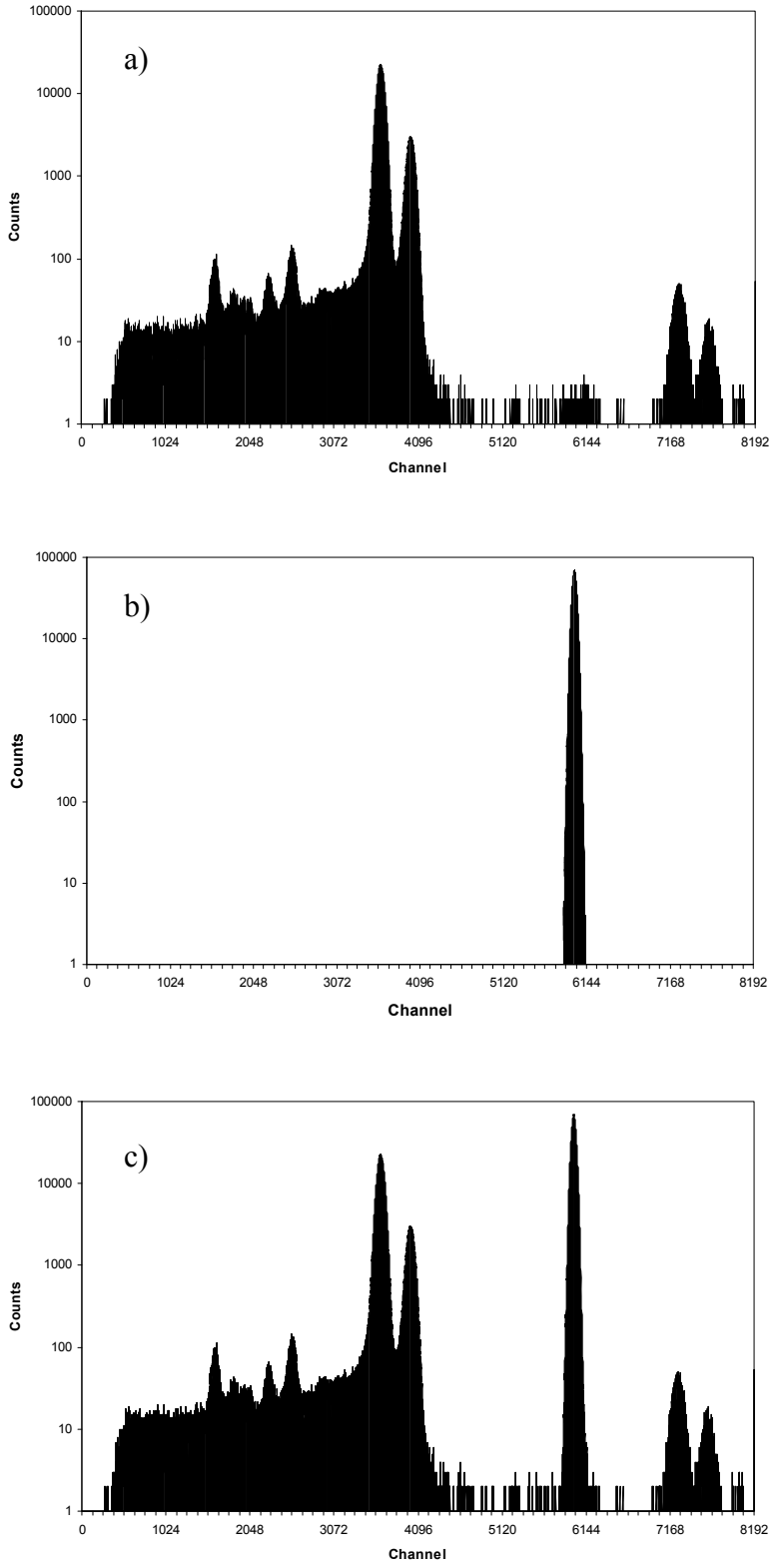

FIG. 4. Examples of X ray spectrum and digital pulser peak.

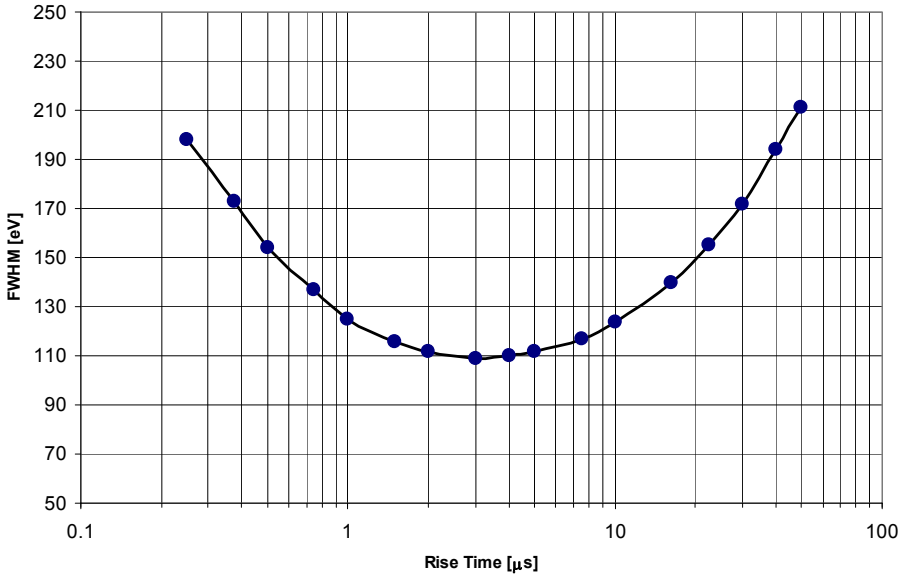

FIG. 5. Electronic noise profile of digital spectroscopy system.

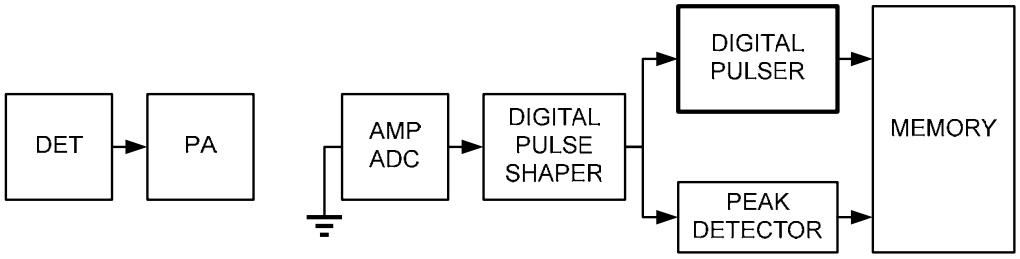

FIG. 6. Test configuration excluding detector and preamplifier from the signal processing chain.

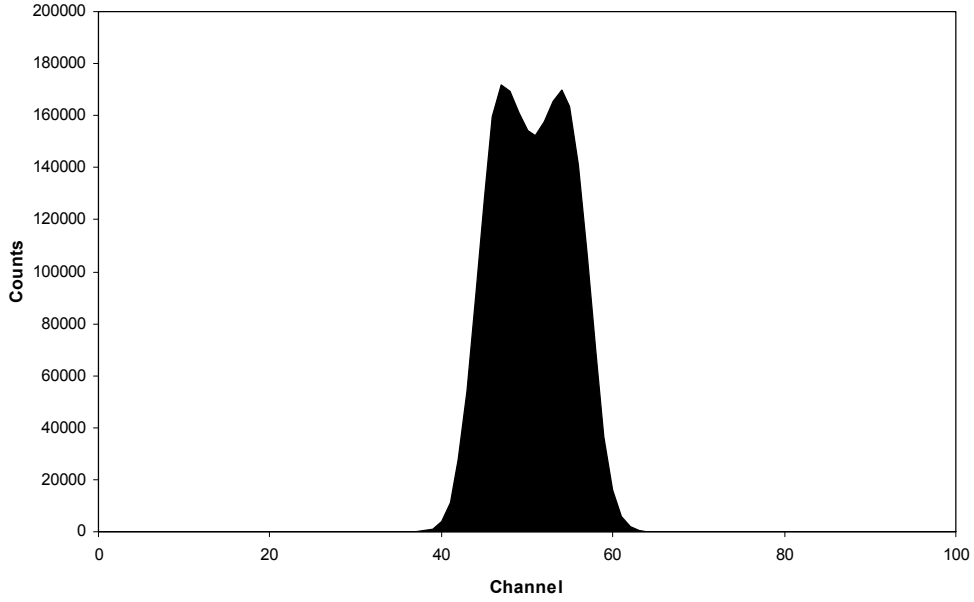

FIG. 7. Digital pulser peak from "grounded configuration" indicating presence of sinusoidal signal.

4. CONCLUSION

The digital pulser is a simple but powerful concept that can be easily incorporated in most digital spectroscopy system. The digital pulser does not add noise to the spectroscopy system and does not interfere with the pulse processing and the spectrum acquisition. Its accurate estimation of the intrinsic electronic noise makes it an indispensable tool in the optimization of the digital pulse processing, characterization and optimization of the detector frontend electronics, accurate measurement of detector parameters such as Fano factor, quality control etc. Other traditional tasks, such as pole-zero adjustment, counting losses estimation may also benefit from the use of the digital shaper.

REFERENCES

[1] MILLER, G.L., et al, Silicon p-n Junction Radiation Detectors, IRE Trans. Nucl. Sci. 7-2 (1960) 185–189.

[2] STRAUSS, M.G., et al, Ultra Stable Reference Pulser for High Resolution Spectrometers, IEEE Trans. Nucl. Sci. 15- 3 (1968) 518–530.

[3] ANDERS, O.U., Experiences with the Ge(Li) Detector for High Resolution Gamma Ray Spectrometry and a Practical Approach to the Pulse Pileup Problem, Nucl. Instr. Meth. 68 (1969) 205–208.

[4] JOHNSON, L.O., et al, Utilization of Concurrently Gathered Pulser Data for Complete Spectral Validation of Gamma Ray Spectra from Germanium Detectors, IEEE Trans. Nucl. Sci. 28-1 (1981) 638–642.

[5] HARTWELL, J.K., GOODWIN, S.G., Pulse Injection with Subsequent Removal: Implementation and Applications, IEEE Trans. Nucl. Sci. 36-1 (1989) 801–805.

[6] THEN, S.S., et al, A pulse generator simulating Ge-detector signals for dead time and pile-up correction in gamma ray spectrometry in INAA without distortion of the detector spectrum, J. Radioanal. Nucl. Chem. 215-2 (1997) 249–252.

DIGITAL SIGNAL PROCESSING FOR OPTIMAL RESOLUTION IN GAMMA RAY SPECTROSCOPY

A. MESSAI, A. NOUR, I. ABDELLANI
Centre de Recherche Nucléaire de Birine,
CRNB – COMENA, Algeria
Email: messai_adnane@yahoo.fr

Abstract

The work described in this paper is based on the digital processing of samples obtained by digitizing the signal pulse as it appears at the output of a γ ray measuring set-up. Consequently, we will discuss the design as well as the implementation on a DSP board, of the various used digital pulse processing techniques in order to provide the main functions required in a generic "Gamma" digital spectroscopic set-up. The first part will be devoted to the design of the digital IIR filter used to compensate the charge preamplifier's slow pole. It will be followed by a practical estimation of the power spectral density characterizing the electrical noise components present in the experiment under consideration. Thereafter, a very detailed attention will be given to the design of the digital optimal filter to be used for the charge measurements. After, we present also another FIR filter. This one deals with the digital estimation of the measurement's reference line in a manner to achieve the role of the classical Base Line Restorer. Finally, we will present the hardware implementation of the whole designed filters using the board: "*TMS320C6713-DSK*", which is a DSP kit developed by "*DIGITAL Spectrum*".

1. INTRODUCTION

In the context of the gamma ray spectroscopy, poor resolution creates a widening of the spectral lines that lead to large inaccuracies in experimental results. One of the principal causes of poor resolution is the electronic noise introduced by the instrumentation used and this especially so when the gamma ray signal is relatively small [1]. The sources of electronic noise include DC baseline fluctuations, pulse pileup effects, electromagnetic and power supply disturbances, as well as thermal and electromagnetic instabilities and disturbances of the power supply [2]. Historically, trying to eliminate or even to satisfactorily compensate all these sources of noise simultaneously using analogue instrumentation has proved very difficult, if not impossible, due to the various interrelations of the noise sources and the complexity of the compensation instrumentation required. Fortunately, this situation has changed during the past few years with the introduction of digital signal processing techniques (DSP) in gamma ray spectroscopy. We have helped develop and implement several proposed digital signal processing methods that have been published in literature, in particular for gamma and X ray spectroscopy [3–8].

Digital processing of the signal emanating from the nuclear radiation detector allows the synthesis of almost any shape of the "*weighting function*" associated with mathematical filters used to process and optimize electronic signals for high resolution spectrometry. Thus we can digitally generate filters close to those theoretically known as optimal ones [6], with an intrinsic adaptability to the various unwanted components of electrical noise in a given experiment. In a typical architecture of the digitized spectroscopic chain (Fig. 1), we generally sample the signal at the output of an analogue pre-filter (charge preamplifier + anti-aliasing filter) at a frequency adapted to the bandwidth of the experiment, which is generally in the range of 5 – 50 MHz. The samples are processed either with dedicated numerical electronics or via the execution of algorithms implemented onboard containing DSP and/or FPGA circuits.

This paper is organized as follows: In section 2, we describe in detail the design of the main digital filters and in section 3 we briefly describes the implementation of the designed digital filters on a DSP board.

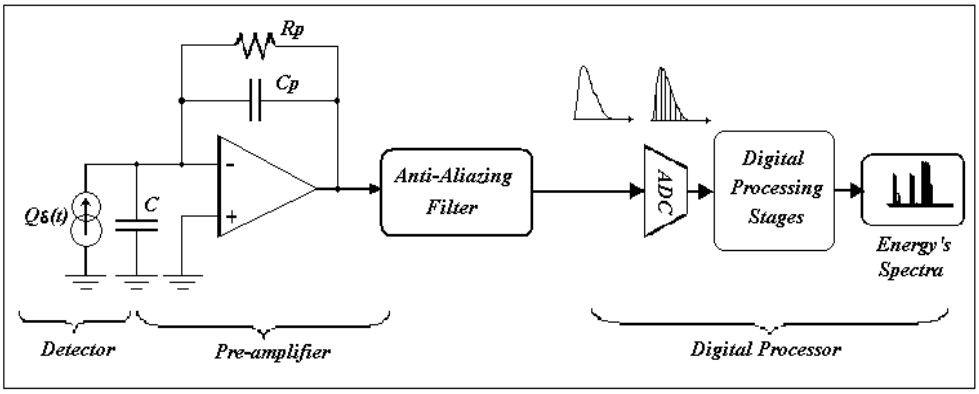

FIG. 1. Typical architecture of the digitized Gamma ray spectroscopic chain.

2. DESIGN OF THE MAIN DIGITAL FILTERS

In general, the main digital filters implemented in digital gamma ray spectroscopy are as shown in Fig. 2:

- The pole zero digital compensator,
- The baseline digital restorer, and
- The energy digital estimator.

For more options, other processing filters can be added but in our case, we were content with these essential ones.

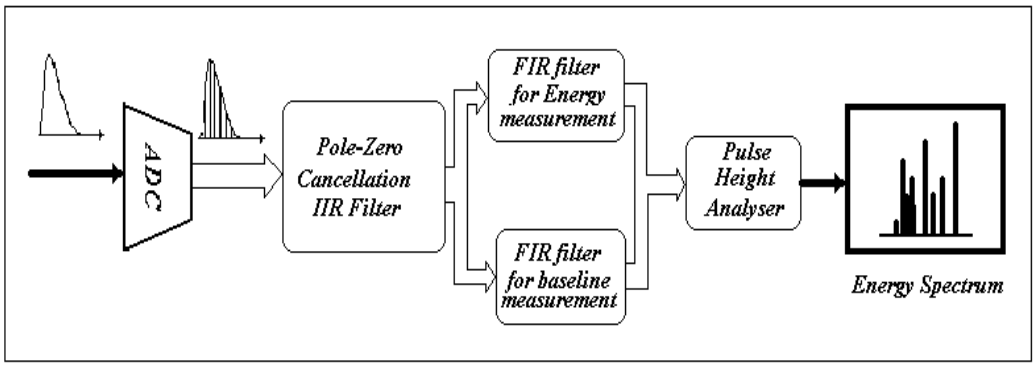

FIG. 2. Schematic representation of the three main digital filters used in gamma ray spectrometry.

The output signal from the ADC undergoes a pole-zero cancellation operation that is necessary to cancel the long exponential decay due to the charge preamplifier. This task is performed using an IIR filter that is self-calibrated so that no human intervention is required for tuning. Baseline instabilities and fluctuations due to the thermal drifts are compensated for in an optimal manner by means of a FIR filter. The pulse's energy determination is carried out in an optimal designed FIR filter that is managed in parallel with the baseline FIR filter. In the

following sections we describe in more detail the design of the three abovementioned digital filters.

2.1. The digital filter to be used for the "pole-zero/zero-pole" compensation

It is well known that in the majority of gamma ray spectroscopic set-ups, the slow time constant introduced by the preamplifier, must be eliminated before the shaping operation. Such a pre-treatment is necessary to avoid both the influence of the temporal persistence of the slow pole on the measurement of successive impulses (risk of the impulses pileup) and saturation of the shaping stage and/or the ADC in the case of a high event rates coming from the detector. To implement this pole-zero (P/Z) cancellation unit, we follow the methodology below.

The effects of the analogue P/Z cancellation is demonstrated by considering the transfer function of the residual couple pole/zero

$$G(s)=\frac{1+s\tau_z}{1+s\tau_p} \tag{1}$$

where τ_p is the time constant introduced by the preamplifier and which is the entity which we want to cancel, and τ_z is the time constant representing the zero introduced by the analogue compensation circuit. To perform the digital PZ/ZP compensation, we insert a digital filter immediately after the ADC circuit to correct the analogue error of compensation on the digitized signal (see Fig. 3).

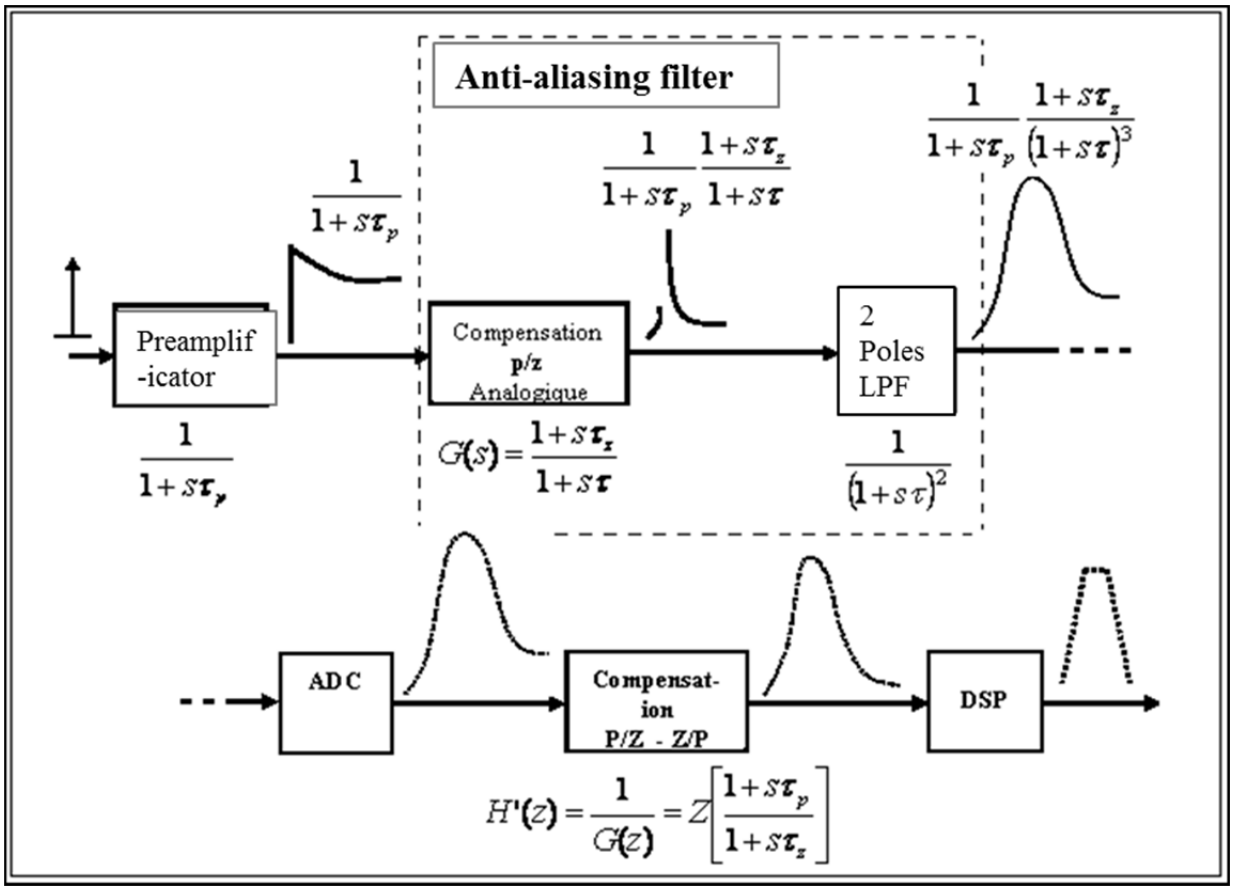

FIG. 3. Generic digital spectrometer with a partial analogue P/Z and a complete Z/P digital compensation.

To design this digital filter, we have followed the three steps [9]:

- Online estimation of the time constant value τ_P introduced by the preamplifier stage
- Online estimation of the time constant τ_Z corresponding to the zero introduced by the shaping stage
- Determination of the IIR digital filter taps, once the structure of the filter IIR, *H' (Z)*, is chosen

To pass from the continuous representation to the discrete form of the filter we have used the bilinear transformation in Eq. 2 [10].

$$s \rightarrow \frac{2}{T_s}\frac{1-z^{-1}}{1+z^{-1}} \tag{2}$$

which gives the equation of the digital filter to be used for the necessary P/Z compensation (Eq. 3).

$$H'(z)=\frac{1}{G(z)}=\frac{T_s+2\tau_p}{T_s+2\tau_z}\frac{1+z^{-1}\dfrac{T_s-2\tau_p}{T_s+2\tau_p}}{1+z^{-1}\dfrac{T_s-2\tau_z}{T_s+2\tau_z}} \tag{3}$$

Figures 4 and 5 depict the shapes of the digitized pulse before and after the "Pole-Zero/Zero-Pole" compensation.

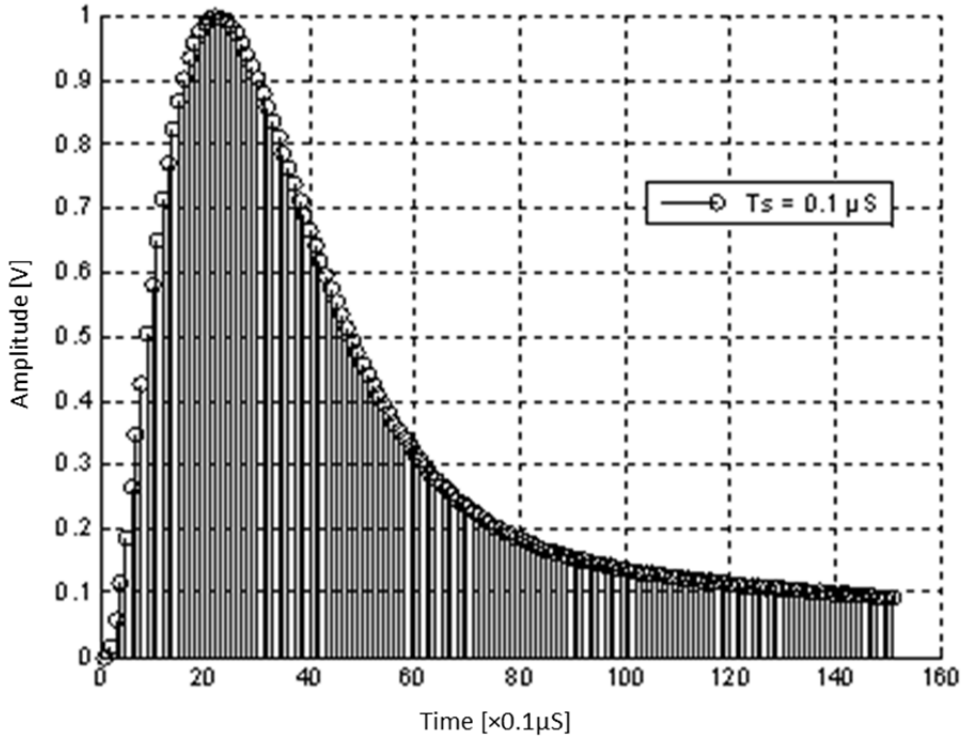

FIG. 4. Digitized nuclear pulse, before the P/Z compensation.

The comparison of the two figures confirms the effectiveness of the method undertaken to get the required filter.

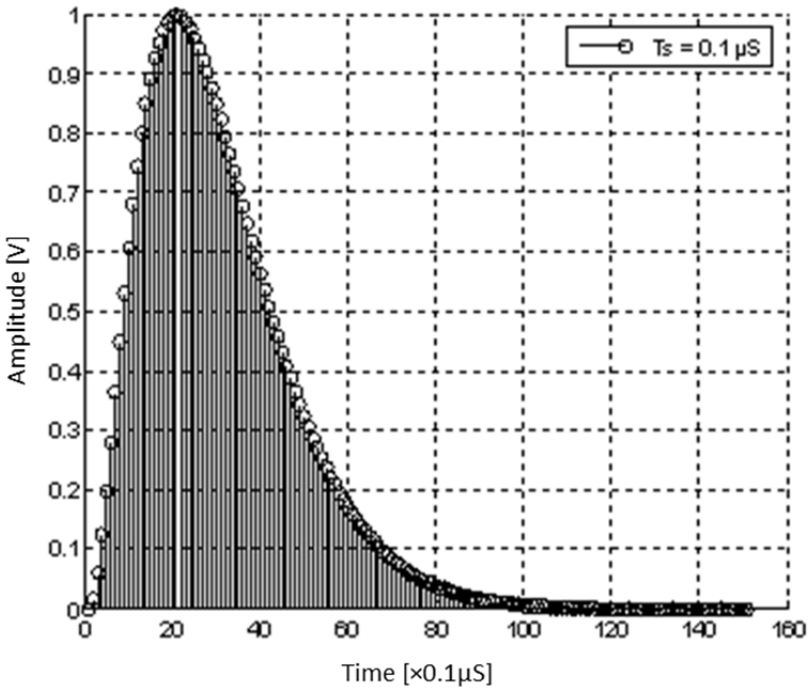

FIG. 5. Digitized nuclear pulse, after the P/Z compensation.

2.2. The optimal digital filter to be used for the pulse energy measurement

The calculation of the optimal filter weighting functions to be used for the measurement of the nuclear pulse energy and the baseline determination requires the characterization of the equipment's current noise components in the frontend electronics. Such a characterization is inevitably done by the calculation and/or the online measurement of the total power spectral density.

2.2.1. The noise power spectral density estimation

To determine the mathematical expression of the power spectral density characterizing the electronic noise at the input of the gamma ray spectrometer, we perform the following tasks:

- Acquisition on a PC of the temporal recordings of the signal at the output of the analogue preamplifier & anti-aliasing filter in the absence of any radioactive source. Acquisitions were made via a digital oscilloscope connected to the PC via a RS-232D link. Several sampling rates were tested before the final choice. Figure 6 illustrates a sample of these temporal records.

- Using these measurements, we calculate an estimate of the power spectral density through the averaged periodogram method (direct method) [10] using MATLAB-R14 software.

The result of one of the calculations using this procedure is shown in Fig. 7.

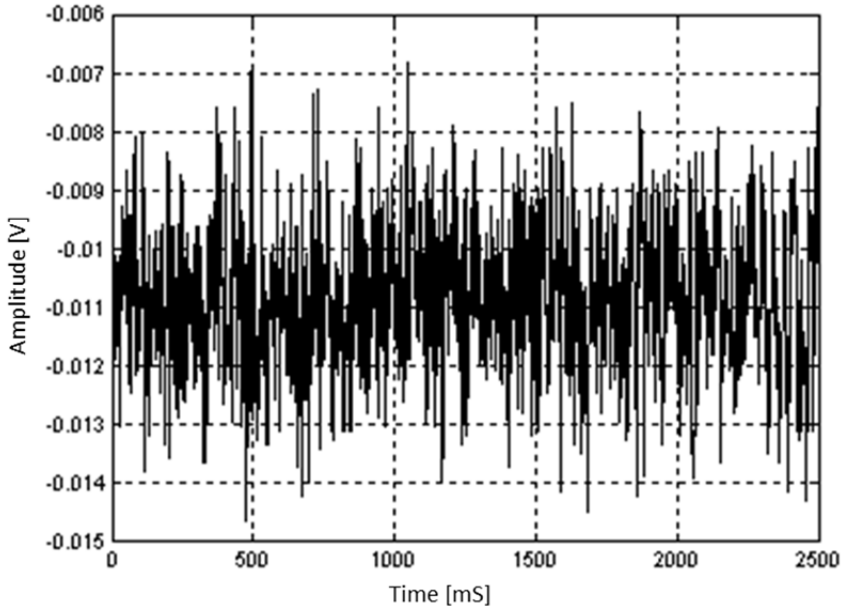

FIG. 6. Sample of the temporal noise recording at the output of the analogue stage.

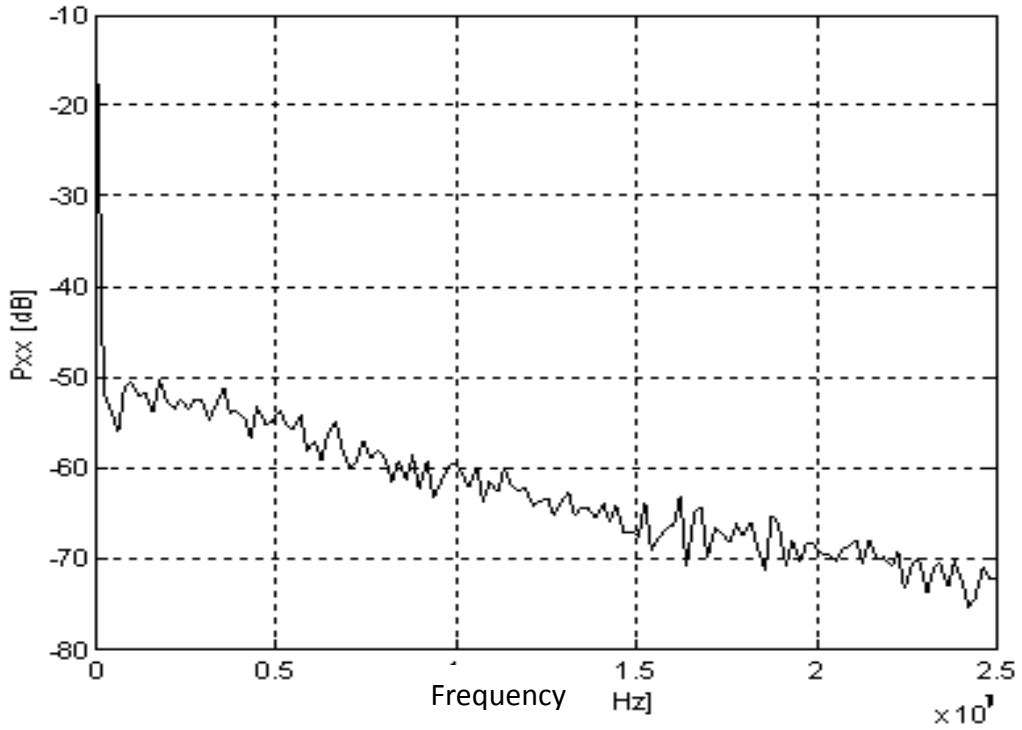

FIG. 7. Experimental noise spectral density.

The power spectral density estimation thus obtained, is brought back to the input of the spectrometer by dividing its output values, point by point, by the squared transfer function characterizing the analogue part of the spectrometer. The mathematical expression of the power spectral density thus obtained is then expressed in negative and positive terms of power of the frequency (Laurent series). To arrive to this result, we have used the weighted least squares method. An example of expressions obtained (in the forms of Laurent series) is given by Eq. (4)

$$N(\omega) = 6.1 \times 10^{-29} f^0 + 4.7 \times 10^{-39} f^2 \, [A^2/Hz]. \quad (4)$$

where N(ω) is the electronic noise at the input of the spectrometer.

2.3. The energy optimal filter design

This design inevitably passes by the minimization of the noise/signal ratio, which is equivalent to the maximization of the signal/noise ratio. In our case, this ratio is calculated using the electric equivalent circuit of a generic gamma ray spectroscopic measuring instrument shown in Fig. 8 [11].

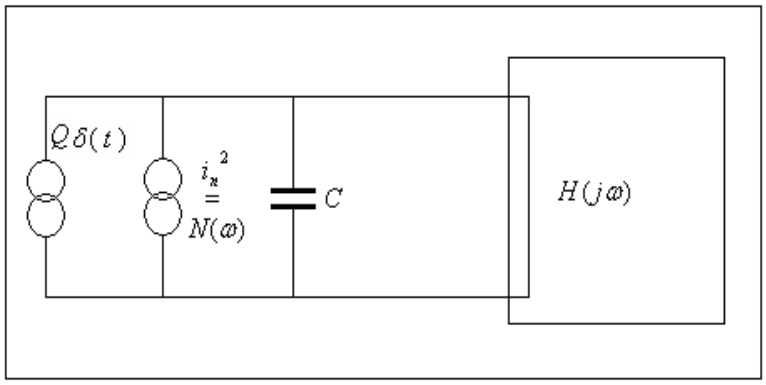

FIG. 8. Reduction of all noise sources to only one equivalent source (current generator) of a power spectral density represented by N(ω).

According to this simplified schematic, the expression of the noise to signal ratio at the output of the studied set-up is given by Eq. (5) [1]

$$\frac{\overline{n}^2}{s^2} = \frac{b\int_{-\infty}^{+\infty} N(\varphi)W(\varphi)W^*(\varphi)d\varphi}{f_c Q^2} \quad (5)$$

where $\varphi = f / f_c$, f_c is the noise corner frequency, b the parallel component of the white noise, $N(\varphi)$ the noise power spectral density at the input of the filter to be designed, $W(\varphi)$ the transfer function of the considered filter, and Q the electrical charge generated in the detector.

To get the parameters of the optimal filter, we have to minimize Eq. (5) with respect to the weighting function $W(\varphi)$ which has constraints (limited duration, flat topped shape, and/or null total surface). To solve such a problem, one can use many mathematical methods available in the field of functional analysis. We have used the variation methods [11] that yield the final expression of the weighting function of the optimal and constrained filter as given in Eq. (6).

$$W_{opt}(\varphi) = \frac{1}{N(\varphi)}(C_0 + C_1 e^{-i\varphi\tau_1} + C_2 e^{-i\varphi\tau_2} + \ldots) \quad (6)$$

Using the theoretical concepts described above, we use MATLAB-R14 to calculate the optimal weighting function $W_{opt}(\varphi)$ (with or without temporal constraints) of the filter necessary for the optimum measurement of energy released by an ionizing radiation in the detector. The inputs to the procedure are the shape of the useful signal and the power spectral density of the actual noise present at the input of the spectrometer under study. Examples of

the shapes obtained after the executions of the weighting function calculation program are illustrated in Figs 9 and 10.

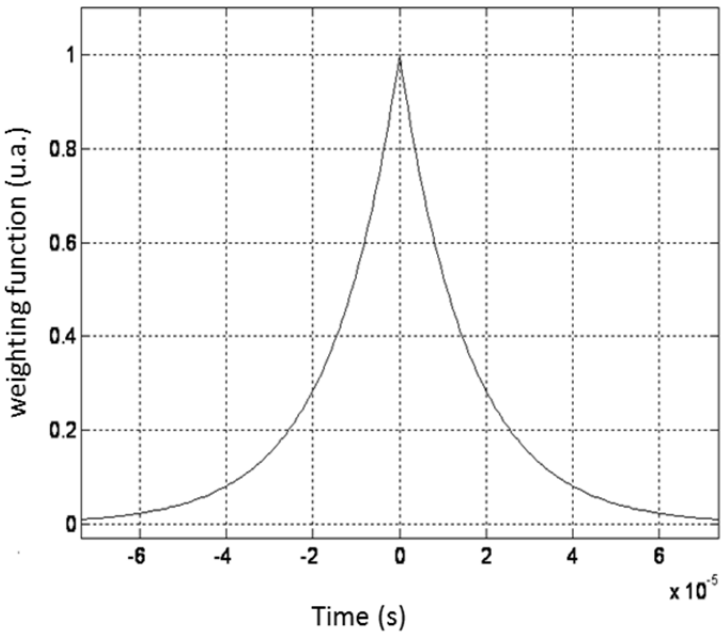

FIG. 9. Optimal weighting function characterizing the optimal filter to be used for the energy measurement (no applied constraints).

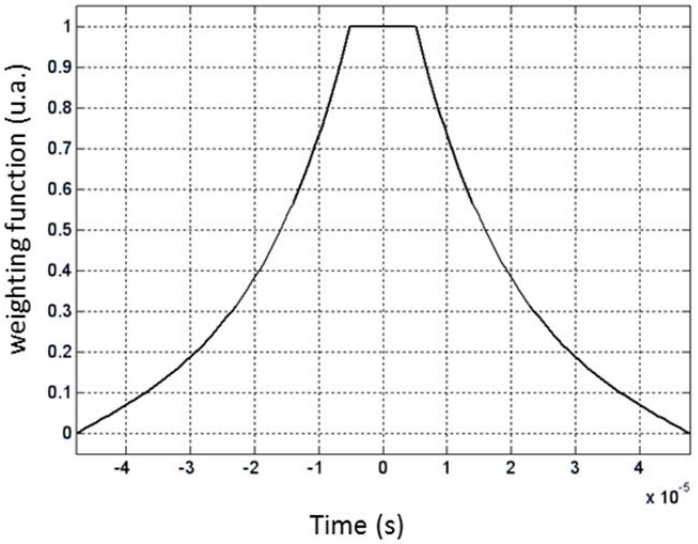

FIG. 10. Optimal weighting function characterizing the optimal filter to be used for the energy measurement (constraints: flat-top, time limitation).

2.4. The optimal digital filter to be used for the baseline estimation

In analogue gamma ray spectroscopic set-ups, signals seen at the output of the amplification and shaping modules are in general, overlapped on a shifted voltage of the baseline. In practical situations, this shift is usually not stable as it depends on the leakage current of the

detector (coupled DC systems with radiation rates inducing pileup phenomenon, or AC coupled systems with a weak P/Z compensation) [9] and thermal drifts of the electronic components. In order to reduce the widening of spectral lines, the amplitude of the base line is determined, and then subtracted from the heights of the measured impulses using a Base Line Restorer circuit.

2.4.1. The baseline estimation optimal filter design

In the context of a shifted base line, a gamma ray spectrometer is schematized electrically by Fig. 11 [12]. We have used this schematic during all our optimal base line filter designs. The followed methodology yields a digital filter that gives an optimized estimation of the base line level seen at the spectrometer's output.

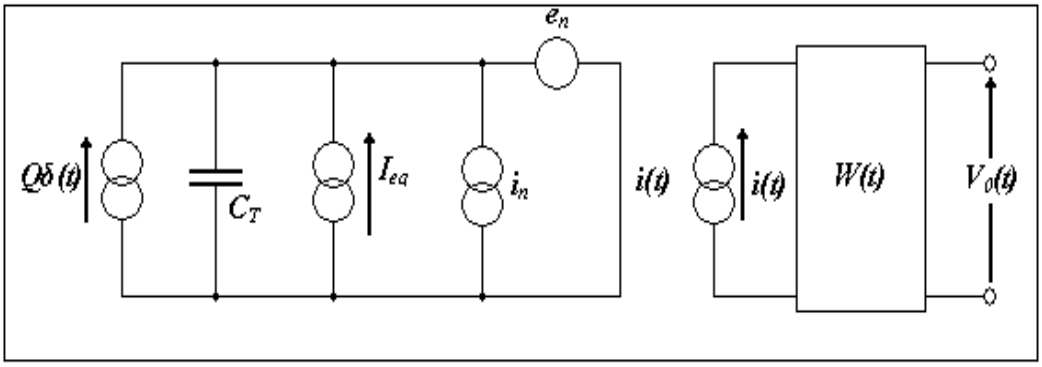

FIG. 11. Basic electrical schematic of a gamma ray spectrometer in the context of a shifted baseline.

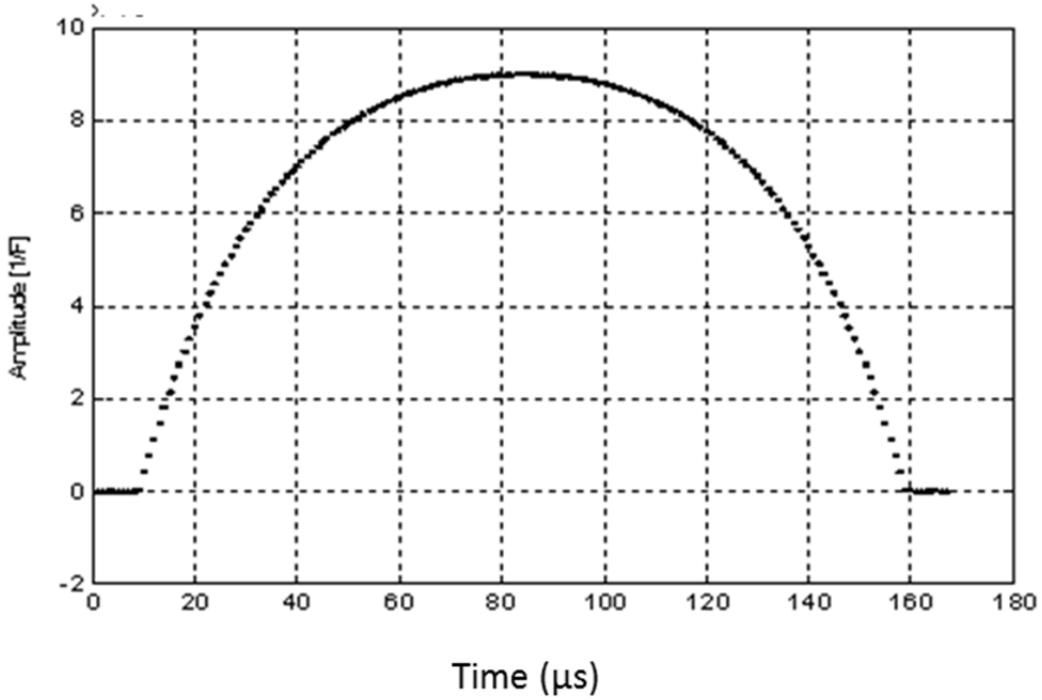

FIG. 12. Weighting function characterizing the optimal filter to be used for the evaluation of the shifted base line.

Using this electrical schematic and by using variational methods to maximize the signal to noise ratio at the output of the sought filter, we derive the weighting function characterizing the minimum noise filter $W_{MN}(t)$ given by the expressions in Eq. (7).

$$\begin{cases} W_{MN}(t)=\dfrac{1/2}{T_f-T_c\tan\alpha}\left(1-\dfrac{\cosh(\alpha t/T_f)}{\cosh\alpha}\right)\cdot\bar{A} & pour\ \ -T_f\le t\le T_f \\ W_{MN}(t)=0 & pour\ \ t\le -T_f\ \ et\ \ t\ge T_f \end{cases} \qquad (7)$$

An example of a weighting function characterizing the optimal filter used for the evaluation of the shifted base line is shown in Fig. 12.

This filter's parameters, which are obtained using Eq. (7), were used to process a DC noised signal (see Fig. 13) representing a shifted baseline. The result, using a theoretically introduced shift of +2, yielded + 1.9965 which is in excellent agreement.

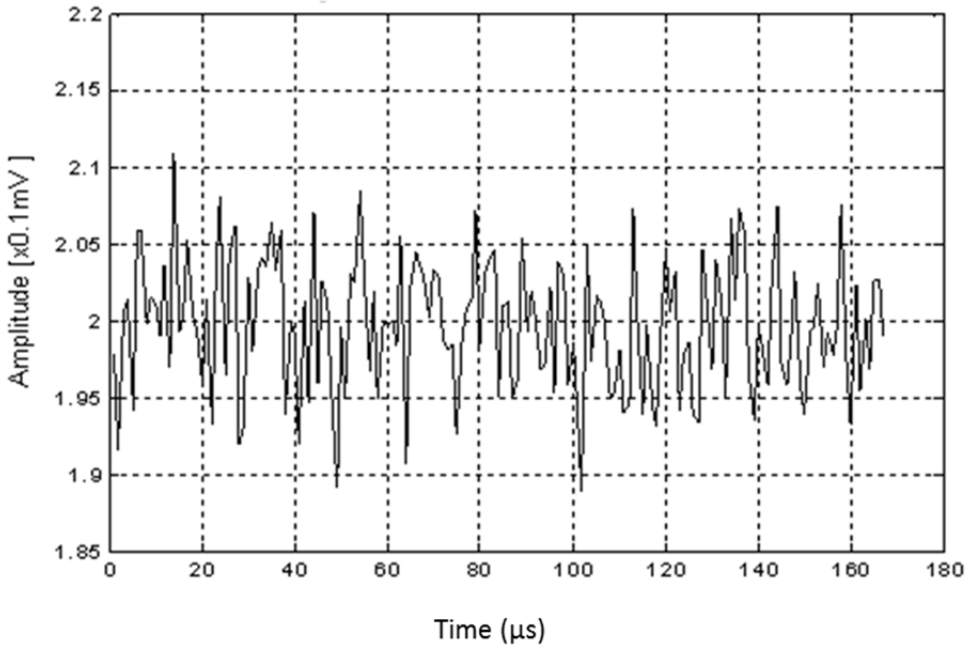

FIG. 13. Noisy baseline shifted towards the positive side.

3. HARDWARE IMPLEMENTATION OF THE DESIGNED DIGITAL FILTERS

DSPs are processors dedicated to the digital signal processing; digital filtering is a particular case of the processing task. The designs of the digital filters to be implemented on DSP chip pose the following problems:

Approximation: Which consists of generating a transfer function that satisfies the specific conditions in the frequency and/or temporal domain. This was described above.
Realization: several types of structures are possible to fulfil a given transfer function (direct form, cascades, parallel, etc.) and which is briefly shown in this section.

The whole filters designed within the framework of this work were implemented and tested separately on a DSP Board (see Table 1) referenced as "*TMS320C1367 DSK*" and made by Digital Spectrum.

TABLE 1. THE IMPLEMENTED DIGITAL FILTERS

DIGITAL FILTER	FUNCTION
Direct form (First order) *IIR* filter	Digital P/Z compensation filter
Direct form (56 coeff.: $a_0 \sim a_{55}$) *FIR* filter	Nuclear pulse energy measurement digital filter
Direct form (167 coeff.:$a_0 \sim a_{166}$) *FIR* filter	Digital baseline restorer filter

The hardware schematic of the DSP board is shown in Fig. 14.

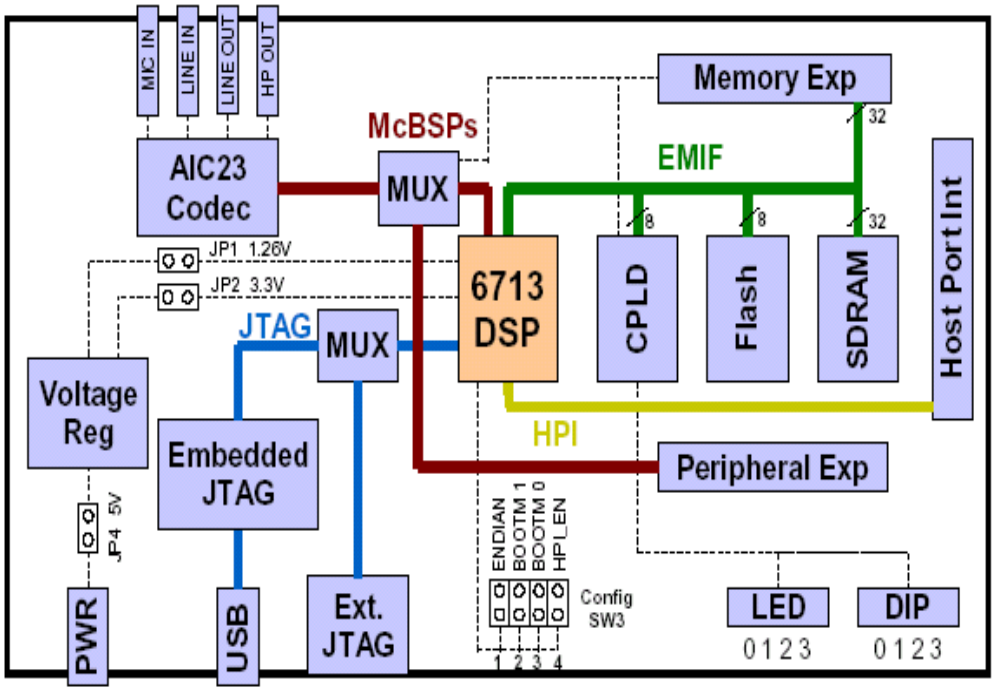

FIG. 14. The block diagram of the DSP used for the designed digital filters implementation.

4. CONCLUSIONS

The task to find the best digital filters, to measure the charge created in the ionizing radiations detector under variable experimental noise components, was described this paper. The filters obtained in the design stage could not be efficiently implemented without contributions of the digital signal processing techniques and tools (soft and hard). These have facilitated the implementation of the designed filters in spite of their specific characteristics (such the insertion of a flat top in the total temporal response of the measuring set-up) and whose realization was impossible using analogue processing tools.

REFERENCES

[1] GATTI, E., MANFREDI, P., Processing the signals from the solid state detectors in elementary particle physics, La Rivista del Nuovo Cimento 9 (1986).

[2] NICHOLSON, P.W., Nucl. Electr., J. Wiley, New York (1974) 315–316.

[3] GEORGIEV, A., et al, An analog to digital conversion based on a moving window deconvolution, IEEE Trans. Nucl. Sci. 41-4 (1994) 1116–1124.

[4] JORDANOV, V.T., KNOLL, G.F., Digital pulse shape analyzer based on fast sampling of an integrated charge pulse, IEEE Trans. Nucl. Sci. 42-4 (1995) 683–687.

[5] RIPAMONTI, G., et al, Digital vs. analog spectroscopy: a comparative analysis, IEEE trans. Nucl. Sci. 42-4 (1998).

[6] GATTI, E., et al, Digital penalized lms method for filter synthesis with arbitrary constraints and noise, Nucl. Instr. Meth. A523 (2004) 167–185.

[7] GAST, W., et al, Digital Signal Processing and Algorithms for Gamma Ray Tracking, IEEE Trans. Nucl. Sci. 48-6 (2001).

[8] ENGELS, R., et al, A Flexible Data Acquisition Board for Nuclear Detectors, IEEE Trans. Nucl. Sci. 49-1 (2002).

[9] GERACI, A., PULLIA, A., RIPAMONTI, G., Automatic Pole-Zero/Zero-Pole Digital compensator for High Resolution Spectroscopy: Design and Experiment, IEEE Trans. Nucl. Sci. 46-4 (1999).

[10] OPPENHEIM, A.V., SCHAFER, R.W., Digital Signal Processing, Prentice Hall (1998).

[11] PULLIA, A., How to derive the optimum filter in presence of arbitrary noises, time domain constraints, and shaped input signals: a new method, Nucl. Instr. Meth. A397 (1997) 414–425.

[12] PULLIA, A., et al, Minimum noise filter for base line estimation irradiation detection systems, Nucl. Instr. Meth. A403 (1998) 455–464.

QUALITY ASSURANCE VIA DIGITAL SIGNAL PROCESSING

T. PAPP, J.A. MAXWELL,
Cambridge Scientific,
Guelph, Canada
Email: tibpapp@cambridgescientific.net

J. GÁL, B. KIRÁLY, J. MOLNÁR, J. TÓTH
Institute of Nuclear Research of the Hungarian Academy of Sciences,
Debrecen, Hungary

Abstract

We have developed a fully digital signal processor for the aim to collect true spectra and supply all the information what is necessary for physics based measurements. In practice all previous signal processors or data collection system used several discriminators to reject unwanted events. However it is necessary to know the reason for the rejection. The signal processors have not supplied the necessary information about the spectra, and therefore the true spectra could not be reconstructed. We have developed a signal processor to supply the necessary information. It has been successful in X ray analysis, and we have made a pilot study in gamma ray spectroscopy as well. We present some observations here. The difference is our signal processing approach, that it analyses all the events and sort them to several spectra, based on whether they have passed or failed the discrimination criteria. It offers quality assurance capability. It also very useful in training and education, as the reason of rejection can be seen visually, whether it was a noisy event, a pile up of two true events, a pile up with a noise, an imperfect signal or a Compton scattered event into the detector. The presented examples demonstrate how differently the measurements need to be designed.

1. INTRODUCTION

While dealing with X ray spectroscopy and X ray based analytical techniques, we were baffled by the very serious shortcomings of the X ray database [1–5] and the very tedious calibration techniques that were necessary for consistent measurements. Since the beginning of the use of solid state detectors it was indicated that the detector electronics, which are used to process the raw signal from the detector in order to produce the spectrum, produce spectral distribution dependent spectra. While trying to make reliable measurements, we have dealt with more than twelve Si(Li) detectors and electronics from different manufacturers. The results were not consistent or satisfactory and this led us to studying the detector response function [6–8]. It was obvious that there is a large variation in the shape of the response function from one detector system to another and that the settings of the electronics will impact on the observed response function. Based on the extensive study of the electron transport processes in the detector materials we were able to derive the expected response function from the experimental response function [7].

It is customary in the detector response function models to incorporate various layers such as incomplete charge collection, dead layers, and with Monte Carlo simulations usually a good agreement could be achieved with the spectra created by the detector and signal processor. However, the effect that the signal processor has on the response is always ignored in these studies. All signal processors have some discriminating criteria to improve the spectral quality. Therefore, it is hard to know the impact of the discriminators, or in other terms, thresholds, on the observed spectrum. There are several reasons why an event might not pass a given discriminator test but the individual reason was not known or recorded.

It became obvious that one of the reasons for the unreliability of the data were rooted in the signal processing electronics. To overcome this difficulty, we have developed a signal processor that differs from every previous one in concept and functionality. This signal processor not only provides the best resolution and line shape, it allows one to make absolute (not just relative) measurements and to determine the true input rate. This is achieved by

processing all events and then sorting them to several spectra based on whether they passed or failed the discriminator tests.

We have applied these techniques to gamma ray measurements with HPGe detectors and present some results here. The observations will cover ghost peaks, reduced Compton plateaus, improperly developed events, and the determination of the input rate. It also allows the quantification of the electronic efficiency. Seeing all events is very useful in education and training. It is also useful in identifying the origin of the size and Compton plateau and is mandatory if one wants to model the background, as the background shape depends on the signal processing electronics. Good signal processors can greatly reduce the background.

2. ENERGY TRANSFER IN DETECTOR MATERIALS

We have observed that in Si, Ge, CdTe, CZT, GaAs, InSb semiconductor detectors and in CsI, BaF2, GOS, LYSO, LSO scintillators, the dominating energy transfer channel is a collective excitation which has a uniform energy, thus producing detectors with reasonably good resolution efficiency. With doping, the breadth of the energy channel can be narrowed presumably yielding better resolution. This is a very promising direction.

In Ge detectors, the dominating energy channel is the plasmon creation by energetic electrons. From the decay of the collective excitation, the number of the created electron hole pairs as a function of X ray or gamma ray energy can be derived. The situation is simple for Si or Ge detector materials. In Fig. 1, the electron energy loss spectrum of Ge is presented. The energetic electrons lose energy via plasmon creation.

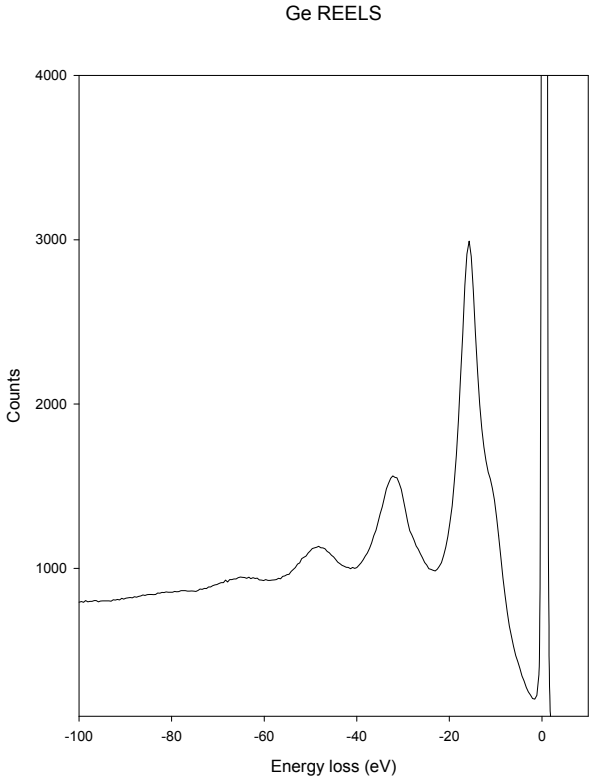

FIG.1. REELS spectrum of Ge.

In other detector materials, several competing collective excitation modes are present, and the calculation of the number of electron hole pairs can be very cumbersome. A good example is the CdTe detector material. In Fig. 2 it is shown that in addition to the plasmons, there are two peaks corresponding to collective excitations. Their decay mode and electron hole pair creation is different from that of the plasmons.

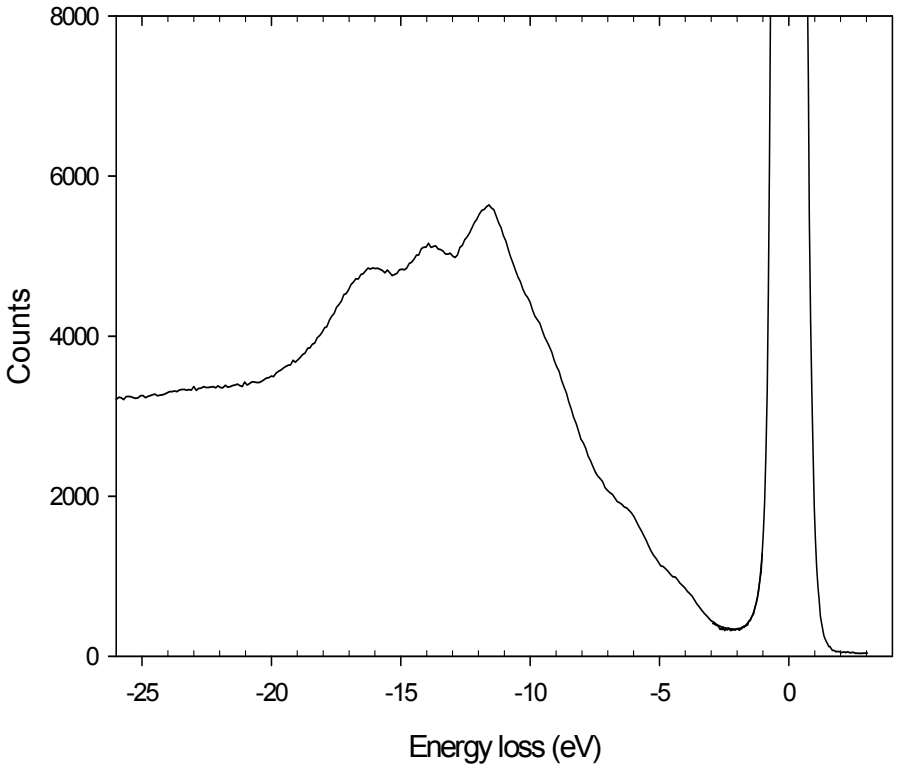

FIG. 2. REELS spectrum of CdTe detector material.

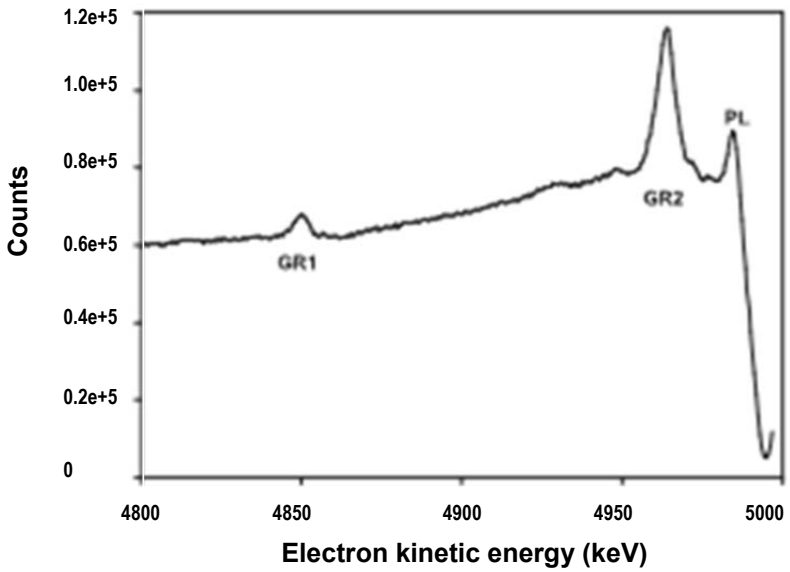

FIG. 3. The electron energy loss spectrum of a GSO scintillator crystal.

Especially abundant is the type of collective excitations in scintillator materials. For scintillators, the typical collective excitations are giant resonances. The significance of collective excitations, and their role in the energy transport processes can be studied by high energy REELS (Reflection Electron Energy Loss Spectroscopy). It is ideally suited to determine the band gap, the level energies and the energy and magnitude of the intrinsic trapping sites. The observed collective excitations already indicate the need to rethink the details of the energy transport processes. A REELS spectrum of a GSO sample measured at high energy resolution is displayed in Fig. 3. Giant resonance peaks, GR1 and GR2, at 149 and 35 eV respectively are indicated in the spectrum.

The presented examples above show the variety of the elementary processes and the energy linearity and consequently, the resolution function can be complicated. For different detectors one would expect different functional forms. Some of the collective excitations can act as charge traps and therefore, the signal processor approaches should be flexible enough to handle charge collections on the different time scales.

3. SPECTRUM SHAPE AND GHOST PEAKS

The signal processing generates the spectra. In X ray detection it is frequent to find ghost peaks in the spectra, an example is presented in [9] with a very excellent Ge detector and signal processor. In gamma ray spectroscopy with Ge detectors one would assume to find similar difficulties, as the detector is much larger, the penetration of the gamma radiation is much further and partial energy deposition has a much higher possibility. While X rays can be collimated to the good part or central region of the detector, such a possibility is not forthcoming for high energy gamma radiations. In X ray spectroscopy, the spectrum quality and trueness can be judged from the resolution, and the presence of the spectral artifacts caused by the finite size of the detector [7]. Such a quality check is not available for a general gamma ray spectrum.

To overcome the contradictions in the X ray field, we have developed a quality assurance capable signal processing approach. It has improved the possibility and already offered solutions for various contradictions, ranging from problems such as the 17 keV neutrino puzzle or the background treatment in the dark matter search. We have been asked by a metrology institute to make some measurements on their big volume gamma detector that has been recently commissioned. This pilot study challenged us and we ended up making two set of measurements, one in the metrology institute and another in a nuclear research centre. The results were sufficiently surprising to warrant a dissemination of the information. In both cases we have made two set of measurements, one with their standard system, and one with our CSX4 digital signal processor. In the metrology institute the preamplifier was a pulse shape type, having a staircase like preamplifier signal. In the nuclear research centre, their regular system is a good quality HPGe detector, and an analogue amplifier with a built in pole-zero compensator and pile up rejector. The preamplifier has a continuous feedback preamplifier with a decay time constant of 100 μs. A circuit was built to transform the preamplifier signal to staircase like signal, which is favourable for digital signal processing. Our CSX system is a digital signal processor, which will be discussed below.

4. QUALITY ASSURANCE CAPABLE SIGNAL PROCESSING

The description of the signal processing approach and its applications were described in [5]. They have various pulse shaping options, including cusp shaping, which could give superior resolution. All parameters are set via the user interface program, and no parameter is set via

any hardware potentiometer or switch. It counts the input rate, the preamplifier reset rate, it allows proper handling of the so-called bucket effect, and has a user friendly set-up. All the measurements can be made in set-up mode where in addition to the two spectra of accepted and rejected events; the spectra of events rejected by each individual discriminator alone are presented to the analyst. Because the detector is aging and can change its performance with time, and because the electronic noise and disturbances are different at the analyst's site than in the factory, the optimum manufacturer's set-up is not necessarily valid in the analyst's laboratory. If it is noisier, then more events will be rejected than is optimum, and in any case the analyst should establish the electronic efficiency. If the rejection criteria are set to be very weak, then the line shape, pileup and resolution will not be optimum. The CSX4 signal processor also generates additional spectra for the events rejected by the specific discriminators. In the additional spectra, the analyst immediately sees the effect of each discriminator on the measurement, and can choose an optimum value for the discriminator via the user interface program. The cusp shaping is expected to give the best resolution therefore we have used that in these measurements.

The CSX series of digital signal processors from Cambridge Scientific, Canada [2, 8] work by digitizing the staircase signal from a reset type preamplifier, use various digital discriminators to produce two spectra, one of the normal accepted events and the other of all the rejected events. Adjusting the various discrimination levels, and observing the effects on both the accepted event and rejected event spectra, one can readily see that the electronics is not just a simple "black box device" for reproducing the event energy signal from the detector but instead, has its own effect on the line shape and content of the accepted event spectrum and therefore the analysis. As mentioned above, the CSX digital signal processor acts by digitizing a staircase like preamplifier signal. This digitized stream is processed by algorithms implemented on a digital signal processor chip to produce one or more spectra (usually two) of events that are downloaded to a computer for storage and analysis. Many of the details of the CSX processors, including quality of spectra, throughput rates, pileup, ease of set-up, etc. can be found in [10] and have been discussed in other literature [2–8,10–12].

Different models (CSX2, CSX3, CSX4, Noise Analyzer, etc.) and modes of operation (batch mode, interactive mode (single accepted spectrum only), interactive with quality assurance mode (2 spectra — accepted events & rejected events) and interactive full report or set-up mode with up to 6 spectra) allow the user various levels of functionality. The CSX2 uses 2 digital discriminators based on rise time and fast pileup rejection; the CSX3 uses three digital discriminators based on noise (proportional to the standard deviation), shape (proportional to the index of similarity) and rise time discrimination; and the CSX4 uses four digital discriminators based on noise, shape, rise time and fast pileup recognition. The most frequently used mode, interactive with quality assurance, simply produces two spectra for each measurement, a spectrum of accepted events for deconvolution and determination of peak areas and a spectrum of rejected events to act as a quality control for the given measurement as well as providing necessary information on the number and nature of the lost events that is needed for determining the true event input rate and thus correcting the deconvoluted peak areas for lost events [3, 11]. A second mode, interactive full report mode, often referred to as set-up mode as it is useful for setting the discrimination levels, produces up to six spectra of events, the accepted event spectrum, the total rejected event spectrum and the spectra of events rejected solely by each discriminator alone. A typical measurement with six spectra is presented in Fig. 4 for a ^{152}Eu radioactive source measured with an HPGe detector and CSX4 signal processor.

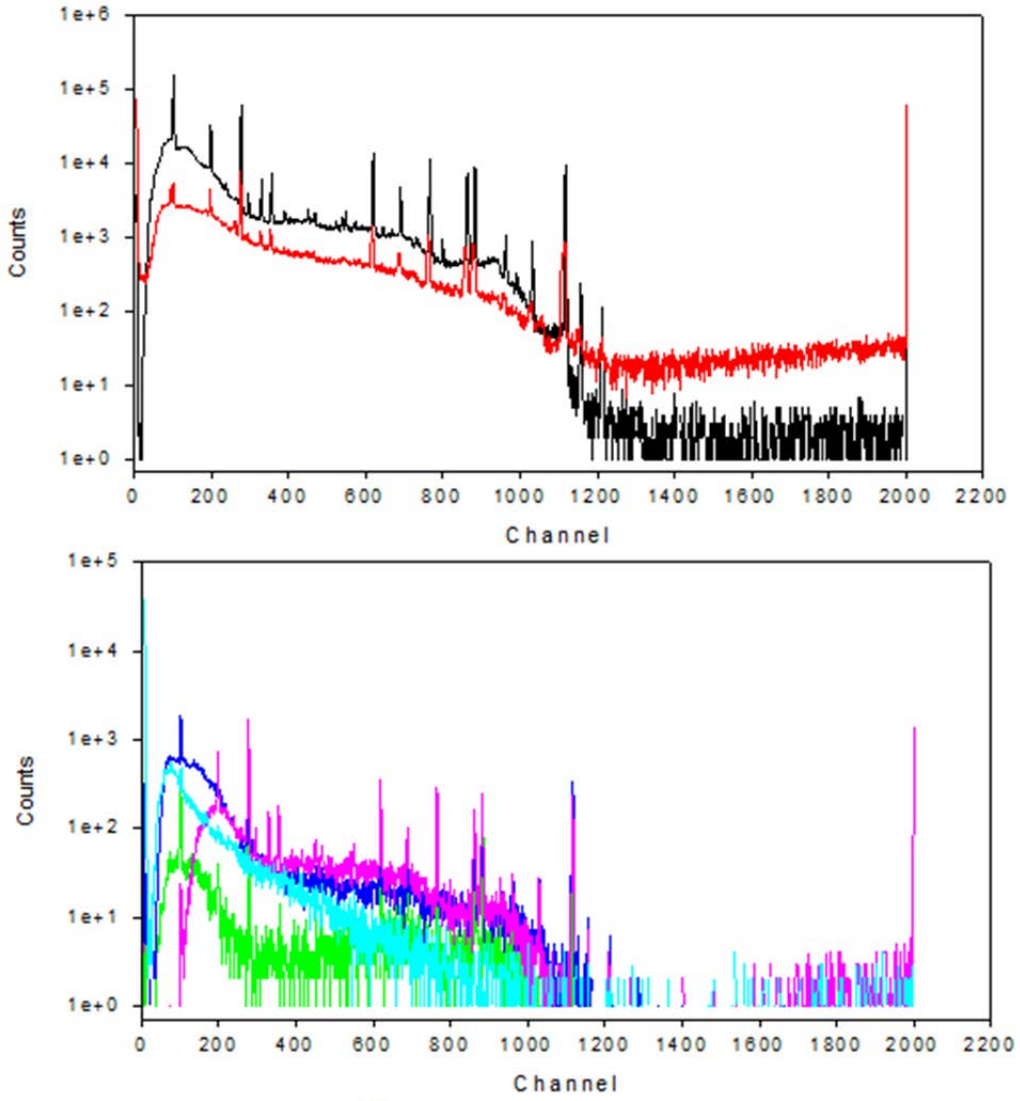

FIG. 4. The gamma spectrum of ^{152}Eu measured with a coaxial HPGe detector and a CSX4 digital signal processor. The CSX4 digital signal processor has four discriminator criteria, pulse shape, noise, fast pile up and rise time. The processor generates six spectra, the accepted, the rejected, and four additional spectra storing the events, rejected by each individual discriminator. The upper panel presents the accepted or desirable (black line) and the rejected or undesirable (red line) spectra. The lower panel presents the spectra of those events which were rejected by one discriminator only; shape discriminator (green), noise discriminator (blue), fast pileup (pink), rise time (cyan).

The signal processor inspects the signal coming from the preamplifier and decides whether it has the desired quality or should be rejected. The rejected signal is usually counted and indicated in the dead time, and pileup counter with other systems. However, the rejected events will include noise events, noise piled up with noise and real events, single event rejection peaks for those individual events that do not pass the event discrimination tests, multiple event pileups as well as non X ray or gamma ray (particle or high energy) events that generate a signal in the spectrum. Therefore, we have actually independent rates for the noise, the electronics disturbances, distorted events and real events. In order to determine the true event input rate we might have to determine up to four separate rates and the usual systems do not offer the necessary information.

We have developed a procedure to account for these different factors and determine the true event input rate. It is based on the signal processor capability to analyse all recognized events and place them in either the accepted event or rejected event spectrum. Such a spectrum pair is shown in the Fig. 5. It also explains many new features in the response function, and possible origins of the varying electronic efficiency of several other systems.

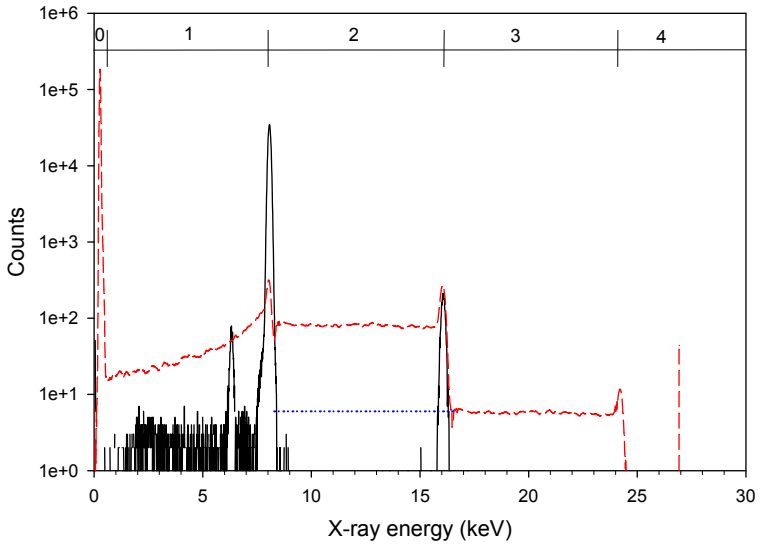

FIG. 5. The x ray spectrum of Cu $K_{\alpha 1}$ line from an X ray monochromator measured with a Si(Li) detector and a CSX4 digital signal processor (after [11]). The processor separates the events to desirable and non-desirable events. The rejected (non-desirable) events spectrum is presented with a dashed line. The settings of the parameters of the measurements were selected for the purpose of explanation, namely the signal recognition was set to a low level to allow the presence of the noise peak in the rejected spectrum. A full description is published online www.cambridgescientific.net.

5. NOISE ANALYSIS

Another model of the CSX signal processor series is the noise analyser, which can be used to show two measures of the signal noise and shape on an event by event level based on the noise and shape algorithms used by the CSX3 CSX4 models. It produces a spectrum of the average noise and shape parameter for each event in each channel, that is, the sum of the noise or shape measure for each event in a given channel divided by the number of events in that channel.

Noise in the system can also be dependent on the energy of the event. In Fig. 6 we show an ^{55}Fe measurement on a Si(Li) detector using the Cambridge Scientific noise analyser. It produces a spectrum of the event energies as before along with two additional spectra of the average noise measure and shape measure values associated with the events of each channel. For this particular detector system, the average amount of noise increases with energy while the average shape measure shows no energy dependence. If the noise discriminator is not set to allow for this variation then the fraction of events rejected at each channel will change resulting in an energy dependent electronic efficiency factor that is often reported in the literature.

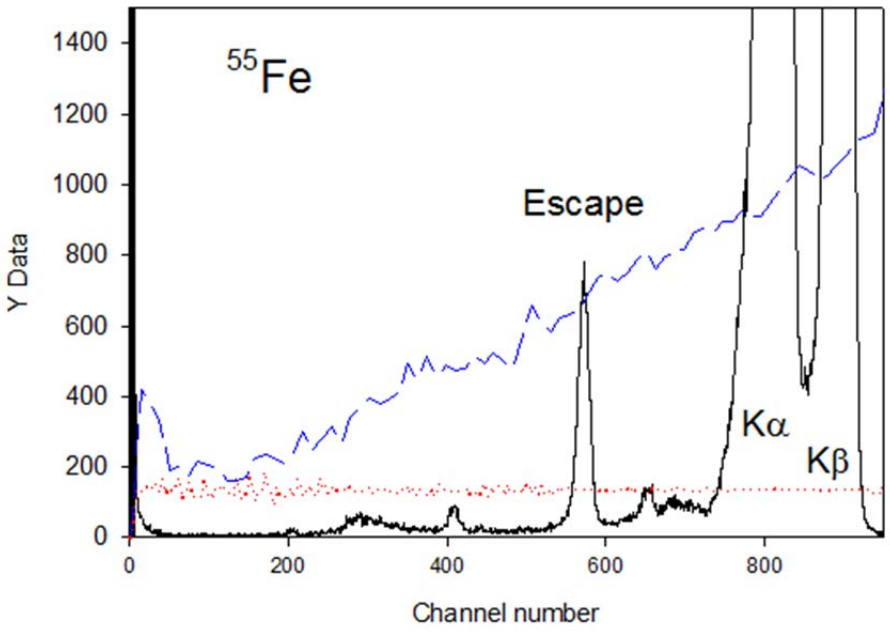

FIG. 6. An expanded scale ^{55}Fe spectrum taken with a Si(Li) detector and the Cambridge Scientific noise analyser. Superposed on the spectrum (solid line) we see two measures of signal noise and shape. These measures are the average noise (dashed line) and shape measures (dotted line) for the events in each channel smoothed here for display purposes. We see that the measure of noise is energy dependent suggesting that the noise discriminator needs to be set up with similar energy dependence to avoid uneven discrimination across the spectrum or an electronic efficiency factor. In this case, the shape discriminator can be set as a constant reflecting the fact that there appears to be no energy dependence of the shape measure.

In X ray spectra one often observes an unexplained elevated number of counts between the escape peak and the parent peak. A noise analysis in this region shows a similar increase in the average noise of events in this region as seen in Fig. 7. In many systems there appears a truncated shelf extending down from the peak to somewhere between 0.5 and 0.8 of the peak energy, which had been proposed earlier as originating from thermal electron out-diffusion [6, 12–18]. The present observation may provide additional insight in finding the origin of this undesired phenomenon. In this system we see the same effect but its events have a much higher average noise value that can be discriminated against so that the feature does not appear in the spectrum of accepted events. This suggests the possibility that with proper discrimination, this artifact could be removed from many systems, as we have demonstrated with our signal processors.

The noise analysis demonstrates that the noise measure is not a constant in the spectra as a function of energy but can have an unpredictable behaviour. Therefore, the number of rejected noise, or noisy events may change. This is an indication that knowledge of the nature of the rejected events is necessary.

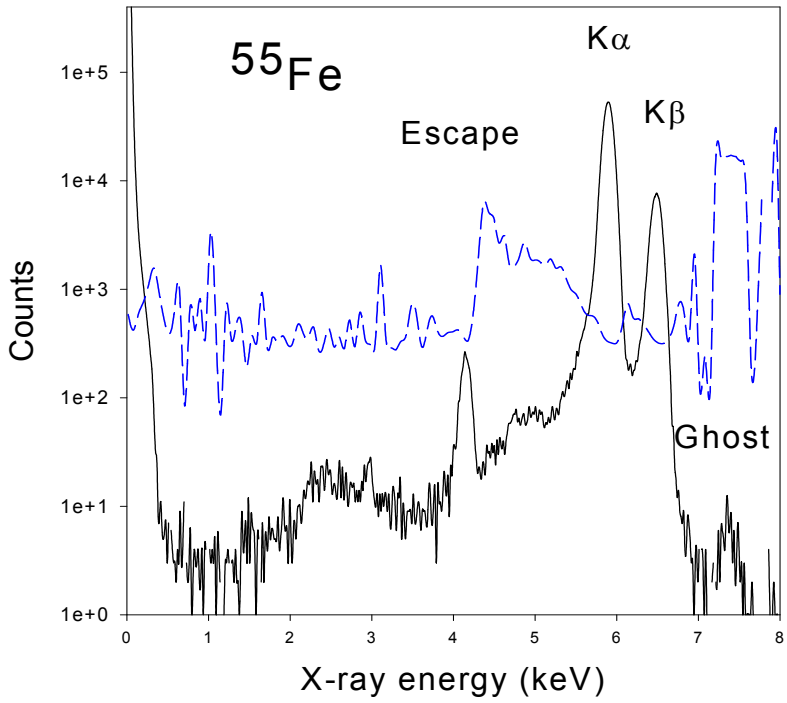

FIG. 7. An ^{55}Fe spectrum (solid line) acquired with a Si(Li) detector and the CSX noise analyser. The region between the escape peak and the parent peak is populated by events with higher than average noise measure, as seen in the noise spectrum (dashed line), which can be discriminated against to improve spectral quality. This is the region where a relatively high amplitude truncated shelf is often seen with many detector systems extending from the peak down in energy to somewhere between 0.5 and 0.8 of the peak energy. Although it is present in this system as well it can be discriminated against to remove this feature from the accepted event spectrum.

6. Si DETECTORS

For Si detectors we have obtained the expected line shape, which was interpreted with measured energy transport components. We were able to explain why other systems are not reaching the low level of tailing that we regularly obtain. The main feature is a sharp step at 1.8 keV for silicon, which is the photoelectron escape edge convoluted with the detector resolution. For Ge detectors such edges are expected at the energy of each absorption edge as well as the electrode's Auger lines [7].

7. Ge DETECTORS

We have made a measurement with our signal processor and a metrology level HPGe detector and associated digital signal processor electronics. The preamplifier was a pulsed shaped type preamplifier. The measurement was made in parallel by two processing systems by splitting the preamplifier signal, and feeding it to the two electronics simultaneously. The spectra obtained are presented in Fig. 8. The measurement was made using a ^{152}Eu source. The black line is our signal processor accepted spectrum, while the red is the rejected. The light green line represents the spectrum of the detector manufacturer signal processor.

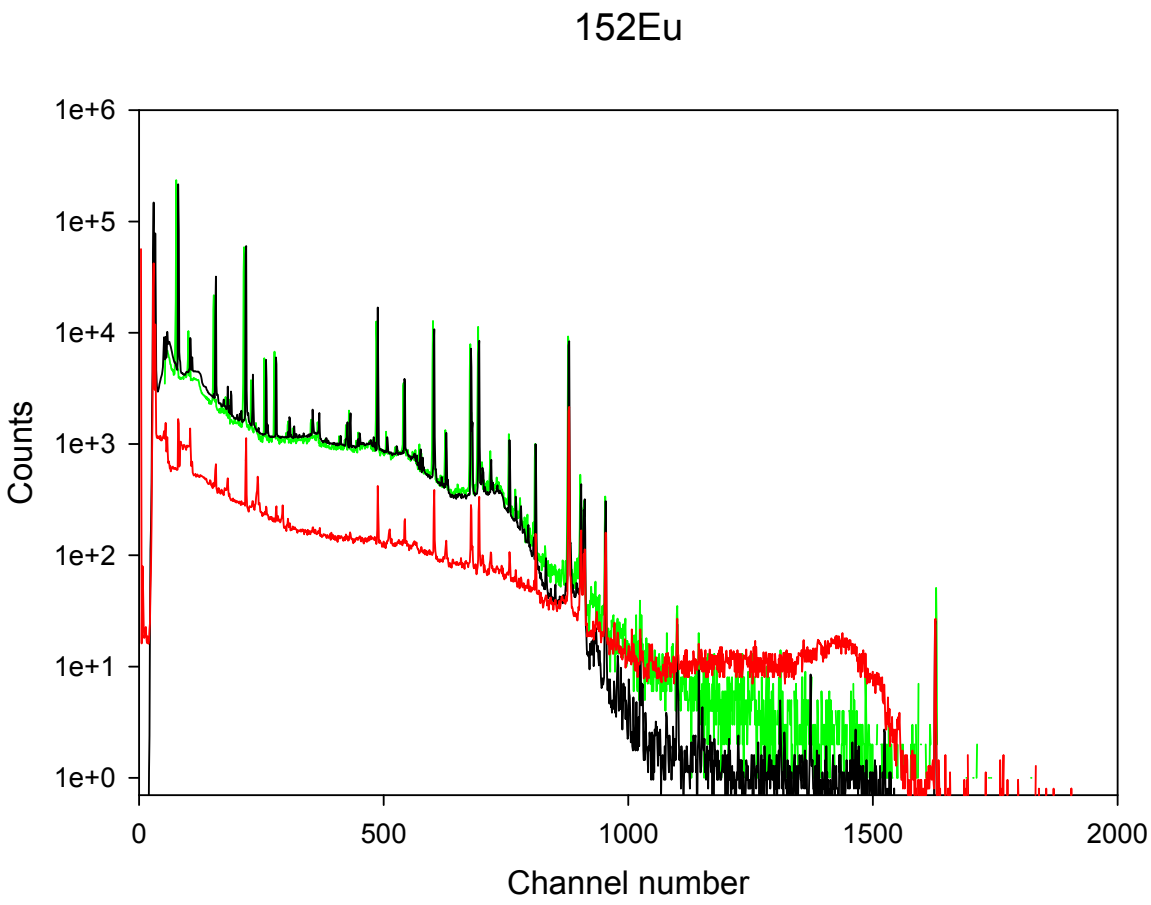

FIG. 8. The gamma ray spectrum measured with an HPGe detector and two digital signal processors simultaneously. The detector manufacturers signal processor generates only a single spectrum (green line). The CSX4 signal processor in quality assurance mode generates two spectra, one for the accepted (black line) and one for the rejected spectra (red line). The advantage of the CSX4 signal processor is obvious.

Having only the green line spectrum available one would wonder on the origin of the 1408 keV gamma line that is at channel 890 in Fig. 8. Having the rejected spectrum available, it is clearly identifiable as a Compton peak, probably from the lead shielding. Its removal will allow seeing lower intensity lines in the spectrum as it is clearly visible in the channel range 1000–1500.

In the second measurement site we had access to a coaxial detector with a linear amplifier and its associated commercial analogue electronics. We have made consecutive measurements feeding the preamplifier signal to the two systems. The first set of measurements was made using the ^{152}Eu source. The two spectra are presented in Fig. 9. The upper panel was made with the analogue nuclear electronics, and the lower panel with our digital processor. This lower panel figure is the same measurement as presented in Fig. 5.

Comparing the two spectra, the following observations can be made. The CSX4 signal processor counted about 15 times more events while still providing a little better resolution. The analogue spectrum has two extra peaks, both with proper line shapes that could therefore be identified as valid peaks (marked with arrows). Since the second measurement was made immediately after changing only the BNC cable connection from the analogue to the digital system, the origin of the extra peaks is almost certainly an artifact of the electronics.

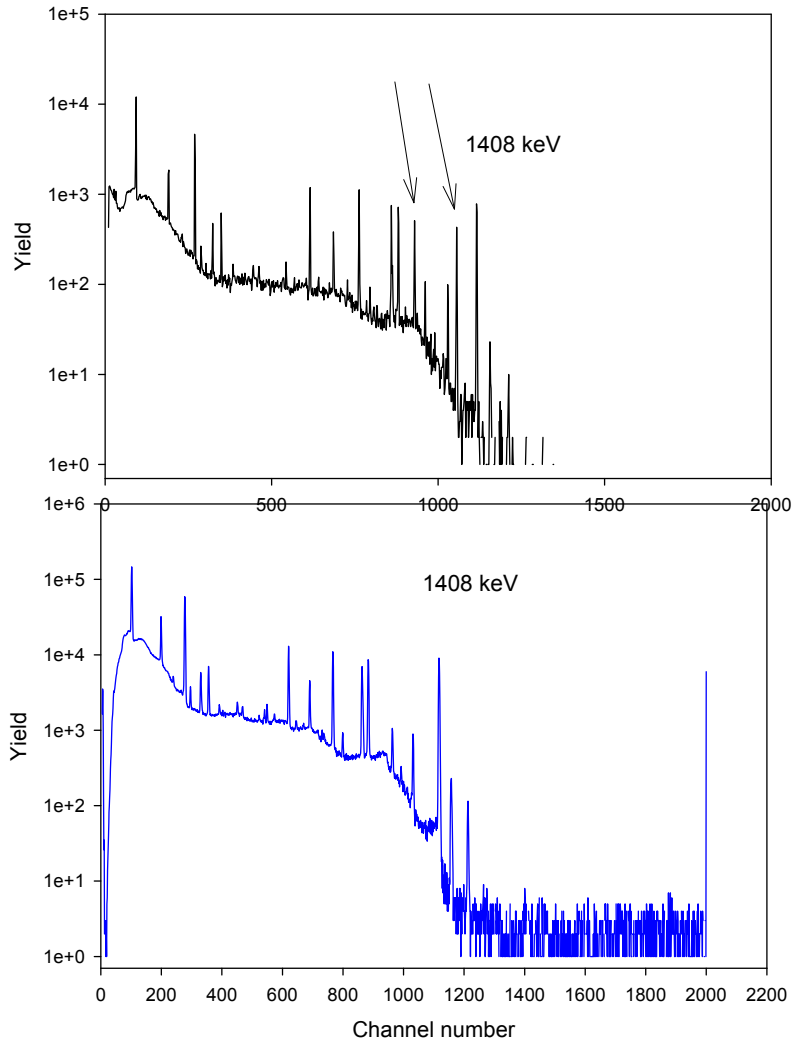

FIG. 9. The ^{152}Eu spectra were measured consecutively feeding the preamplifier signal to an analogue signal processing chain (upper panel), and to a digital signal processor, CSX4 (lower panel). In the upper panel spectrum two unidentified peaks, possible ghost peaks are marked with arrows. The measurement was made for the same time duration. The difference in the yield is more than an order of magnitude.

If we analyse the meaning of the rejected spectra, we observe that some fractions of the peaks are rejected. The upper panel of Fig. 5 presents the accepted and rejected spectra for this measurement on ^{152}Eu, and the black line is the same as the lower panel of Fig. 9. Part of the upper panel of Fig. 5 is presented in Fig. 10 in a magnified plot. The rejected spectrum has only the tail part of the spectrum that has the advantage of improving the line shape in the accepted or desirable spectrum, while keeping an accurate account of the total events for each peak by storing the tail events in the rejected spectrum. The benefit is we can have both the good part for analysis and the rejected events to compensate for lost counts.

The second measurement was made using a natural thorium salt. The measurements were made for the same time duration consecutively. The CSX4 digital signal processor spectra are presented with red line, while the analogue system with black line in Fig. 11. At this time we will not go into the details of the possible reason for the difference in the low energy continuous spectrum features of the two spectra as it is beyond the scope of this paper.

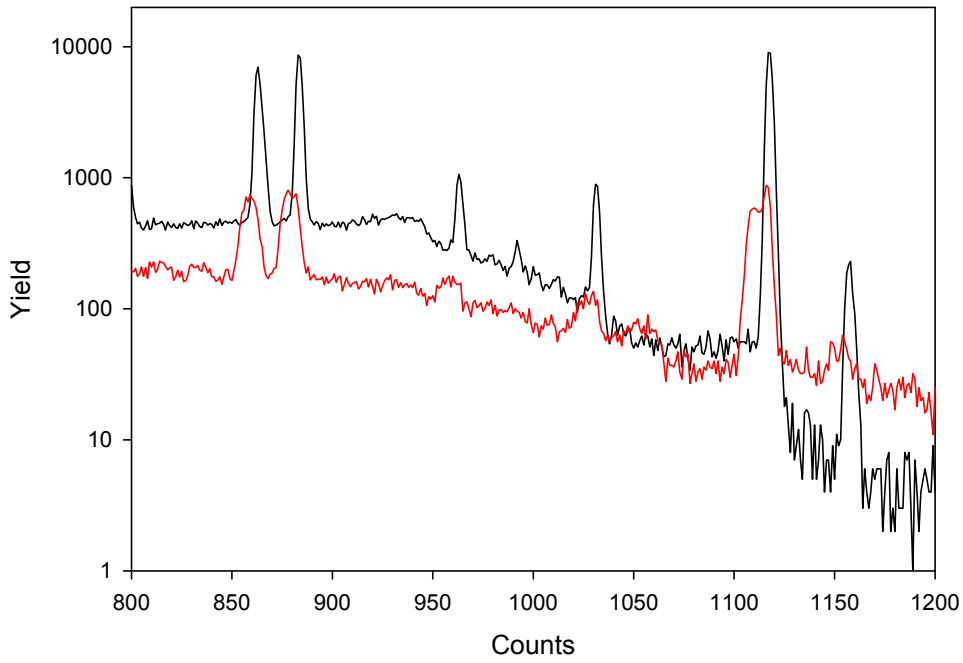

FIG. 10. The magnified plot of Fig. 5. It demonstrates that the peak related features are detector tailing in the rejected spectrum, and the CSX4 rejects the peak tailing efficiently.

In Fig. 12 we present the CSX4 spectrum with the rejected event spectrum as well. The rejected spectrum seems to have a ghost peak that was rejected. In the CSX4 spectrum, the peaks have a nice shape, and a reasonably good resolution. However if we look into the spectra of the analogue system, there are puzzling aspects of the line shape. In the low energy side of the spectrum, Fig. 13 upper panel, the peaks have a good line shape. However, in the high energy side, Fig. 13 lower panel, the peak shape is distorted. It remains to be resolved whether this represents an additional peak, a pile up with noise, a simple ghost peak, or it is the original peak with this line shape that has to be accounted for as one peak.

These are standard clean relatively simple spectra. In in-beam measurements where a large number of unknown peaks are present it is impossible to identify their origin. However having a rejected spectrum available, a ghost peak in the accepted spectrum would present itself as a ghost deficit in the rejected spectrum, as an event is either in the accepted or in the rejected spectra. In coincidence measurements, these "ghost peaks" would erroneously give a time signal thus degrading the measurement. In such measurements, a system is necessary that not only guarantees quality but whose performance is always easily verifiable. The CSX systems offer such verifiable quality assurance.

It is interesting to observe the performance when the input rate is high. The preamplifier signal decay time constant is 110 μs. We have measured a ^{137}Cs source spectrum with the digital signal processor at 9600 Hz input rate. At this rate, the analogue system did not give a meaningful spectrum. Since the digital signal processor is a non-paralyzable system, and has successfully operated for input rates of the order of a few million with X ray detectors, we expected some spectra. The spectra are presented in Fig. 14. The 661.65 keV gamma ray line of ^{137}Cs, has a good line shape, and even the gamma line of ^{40}K is well above the pileup level. Having the rejected spectrum available, quantitative data can be obtained.

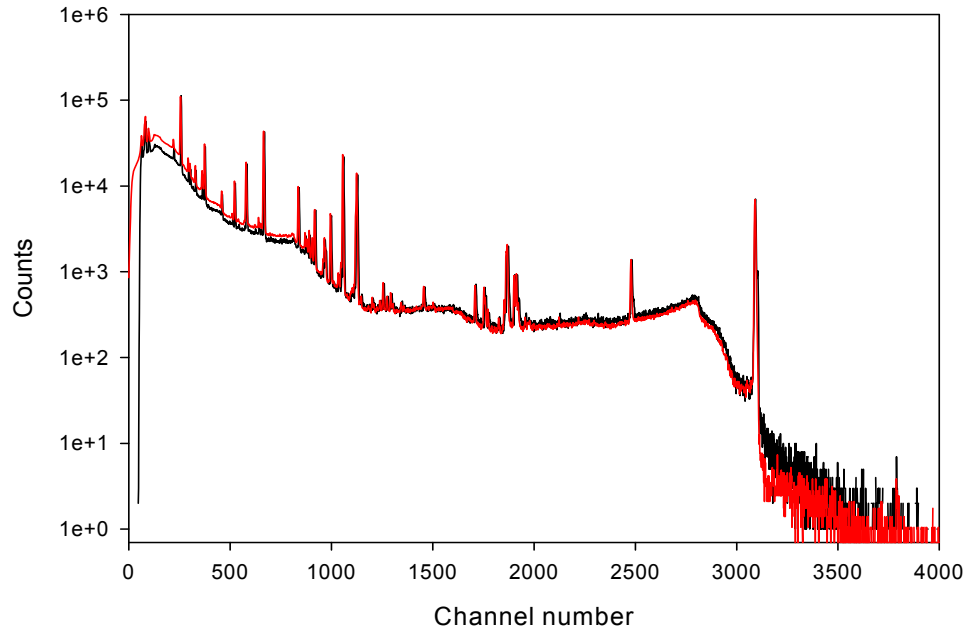

FIG. 11. The gamma ray spectra of natural thorium salt measured under the same circumstances, except the preamplifier signal was fed to two different signal processing chains. The black line is the detector systems own analogue electronics. The red line is the spectrum of the CSX4 fully digital signal processor.

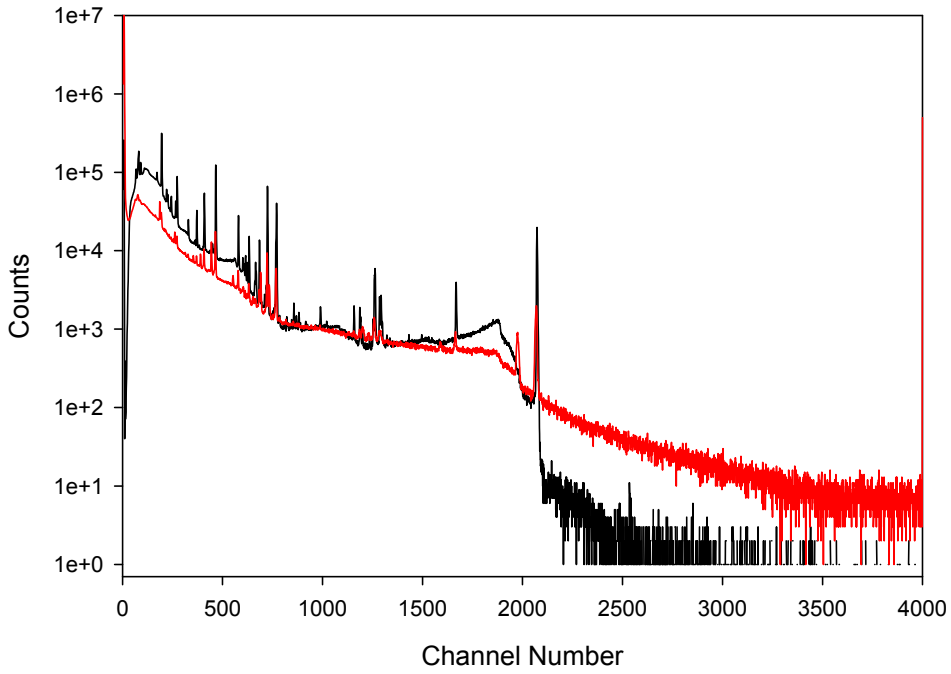

FIG. 12. The gamma ray spectrum of natural thorium salt, measured with a HPGe detector and a quality assurance capable signal processor, CSX4. Black line is for the accepted spectrum, and red line is for the rejected spectrum.

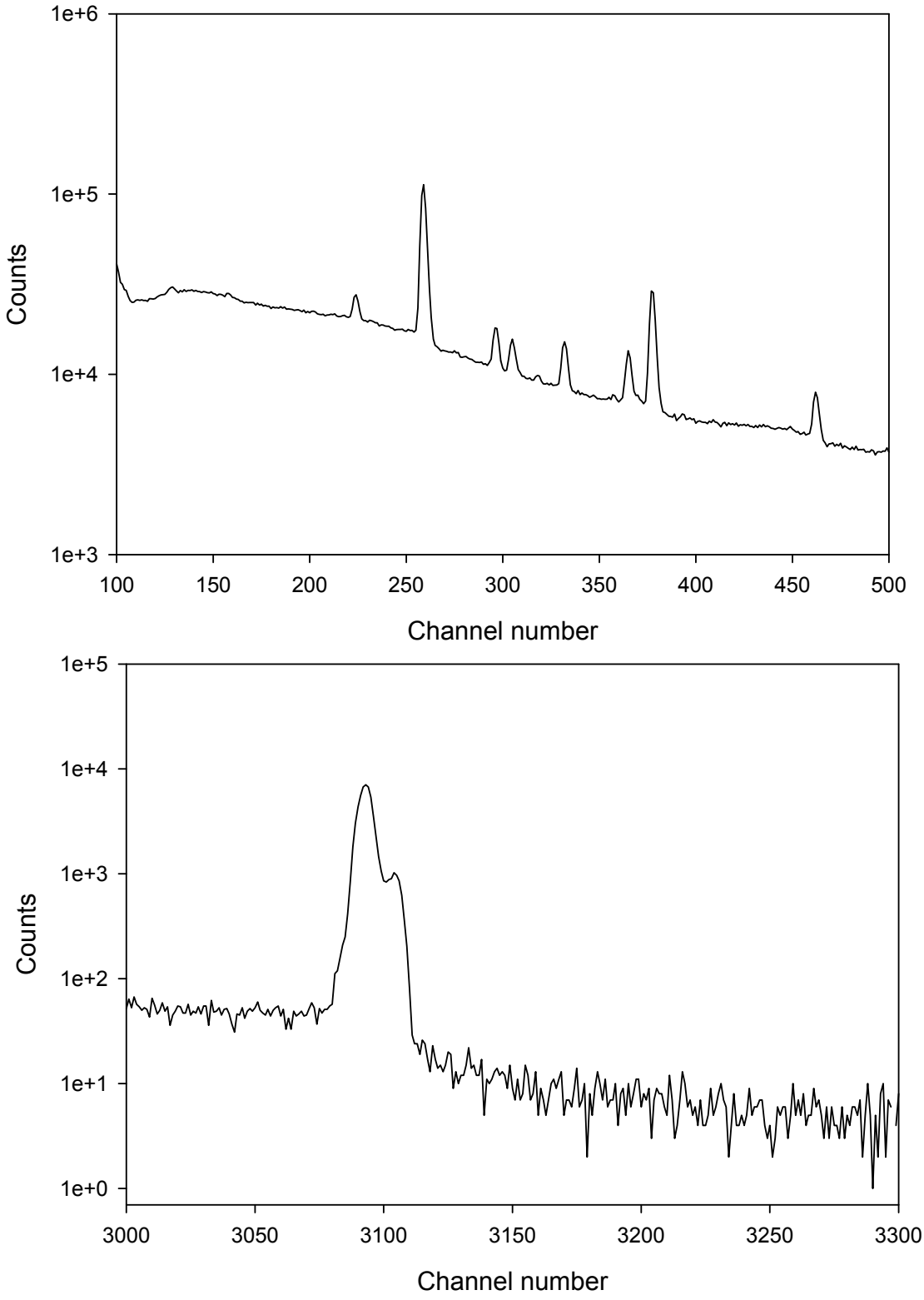

FIG. 13. A detailed view of the spectrum of the analogue system. The upper panel shows the low energy part and the lower panel the high energy side. The origin of the shape of the lower panel gamma line is unknown. The shape of this line is normal when measured with the digital processor.

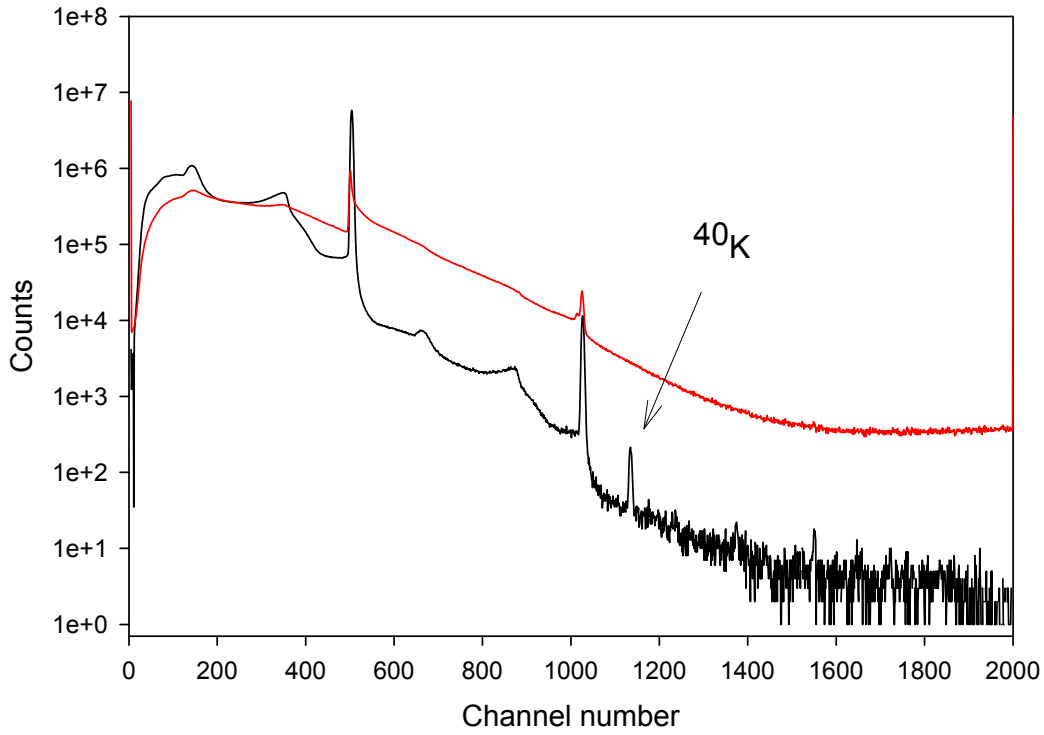

FIG. 14. The 661.65 keV gamma ray line of ^{137}Cs measured with the CSX4 signal processor. The black line is the accepted spectrum while the red line is the rejected spectrum. The gamma ray line of ^{40}K is well visible because of the pile up recognition and rejection. The measurement was made at 9600 Hz input rate with a preamplifier having 110 μs decay time constant.

8. CdTe DETECTOR

We have made a measurement with our signal processor and a metrology level HPGe detector and associated digital signal CdTe may provide excellent detector materials by proper modification of the collective excitation channel. Although we consider the development of the proper doping important, we were interested to see what resolution can be achieved with the presently available detector materials. For testing purposes we have made measurement on a 1 mm thick CdTe PIN diode. Its compact size with a Peltier cooled approach allows its application in portable devices. Of course, one important issue is the line shape and resolution. Frequent comparisons on the resolution and line shape are made on the 662 keV lines of ^{137}Cs and we present such a spectrum in Fig. 15. We are pleased to show the excellent resolution that can be readily seen from the well resolved escape peaks. In this particular measurement the resolution was 1.9 keV for the 662 keV line. Previous studies on these material used strong discrimination and rejection [19].

The applied risetime discrimination strongly reduced the tailing on the 59.6 keV gamma ray line of ^{241}Am. As seen in Fig. 5 of the authors, the discrimination hardly changed the intensity of the lower energy X ray lines, but reduced the intensity of the gamma ray line by more than a factor of two. This is a clear indication that such discrimination would introduce an energy dependent signal processing efficiency. Therefore, a rejected spectrum in this context should also be considered mandatory.

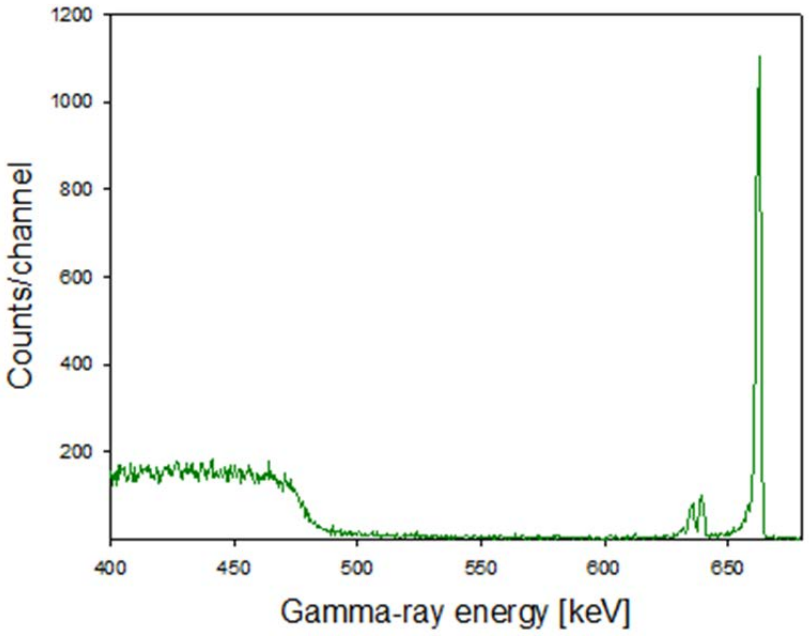

FIG. 15. A spectrum of the 661.65 keV gamma line of ^{137}Cs, measured with a CdTe PIN diode (3 x 3 x 1 mm^3). The well resolved escape peaks demonstrate the resolution capability.

9. TRAINING AND EDUCATION

The presented examples demonstrated that even in expert laboratories the system adjustment and tuning needs special expertise. The noise condition can change and therefore monitoring the system performance is a demanding task and needs high level knowledge of several fields. The detector and electronic can age or deteriorate requiring readjustment as necessary. The examples above provide clear demonstrations of several of the potential problems facing the analyst.

The majority of the spectra are continuous having background, pileup, and Compton scattering components. Therefore, the geometrical and noise environment set-up requires experience. The peak shapes are also modified by the set-up and capability of the signal processing electronics.

The training and education can be made easy using a plug and play system. The effect of the signal processor settings can be seen immediately by showing the effect each discriminator has on the overall spectrum as well as the individual features. The CSX processors can also provide a wealth of information on detector physics, allowing identification of the signals resulting from slow rise time, or distorted signals originating from imperfections. The effect of system noise hunting can be monitored. All the user adjustable parameters are made by the API, or interface program, therefore remote set-up and control is possible via USB communication port, minimizing the time spent close to the radioactive source. The storing of the rejected spectra allows for future inspection of the measurement conditions, and thus a better interpretation of the spectra.

10. CONCLUSIONS

It became evident in the X ray detection field that quality assurance is necessary. It seems to be the case in the field of gamma ray detection as well. The presented approach offers the

opportunity to determine the true input rate. The storing and subsequent analysis of all events helps guarantee quality measurements. The rejected spectra of each discriminator give additional support to identify the various spectral features that are usually present in the spectrum.

ACKNOWLEDGEMENTS

The preparation of the manuscript was supported by a Marie Curie International Reintegration Grant within the 7th European Community Framework Programme. The authors thank the laboratory of Prof J. L. Campbell of University of Guelph, Canada, the Osaka Electro-Communication University, Japan; M.C. Lepy of the Laboratoire National Henri Becquerel (BNM/LNHB) CEA / Saclay, France, and J. Pantazis, Amptek Inc, Bedford, MA, USA for support of some of the research presented in the paper.

REFERENCES

[1] CAMPBELl, J.L., X Ray Energies: Transition Probabilities, Fluorescence and Coster-Kronig Probabilities, report prepared for the International Initiative on X ray Fundamental Parameters. www.canberra.edu.au/irps/xray.pdf

[2] PAPP, T., PAPP, A., MAXWELL, J.A., Quality assurance challenges in x ray emission based analyses, the advantage of digital signal processing, Anal. Sc. 21 (2005) 737–745.

[3] PAPP, T., MAXWELL, J.A., PAPP, A., The necessity of maximum information utilization in x ray analysis, X ray Spectr. 38 (2009) 210–215.

[4] PAPP, T., MAXWELL, J.A., PAPP, A., A maximum information utilization approach in x ray fluorescence analysis, Spectrochimica Acta Part B: 64 (2009) 761–770.

[5] PAPP, T., MAXWELL, J.A., PAPP, A.T., The necessity of recognizing all events in X ray detection, Appl. Rad. .Isot. .68- 4/5 (2010) 561–565.

[6] PAPP, T., CAMPBELL, J.L., VARGA, D., KALINKA, G., An alternative approach to the response function of Si(Li) X ray detectors based on XPS study of silicon and front contact materials, Nucl. Instr. Meth. A 412 (1998) 109–122.

[7] PAPP, T., On the response function of solid state detectors, based on energetic electron transport processes, X ray Spectr. 32 (2003) 458–469.

[8] PAPP, T., MAXWELL, J.A., The effect of the signal processor on the line shape, Adv. X ray Anal. 53 (2011).

[9] LÉPY, M.C., PLAGNARD, J., FERREUX, L., Measurement of ^{241}Am L X ray emission probabilities, Appl. Rad. Isot. 66 (2008) 715–721.

[10] PAPP, T., MAXWELL, J.A., A robust digital signal processor: Determining the true input rate, Nucl. Instr. Meth. A619 (2010) 89–93.

[11] PAPP, T., MAXWELL, J.A., PAPP, A., NEJEDLY, Z., CAMPBELL, J.L., On the role of the signal processing electronics in X ray analytical measurements, Nucl. Inst. Meth. B219 (2004) 503–507.

[12] LARSSON, N.P., TAPPER, U.A.S., MARTINSSON, B.G., Characterization of the response function of a Si(Li) detector using an absorber technique, Nucl. Instr. Meth. B43 (1989) 574–580.

[13] GOTO, S., Response function of a Si(Li) detector from 1 to 10 keV, Nucl. Instr. Meth. A333 (1993) 452–457.

[14] TORII, K., TSUNEMI, H., MIYATA, E., HAYASHIDA, K., Some characteristics of a solid state detector in the soft x ray region, Nucl. Instr. Meth. A361 (1995) 364371.

[15] GARTNER, R.P., YACOUT, A.M., ZHANG, J., VARGHESE, K., An investigation of the possible interaction mechanisms for Si(Li) and Ge detector response functions by Monte Carlo simulation, Nucl. Instr. Meth. A242 (1986) 399405.
[16] GOULDING, F.S., Some aspects of detectors and electronics for X ray fluorescence analysis, Nucl. Instr. Meth. 142 (1997) 213223.
[17] CAMPBELL, J.L., MCDONALD, L., HOPMAN, T., PAPP, T., Simulations of Si(Li) X ray detector response, X ray Spectr. 30 (2001) 230241.
[18] LÉPY, M.C., CAMPBELL, J.L., LABORIE, J.M., PLAGNARD, J., STEMMLER, P., TEESDALE, W.J., Experimental study of the response of semiconductor detectors to low energy photons, Nucl. Instr. Meth. A439 (2000) 239246.
[19] OWENS, A., BUSLAPS, A.T., ERDA, C., GRAAFSMA, H., LUMB, D., WELTER, E., Hard X ray and γ-ray measurements with a 3×3×2 mm^3 CdZnTe detector, Nucl. Instr. Meth. A563 (2006) 268.

DIGITAL SET-UPS FOR POSITRON ANNIHILATION SPECTROSCOPY AT PAS LABORATORY FEI STU BRATISLAVA

M. PETRISKA, V. SLUGEŇ, J. VETERNÍKOVA, S. SOJAK
Slovak University of Technology, FEI,
Bratislava, Slovakia
Email: martin.petriska@stuba.sk

Abstract

Current status of the digitization in Positron Lifetime and Coincidence Doppler Broadening spectroscopy set-ups at the Slovak University of Technology in Bratislava is described in this paper. In PALS set-ups two digitizer cards Acqiris DP-240 and Ztec ZT4612 with different parameters and abilities were tested. The first results from the Coincidence Doppler Broadening set-up using Adlink PCI-9820 digitizer card are presented.

1. INTRODUCTION

The Positron Annihilation Spectroscopy Laboratory at the Department of Nuclear Physics and Techniques in Bratislava is specialized in research of the alloys for fission and fusion technology. In this area, many useful applications and outputs have been obtained [1, 2]. From a technical point of view, to observe material changes in alloys and steels in PAS LT measurements, good time resolution (FWHM) of the measurement set-up is needed. Improvements in decreasing the FWHM started in 2003 when plastic scintillators with anode timing from XP2020 photomultipliers were changed to BaF_2 scintillators with dynode timing from XP2020Q photomultiplier tubes. This change brought improvements in FWHM from 450 ps in our old system to a best resolution of 180 ps in our new set-up. To achieve better results and measurement stability, system digitalization was chosen.

2. POSITRON ANNIHILATION SPECTROSCOPY METHODS

A positron is the antiparticle to the electron, having the same mass but positive charge. It was predicted by Dirac in 1928 and discovered by Anderson in a cosmic ray in 1932. Positrons are used as a microstructure probe for defects in materials. There are three main positron annihilation spectroscopy methods: Positron Annihilation Lifetime Spectroscopy (PALS), Doppler Broadening of the annihilation ray, and Angular Correlation of the Annihilation Radiation (ACAR). These three different methods are shown in Fig. 1.

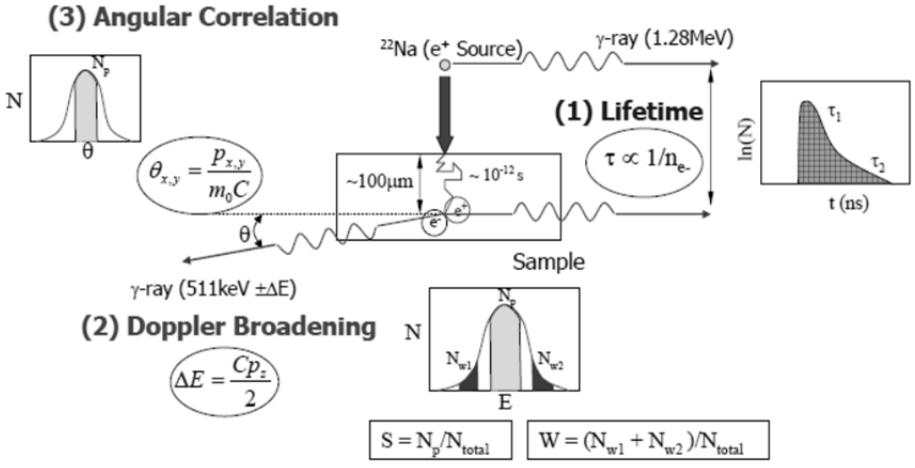

FIG. 1. Principles of the positron annihilation spectroscopy techniques.

2.1. PALS — positron annihilation spectroscopy

Positrons from ^{22}Na are emitted with a mean kinetic energy about 250 keV. A gamma ray with energy 1274 keV is emitted 3.5 ps after positron emission. This gamma ray is used as a positron "born" indicator. In solids, a positron is losing his kinetic energy by thermalization. After the thermalization, a diffusion process starts as shown in Fig. 2. The diffusion length is about 100 nm. During the diffusion, annihilation with electrons can occur. If there are defects such as vacancies or vacancy clusters, the positron is trapped in the vacancy and its lifetime is prolonged. This effect is used to determine the occurrence of defects in materials. When the positron annihilates with the electron, two annihilation rays with energies 511 keV are emitted in opposite directions. The direction and energy of the annihilation rays are affected by the annihilated electron's momentum before the annihilation.

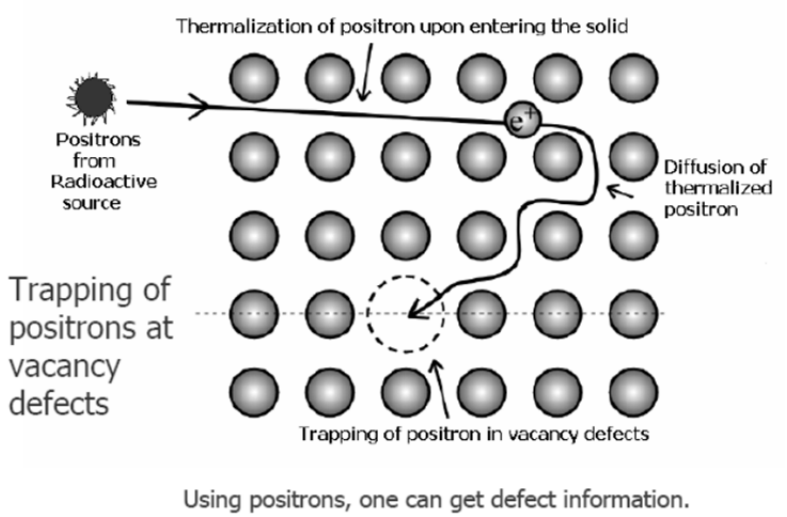

FIG. 2. Positron trapping model [3].

2.1.1. PALS – analogue set-up

To measure the time between the born positron and its annihilation in the material, the measurement set-up in Fig. 3 should be used. This set-up consists of two scintillation detectors, constant fraction discriminators with single channel analysers (CFD+SCA), a time to amplitude convertor (TAC) and a multichannel analyser (MCA). A delay in the stop part of the set-up is used to shift the time annihilation spectra to position it in the middle of the multichannel analyser range. There are two possible set-ups: fast-slow, where start-stop events are selected on the energy base after time measurement in separated hang, or fast-fast set-up using differential constant fraction discriminators with start-stop events selection during time measurement.

2.1.2. Digital PALS set-up

New fast digitizers with sampling rates higher than 1 GS/s avoid building pure digital PALS set-ups. In these set-ups, pulses from detectors are sampled with a digitizer and the software makes all timing, processing and storing data to histograms.

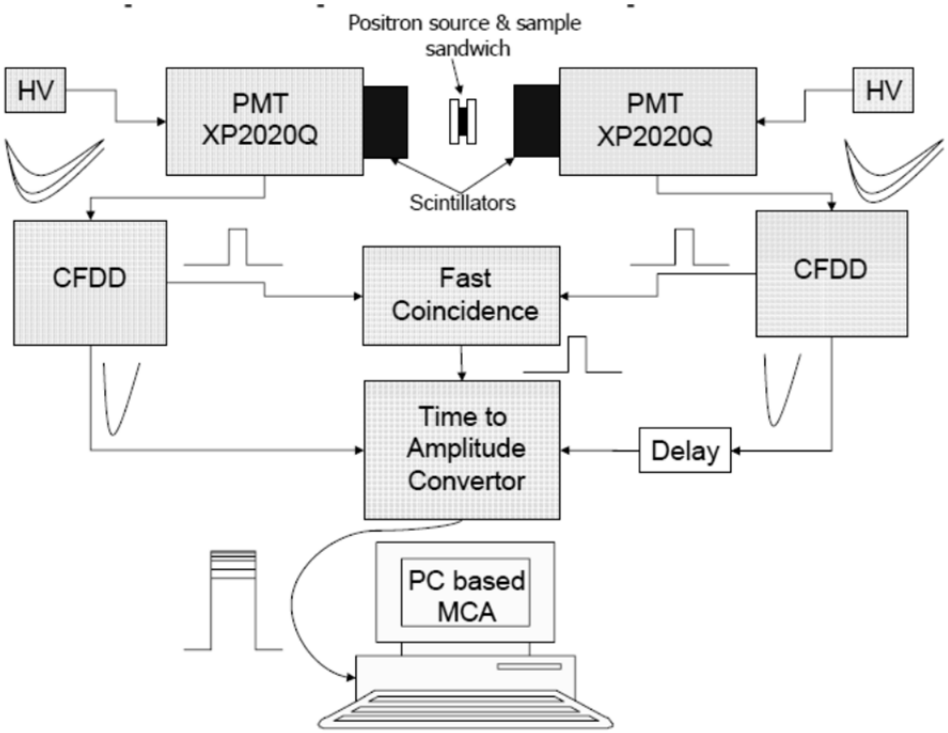

FIG. 3. PALS set-up (fast-fast) [3].

2.1.3. Digitizing pulses from detector

For digital PALS systems, the most important part is obtaining the timing information from the digitized pulses. It was found [4, 5] that best results are given by the constant fraction method in both analogue and digital set-ups. In the analogue set-up, extracting timing information is performed by the CFD module by process shown in Fig. 4. In the digital set-up, the same operation is made by calculating the constant fraction from pulse shape extrapolated over samples (Fig. 5).
Extrapolation of the pulse shape should be made by linear, parabolic or spline functions (Fig. 6).

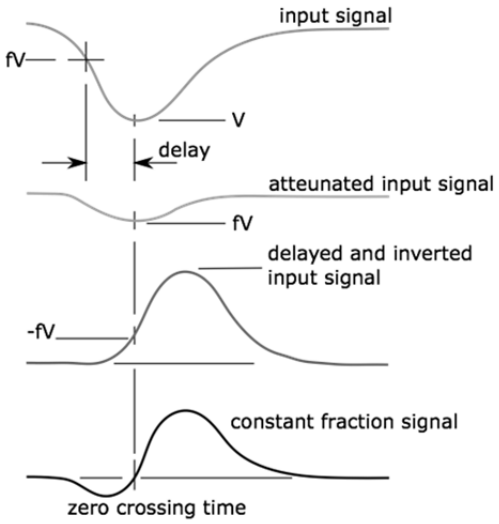

FIG. 4. Analogue constant fraction method.

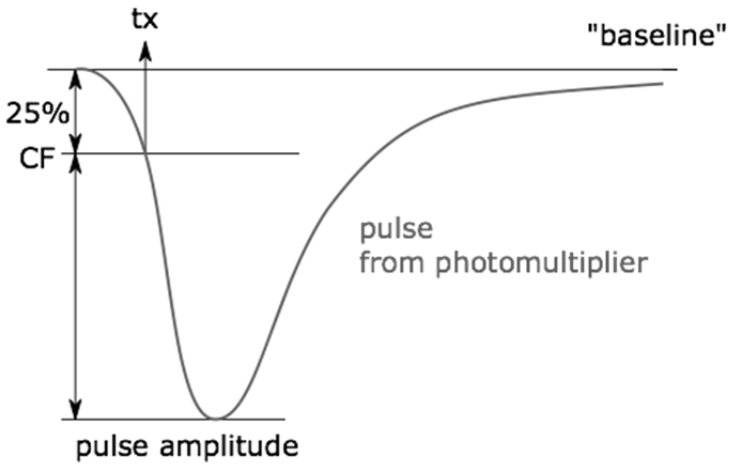

FIG. 5. Digital constant fraction method.

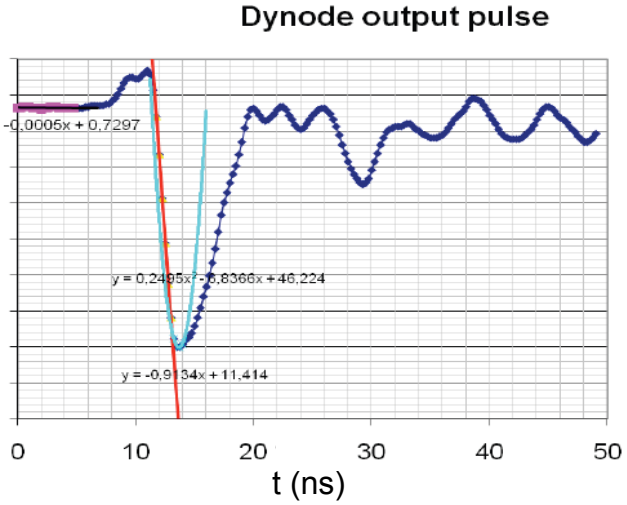

FIG. 6. Digitized pulse from scintillation detector with extrapolation in rising edge and pulse minimum.

2.1.4. PAS LT set-up with Acqiris DP240

In framework of joint activity between STU Bratislava and JRC Petten in October 2006, Acqiris DP240 digitizer was loaned to our laboratory to develop software for positron lifetime measurements. DP240 was connected to our existing analogue PAS LT system to compare analogue and digital systems with minimal impact of the rest parts of the set-up. It was found that a sampling rate of 1 GS/s in double channel mode was not sufficient to process dynode timing signals from our set-up. In the joined mode (Fig. 7b) where the signal from the stop detector is delayed and added to the start signal, results comparable with the standard analogue set-up were obtained [6] and which is presented in Table 1. For signal processing, linear and parabolic approximations of the sampled pulses was used.

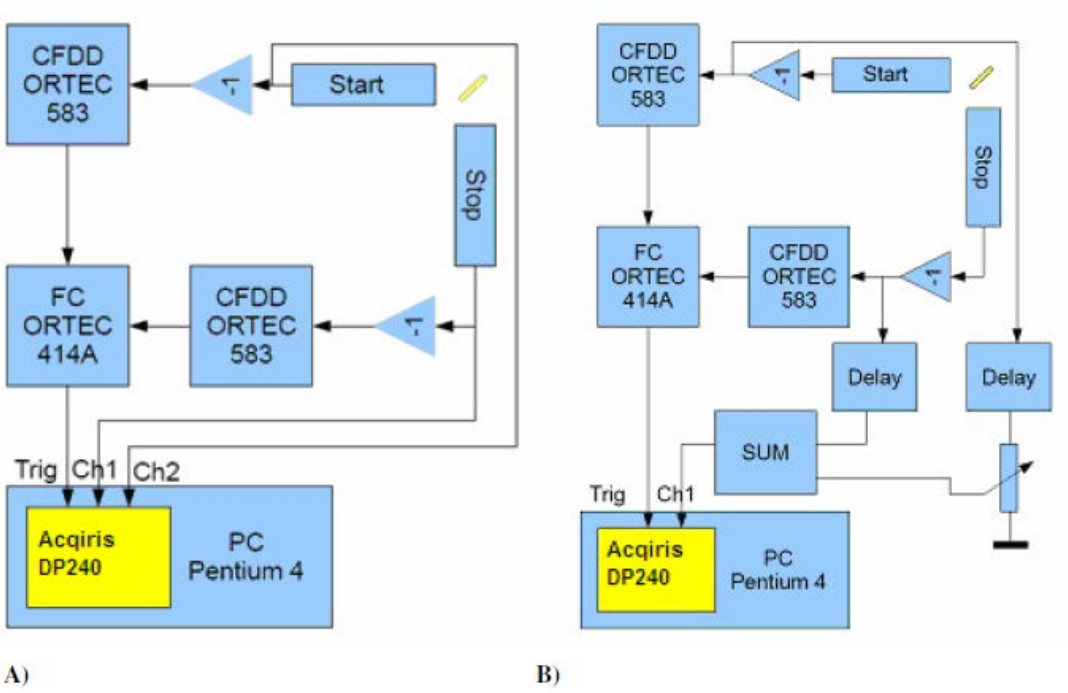

FIG. 7. DPA240 based digital PALS set-ups a) two channel mode, b) joined channel mode.

TABLE 1. COMPARISION ANALOGUE AND DIGITAL SET-UP WITH DP240

Set-up	**Sample**	**τ1 (ps)**	**τ2 (ps)**	**I1 (%)**	**I2 (%)**	**FWHM (ps)**
Digital	Si	222.2 ± 2.0	1690 ± 150	97.34 ± 0.12	2.63 ± 0.12	230.4
	Ni	110.6 ± 0.2	3910 ± 370	98.81 ± 0.05	1.19 ± 0.05	214.9
Analogue	Si	222.9 ± 1.7	1609 ± 43	97.40 ± 0.08	2.60 ± 0.08	244.4
	Ni	118.3 ± 0.5	3310 ± 83	96.06 ± 0.07	3.94 ± 0.07	210.6

2.1.5. PAS LT with ZTEC ZT4612

Ztec ZT4612 is a 4-channel LAN based digitizer with a maximum sampling rate of 4 GS/s in two channel mode, and 2 GS/s sampling rate in four channel mode. These parameters, with a good price, were the main reasons to purchase this digitizer. The ZT4612 card has a wide palette of signal processing functions that enables users to build measurement systems without external software processing in the hosting PC. Unfortunately, the processing speed together with the data transfer speed limits through the 10 Mbit LAN interface from digitizer card to PC were a big obstacle to overcome to obtain a usable measurement set-up. The maximum obtained coincidence rate with the joined one channel mode was 150 Hz in the mode when all processing in PC is done. In comparison, using the internal ZT4612 functions to achieve times between two joined pulses has a maximum measurement rate ~15 Hz. Using more inputs for measurement from more detectors means more data needs to be transferred through the Ethernet interface so measurement speeds is even slower. The USB connection which is available as hardware part of the ZT4612 is not yet supported by internal software and device drivers. However, this set-up brings new ideas to process digitized pulses. New algorithms based on filtering sampled data with moving average filters were tested. For using

the system in real measurements, an external triggering module to select only important pulse events is needed. In our set-up, parts from an old analogue system were used.

2.1.6. Digital set-up improvements

In analogue set-up detectors start and stop signals are separated, but both of them are detecting both gamma rays of 1274 keV and 511 keV. With digital set-ups it is possible to measure simultaneously two spectra. One where the first detector detects a start signal from 1274 keV and second 511 keV, and second when first detector detects stop signal from 511 keV and second 1274 keV. By measuring two spectra simultaneously, it is possible to collect the same number of events in half the time. Set-up based on this principle is has been published [5, 7].

Another system improvement is possible when three detectors are used. This set-up is detecting both 511 keV annihilation rays. In an analogue set-up it is often used to reduce the background from ^{60}Co. In a digital set-up it is possible to compute the lifetime precisely by averaging two lifetimes measured from one annihilation event. This improvement has been described in the published literature [8]. It was shown that by averaging two lifetimes, the FWHM is decreased from 144 ps in the single stop to 119 ps in the double stop mode.

2.2. Positron annihilation Coincidence Doppler Broadening

To study the electron structure in solids and for defect investigations, the electron momentum distribution obtained from Coincidence Doppler Broadening (CDB) of the annihilation peaks is used. For this technique a new set-up was built at our laboratory (Fig. 8) which consists of two Canberra GC2019 HPGe detectors each with relative efficiency 20% and resolution 1.9 keV at 1.33 MeV. The HPGe detectors are cooled by a Cryo-JT electronic cooling system.

For these measurements, a good pulse amplitude resolution is needed. An Adlink PCI-9820 digitizer with 14-bit resolution and 65 MS/s sampling rate was chosen. It is possible to process signal from spectral amplifiers, or to process signals before from the preamplifier output of the detector. The first solution uses a spectroscopy amplifier (Canberra 2022) as the pulse processing module. The digitizer card is using as pulse amplitude meter. The first CDB spectra measured with such set-up is shown in Fig. 9. The pulse shape time constant of the spectroscopy amplifier was set to 5 μs. The data transfer and processing speed of the PCI-9820 is suitable to construct this set-up without an external triggering part. Work on the software is still in progress.

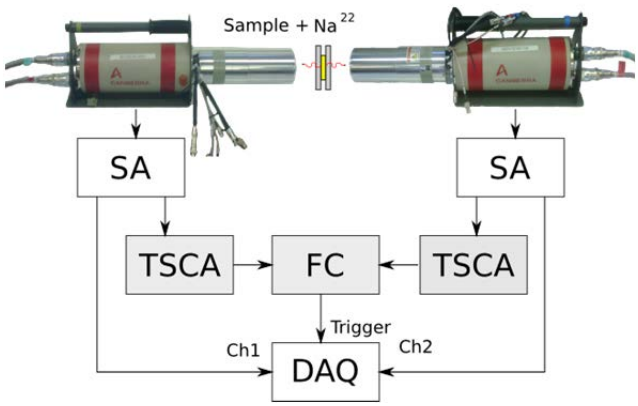

FIG. 8. CDB schematics: SA (spectroscopy amplifier), TSCA (timing single channel analyser), FC (fast coincidence), DAQ (digital acquisition card).

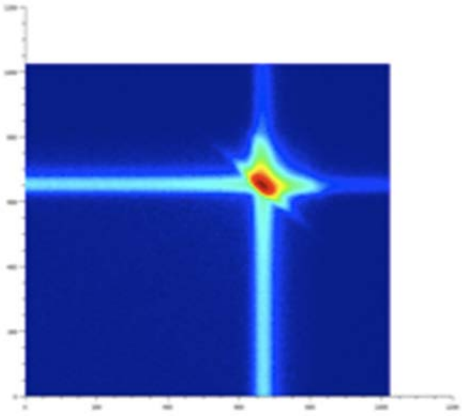

FIG. 9. First logarithmic spectra from CDB at FEI STU, reference SI sample.

3. CONCLUSIONS

Digitization in positron lifetime set-ups is a growing trend. To build digitized set-ups, careful attention to choosing right digitizer card is needed. Except sampling rate, data transfer rates between card and PC is very important parameter. Triggering abilities of the cards used in our lifetime measure set-ups were insufficient to work without using an external trigger module. For Coincidence Doppler Broadening, a set-up using internal software triggering is possible.

REFERENCES

[1] SLUGEN, V., et al., Positron annihilation Investigation of defects in copper alloys selected for nuclear fusion technology, Fusion Engineering and Design 70-2 (2004) 141–153.

[2] SLUGEN, V., KÖGEL, G., SPERR, P., TRIFTSHÄUSER, W., Positron annihilation studies of neutron irradiated and thermally treated reactor pressure vessel steels, J. Nucl. Mat. 302- 2/3 (2002) 89–95.

[3] KRAUSE-REHBERG, R., LEIPNER, H.S., Positron annihilation in Semiconductors, Solid-State Sciences 127 (Springer Verlag, Berlin, 1998).

[4] NISSILÄ, J., et al., Performanc analysis of a digital positron lifetime spectrometer, Nucl. Instr. Meth. A538 (2005) 778–789.

[5] BEČVÁŘ, F., ČÍŽEK, J., PROCHÁZKA, I., High resolution positron lifetime measurement using ultra fast digitizers Acqiris DC211, Appl. Surf. Sc. 255 (2008).

[6] KRILLE, A., "Simulation and Practice of Digital Timing", paper presented at Workshop on Digital Signal Processing in Nuclear Science, Dresden, Germany, 2009.

[7] PETRISKA, et al., Application of fast digitizer card Acqiris DP-240 in positron lifetime spectroscopy, Phys. Status Solidi 6-11(2009) 2465–2467.

[8] SAITO, H., NAGASHIMA, Y., KURIHARA, T., HYODO, T., A new positron lifetime spectrometer using a fast digital oscilloscope and BaF_2 scintillators, Nucl. Instr. Meth. A487 (2002) 612–617.

PARALLEL PORT INTERFACE ADC FOR REAL TIME DATA ACQUISITION

M.M. RASHID, N. JAHAN, G.S. ISLAM, M. ALIUZZAMAN
Institute of Nuclear Science and Technology,
Atomic Energy Research Establishment,
Savar, Dhaka, Bangladesh
Email: mrashid@agni.com

Abstract

A parallel port interface ADC for real time data acquisition has been designed and developed indigenously. The ADC has been designed by utilizing the data input capabilities of the computer parallel port. In addition to a basic ADC chip, it has been required to incorporate some additional hardware and software components such as parallel port data bus interface, control bits decoder, driver software and acquisition software to realize this ADC. The data acquisition software has been developed under the Visual Basic (VB) programming language environment. The driver software, to enable the VB of port access capability, has been obtained from the website. The main hardware component of the developed ADC is AD574 IC. The AD574 chip is a complete 12 bit successive approximation analogue to digital converter with 3-state output buffer circuitry for direct interface to a data bus. 8-bit data bus buffer is used to interface the ADC output to the parallel port data lines. The control pulses, as required by AD574, are generated by decoding the control bits C0–C3 of the control register. C5 bit of the control register is set to the proper logic value to determine the direction of data would be appeared on the data bus (D0 – D7) of the parallel port. Standard features, such as on-line acquisition, data display, data save, data retrieve, etc. options, are included in the acquisition software.

1. INTRODUCTION

Vendor made standard PCI/USB interface ADCs are available in the international market. These ADCs are accompanied by dedicated software. However, a prototype developer does not have easy access to this hardware and software. Our group has good experience of developing ISA based ADC cards [1, 2] for computer based instrumentation and control. The ISA based ADC cards have now become obsolete because modern computers are no longer equipped with ISA slots. Hence, to develop the data acquisition hardware and software, comparatively easier interface approach may be via the utilization of the parallel port data access capabilities of a computer. The parallel port consists of data register, control register and status register having eight I/O data lines, four output control & one data control lines and five input status lines, respectively. A prototype parallel port ADC has been developed and used for the acquisition of the neutron flux signal from the TRIGA research reactor of Bangladesh.

2. DESIGN PRINCIPLE

The main component of this device is the familiar IC AD574 (12-Bit ADC 574AJ, RS Data library, Sheet # 4383, RS Components Ltd, UK). The AD574 chip is a complete 12-bit successive approximation analogue to digital converter with 3-state output buffer circuitry for direct interface to an 8, 12, or 16-bit microprocessor bus. The IC takes a conversion time of 25 μS. It has an important feature that its 12-bit output can be read by a single 8-bit port. For this purpose, it has to be selected for upper 8-bit read mode or lower 4-bit read mode by applying proper logic signal at a special pin (Mode) of the IC. The ADC unit gives standard TTL level digital outputs that are read by the software through the computer interface unit.

2.1. Analogue input interface

The analogue input interface, having very high input impedance, is used to protect any possibility of loading of the input source. The FET input operational amplifier IC CA3140 is used to serve the purpose of analogue input interface. This operational amplifier is very suitable to be used as an input buffer. The input impedance of this operational amplifier is about 10^{12} ohms. This feature of the IC isolates the ADC from the input source.

2.2. Computer port interface

The parallel port interface is used for control and reading the data from the ADC. The bidirectional parallel port [3] allows eight input/output data lines (D0–D7), four output control lines (C0–C3) and five input status lines (S3–S7) through Data Register, Control Register and Status Register, respectively, that can be accessed directly by an external device. Thus, it requires minimum external circuitry to interface this port with an external hardware. A standard parallel port uses three I/O addresses, starting at the base address. They are to access 'Data Register,' 'Status Register' and 'Control Register,' respectively. The required addresses to access these registers are given in Table 1. The directions of the register bits are given in Table 2. As mentioned in Table 2, the direction of the data register bits is controlled by the software setting of the control register bit C5.

TABLE 1. PARALLEL PORT REGISTER ADDRESS

Register	LPT1	LPT2
Data register (base address + 0)	378 (Hex)	278 (Hex)
Status register (base address + 1)	379 (Hex)	279 (Hex)
Control register (base address + 2)	37A (Hex)	27A (Hex)

TABLE 2. PARALLEL PORT REGISTER-BIT INFORMATION

Pin No (DB25)	Direction	Register -bit	Inverted
2–9	In/Out	D0–D7	No
15	In	S3	No
10	In	S6	No
11	In	S7	Yes
12	In	S5	No
13	In	S4	No
1	Out	C0	Yes
14	Out	C1	Yes
16	Out	C2	No
17	Out	C3	Yes
18–25	Ground	-	-
C5	Software use to set data direction: 1=input, 0=output		

2.2.1. Hardware interface

As shown in Table 2, some of the control bits (C0, C1 and C3) give the inverted outputs, from the setting of the control register bits, at the output pins of the parallel port. The inverted control bits are inverted again intentionally by using 74LS04 IC to provide the same control bits, as

setting of the control register. The IC 74LS138 is used for decoding the control bits to provide various control pulses, such as ADC mode select, start conversion and ADC output read as required for the ADC. The control bits decoder shown in Fig. 1 is used to generate the required control pulses (Mode, Start Conversion and Read ADC Out) for the ADC. The TTL buffer IC 74LS244 is used for reading the digital data from the output of the 574 IC.

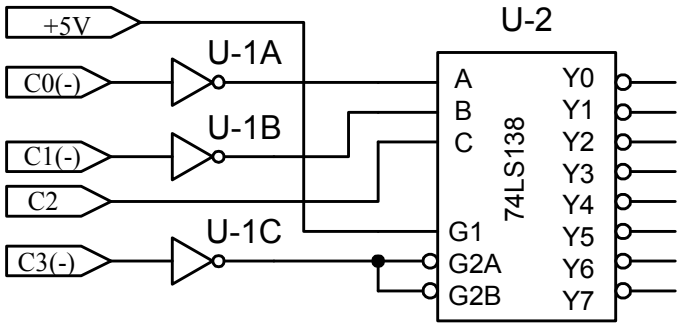

FIG. 1. Control bits decoder.

2.2.2. Software interface

The parallel port registers can easily be accessed from Basic and C languages. Unfortunately, Visual Basic (VB) does not have standard I/O read/write functions to access the mentioned registers. However, the I/O read/write functions can be called in VB environment, importing them from a dynamic link library (DLL) file, declaring them in a VB module file. The DLL file can easily be developed by C++ or by any suitable programming languages to serve as an interface between VB and the external hardware. The DLL file, "inpout32.dll" for parallel port interfacing, is freely available on the internet and has been in our applications. The I/O read/write functions of the "inpout32.dll" are called from the acquisition program by declaring them in a module file as given in the following Program code.

Public Declare Function Inp Lib "inpout32.dll" Alias "Inp32" (ByVal PortAddress As Integer) As Integer

Public Declare Sub Out Lib "inpout32.dll" Alias "Out32" (ByVal PortAddress As Integer, ByVal Value As Integer)

3. ADC WORKING

The circuit diagram of the ADC is given in Fig. 2. The analogue input terminal (ANA-IN) of the device is connected directly to the input source. The 'ANA-IN' signal is fed to the analogue input (Analogue IN) of 574 IC via the unity gain buffer made by 3140. VB based 'Module File' code and 'Acquisition Program' code as required for this ADC is given in the program code below.

```
Out &H37A, &H08
Out &H378, &H00    '(Select ADC mode 0
Out &H37A, &H00    'for 12-bit conversion)
Out &H37A, &H08
```

```
Out &H37A, &H01    '(Start AD conversion)
Out &H37A, &H08

EndConv=0
Do
Status= Inp(&H379)   '(read status register)
Status=Status And &H08   '(Check for Status-3)
        If Status = 8 Then
                EndConv=1
        End If
Loop While EndConv=0

Out &H37A, &HF2
x = Inp(&H378)       '(read upper 8-bit )
Out &H37A, &H08

Out &H378, &H01   '(Select ADC mode 1
Out &H37A, &H00   'for lower 4-bit read)
Out &H37A, &H08

Out &H37A, &HF2
y = Inp(&H378)       '(read lower 4-bit )
Out &H37A, &H08

x = x * 16
x = x And &HFF0
y = y / 16
y = y And &HF
z = x + y
Voltage = z
```

The 'Module File' refers the driver file 'inpout32.dll' for importing the port I/O functions for the acquisition program. The 'Inp' and the 'Out' as declared in the module file, are the port input and the port output functions, respectively, for the acquisition program (Acquire_Data).

The mode input (Mode) of the 574 IC is first set to '0' to enable the chip to 12-bit ADC mode while the upper 8 bits of the ADC output is available for reading. The program then generates the start conversion (Start Conv) pulse for the ADC. As the 574 ADC chip needs a conversion time to complete an A/D conversion cycle a 'DO' program loop is introduced for checking the end of conversion. After the A/D conversion cycle, the 574 IC generates a high pulse 'End Conv' to indicate the end of conversion. The 'End Conv' is detected by reading the S3 of the status register in the 'Do' loop. Upper 8 bits are now available for reading.

After reading the upper 8 bits as 'x', the mode input is set to '1' when the lower 4 bits are available at the ADC output. The lower 4 bits are then read as 'y'. Finally, after masking the value of 'x' and 'y' the actual digital output is found as 'z' which is then assigned to 'Voltage' variable. Successive values of the 'Voltage' variable are to be used for the next steps of digital signal processing.

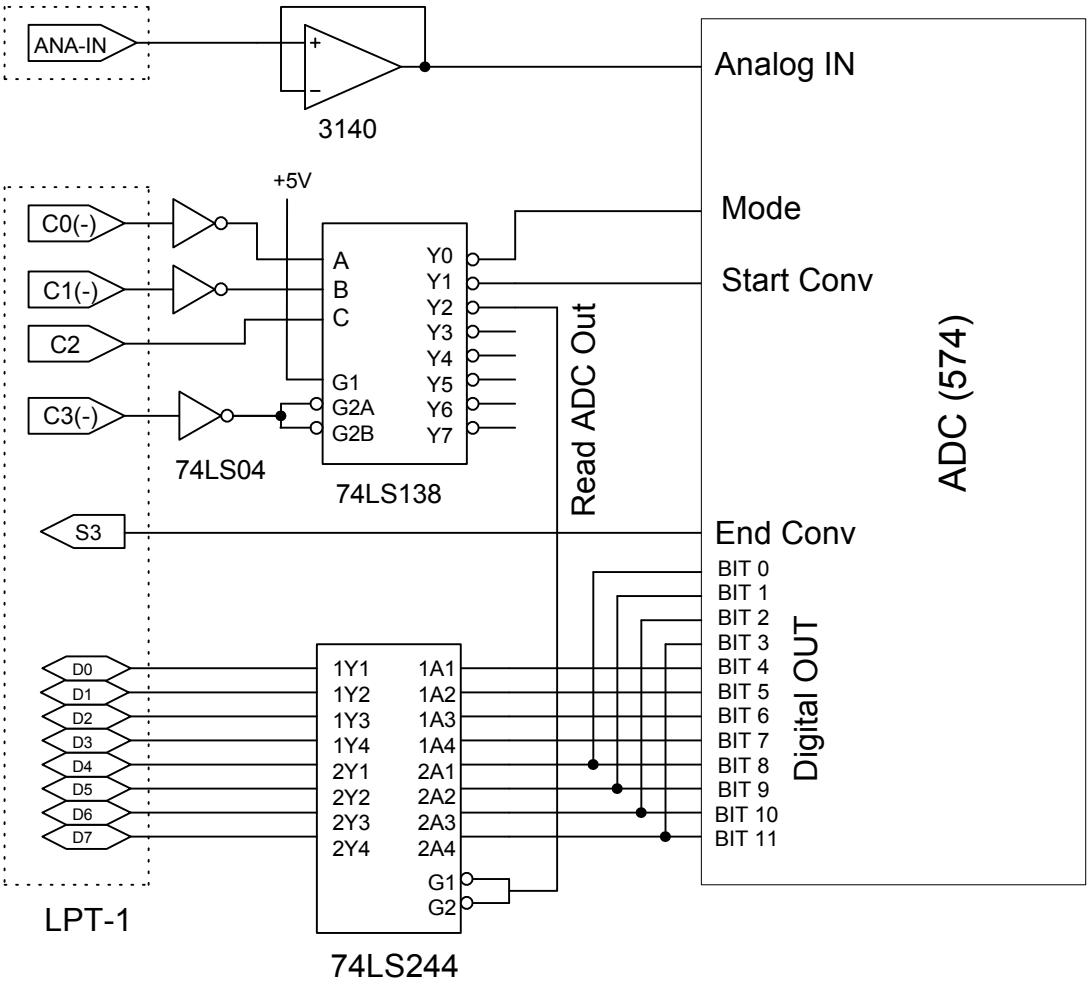

FIG. 2. Circuit diagram of the ADC.

4. RESULTS AND CONCLUSIONS

The ADC has not yet been tested in any radiation detection spectroscopy applications. However, an online digital reactivity meter has been developed by using this ADC [4].

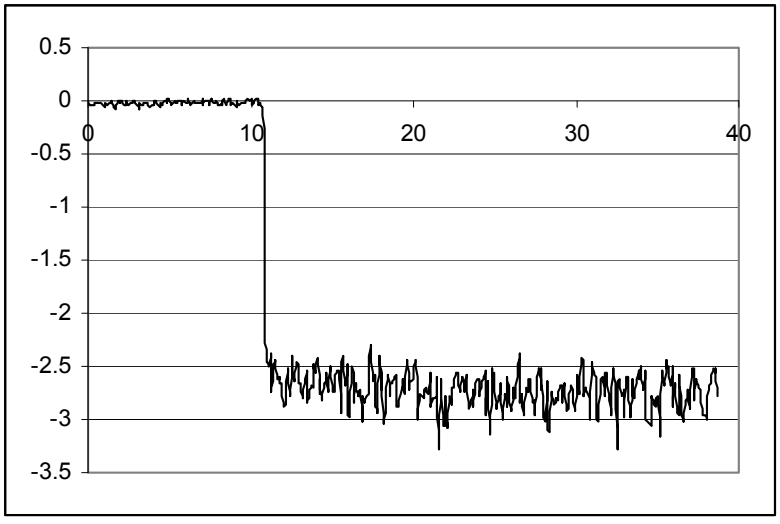

FIG. 3. The plot of time (s) versus reactivity ($).

Additional software functions such as, reactivity calculation by point kinetic equations, online display and plotting of reactivity, saving data, etc., have been developed for the reactivity meter. The digital reactivity meter has been used for measuring the reactivity worth of the TRIGA reactor control rods. Figure 3 is a practical Time (s)–Reactivity ($) plot that shows the reactivity change of the reactor from the critical condition (zero reactivity) for the full-length change of the regulating rod. It has been observed that the parallel port ADC developed for the digital reactivity meter is working properly. Our Institute has a plan to develop field radiation detection and monitoring system based on Cadmium Zinc Telluride detectors. Development of an ADC may be an initial stage of the project.

REFERENCES

[1] INTERNATIONAL ATOMIC ENERGY AGENCY, "Data acquisition system for the 3 MW TRIGA reactor at AERE Savar", Application of Personal Computers to Enhance Operation and Management of Research Reactors, IAEA-TECDOC-1004, IAEA, Vienna (1998) 11–26.

[2] RASHID, M.M., JAHAN, N., KHAYER, M.A., MONDAL, R., Transition from ISA Bus Interface to Parallel Port Interface for Computer based Control & Instrumentation, J. Bangladesh Electr. Soc. 4-2 (2004).

[3] ROSCH, WIN L., Hardware bible, Premier Edition, New Delhi, (1997).

[4] RASHID, M.M., JAHAN, N., AHMED, F., KABIR, N., KHAYER, M.A., Design and Development of a Software Controlled ADC for Digital Reactivity Meter, Proceedings of the International Conference on Electronics Computer and Communication (ICECC 2008), University of Rajshahi, Bangladesh (2008).

REAL TIME DIGITAL PULSE SHAPERS WITH VARIOUS HPGE AND SILICON RADIATION DETECTORS

N. MENAA, B. ZAKRZEWSKI
Canberra Industries Inc.,
Meriden, USA
Email: bzakrzewski@canberra.com

V.T. JORDANOV
Yantel LLC,
Los Alamos, USA

Abstract

Real time digital pulse shaping techniques allow synthesis of pulse shapes that have been difficult to realize using the traditional analogue methods. Using real time digital shapers, triangular/trapezoidal filters can be synthesized in real time. These filters exhibit digital control on the rise time, fall time, and flat-top of the trapezoidal shape. Thus, the trapezoidal shape can be adjusted for optimum performance at different distributions of the series and parallel noise. The trapezoidal weighting function presents the optimum time limited pulse shape when only parallel and series noises are present in the detector system. In the presence of one-over-f (1/f) noise, the optimum WF changes depending on the 1/f noise contribution. In this paper, we report on the results of the evaluation of new filter types for processing signals from CANBERRA HPGe and Passivated, Implanted, Planar Silicon (PIPS) detectors. The objective of the evaluation is to determine improvements in performance over the current trapezoidal (digital) filter. The evaluation is performed using a customized CANBERRA digital signal processing unit that is fitted with new FPGA designs and any required firmware modifications to support operation of the new filters. The evaluated filters include the cusp, one-over-f (1/f) and pseudo Gaussian filters. The results are compared with the CANBERRA trapezoidal shaper.

1. INTRODUCTION

The purpose of nuclear pulse processing hardware is to deliver the optimum resolution and throughput for a given detector system in a manner the user can readily analyse and interpret. Several factors dictate the appropriate data acquisition and analysis hardware needed for best performance. Count rates spanning several orders of magnitude, transient count rates, different detector and preamplifier modalities, the range of gamma ray energies of interest, dynamic environmental conditions such as temperature, are all factors that must be taken into account when choosing an appropriate digital spectrum analyser for a gamma ray spectroscopy system. Digital signal processors in many applications now replaced analogue electronics for spectroscopy systems due to their superior environmental, count rate stability, and processing flexibility.

The performance of such systems is commonly quantified by energy resolution, stability and throughput. The total Full Width Half Maximum (FWHM) energy resolution W_T of a semiconductor detector depends upon a combination of three factors: the statistical distribution in the number of charge carriers W_D, variations in the charge collection efficiency W_X, and electronic noise W_E [1]. These three parameters add in quadrature: $W_T^2 = W_D^2 + W_X^2 + W_E^2$ .The parameter $W_D^2 = F\varepsilon E$ is directly proportional to the energy E deposited by the gamma ray and to the electron-hole excitation energy ε of the semiconductor material (with a typical Fano factor F = 0.11 for Ge). W_X^2 depends on the detector volume, shape and the intensity of the electric field inside the crystal. Electronic noise is a contributing factor to energy resolution in semiconductor radiation detectors. It has been well described in the literature [2] and is considered to come from only a few different sources.

These sources are:

- The shot noise or the parallel thermal noise due to the detector leakage current

- The series thermal noise generated within the channel of the input JFET in the preamplifier due to the total input capacitance (of detector and FET)
- The 1/f noise generated in the detector itself

The total electronic noise is the quadratic sum of these separate components. In order to reduce the total electronic noise component, the signal from the preamplifier is shaped with characteristic parameters, such as the width or shaping time.

The behaviour of the various noise contributions as a function of shaping time varies depending on the noise source. The series noise deceases as the shaping time increase while the parallel noise behaves the opposite. The 1/f noise though, is independent of the shaping time. Lower shaping times are favoured for high rate application where throughput is desired over resolution, while larger shaping times are typically desired for low rate situation. The best operating values of the shaping characteristic parameters depend on each application. In other words, there could be several optimal case scenarios depending on the trade-off between the minimization of resolution and throughput maximization. The trapezoidal digital shaper is a good example that handles well this trade-off. However, in situations where throughput maximization is not a priority (such as low rate applications) and/or 1/f noise is a major noise component, there are other filters that could yield better energy resolution performance.

2. REAL TIME DIGITAL FILTERS

Noise can be defined as an unwanted signal that obscures the desired signal. It can be thought of a random fluctuation of the signal in electronics circuits and amplifiers. The primary efforts in fabricating a semiconductor detector should be directed towards the minimization of the series, parallel and 1/f noise contributions as much as possible. Shaping techniques are intended to improve the signal to noise ratio. Real time digital pulse shaping techniques allow synthesis of pulse shapes that have been difficult to realize using the traditional analogue methods. Using real time digital shapers, triangular/trapezoidal filters can be synthesized in real time, as described in [3], or in quasi real time, as described in [4]. These filters exhibit digital control on the rise time, fall time, and flat-top of the trapezoidal shape. Thus, the trapezoidal shape can be adjusted for optimum performance at different distributions of the series and parallel noise.

The trapezoidal weighting function (W_F) represents the optimum time limited pulse shape when only parallel and series noises are present in the detector system [2, 5–7]. In the presence of 1/f noise, the optimum W_F changes depending on the 1/f noise contribution. Optimum pulse shapes have been derived, as described in [8] for both cases of 1/f voltage and 1/f current noise sources. In this work, we considered new filter types (see Fig. 1) for processing signals from HPGe and PIPS detectors. The objective of the evaluation is to determine improvements in performance over the current trapezoidal (digital) filter. Two parameters are available to control the each of the filters: rise time (sometimes referred to as integration time) and flat-top (sometimes referred to as charge collection time). The rise time is defined as the times it takes for the shaped signal to go from baseline to the start of the flat-top and the flat-top time is the “wait” time after reaching the flat region.

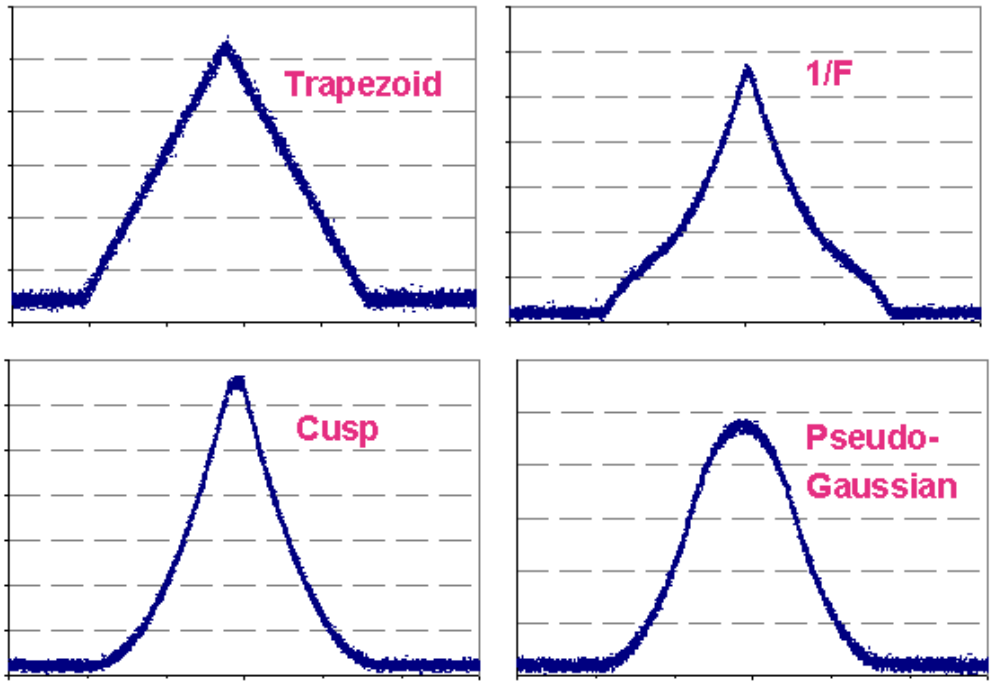

FIG. 1. Actual shaper traces for the trapezoidal, 1/f, cusp and pseudo Gaussian filters using a HPGe detector. The flat-tops for all the filters were set to a very small value for visualization purposes only.

3. EXPERIMENTAL AND RESULTS

The evaluation is performed using a customized CANBERRA digital signal processing unit (LYNX) [4] that is fitted with new FPGA designs and any required firmware modifications to support operation of the new filters. The evaluated filters include the cusp, 1/f and pseudo Gaussian filters. The results are compared with the CANBERRA trapezoidal shaper. A set of detector types is chosen to perform the testing. The choice of detector types was dictated by the expected effect of the filters on the detectors and their availability at the time of the testing. The following CANBERRA detector types were considered:

- BE3820 BEGe: Broad Energy Ge Detectors (LN_2 cooled) [2, 4]
- 30% relative efficiency Medium Coaxial Detector GC3020 (LN_2 cooled) [2, 4]
- X-PIPS Silicon detector (Peltier Cooled) [2, 4]
- GL1015S LEGe: Low Energy Germanium Detector (Canberra Cryo-Cycle Cryostat: redundant electric/LN_2 cooling) [2, 4]
- 52.6% relative efficiency GR5020 REGe: Medium Reverse Electrode Coaxial Detector (LN_2 cooled) [2, 4]

FWHM resolution measurements were performed using ^{55}Fe, ^{57}Co and ^{60}Co sources for the various digital filters by varying the rise time. For each detector, the optimum flat-top is determined based on the trapezoidal filters, and that same value is used for the rest of the filters. The resolution measurements results are shown in Fig. 2 for the REGe, BEGe and XPIPS detectors. The dead-time was approximately 5% with 8.8 μs rise-time and 1.2 μs flat-top for the REGe, 8 μs rise time and 1.2 μs flat-top for the BEGe and 20 μs rise time and 0.2 μs flat-top for the X-PIPS detector. Figure 2(a) suggests that, for short rise times, the trapezoidal filter results in better energy resolutions followed by the 1/f and cusp filters.

The pseudo Gaussian shape gives the worst resolution for almost all the shaping times. We also notice that for larger shaping times the trapezoidal and pseudo Gaussian shapes tend to converge. The same can be concluded for the 1/f and cusp filters too at those large shaping times.

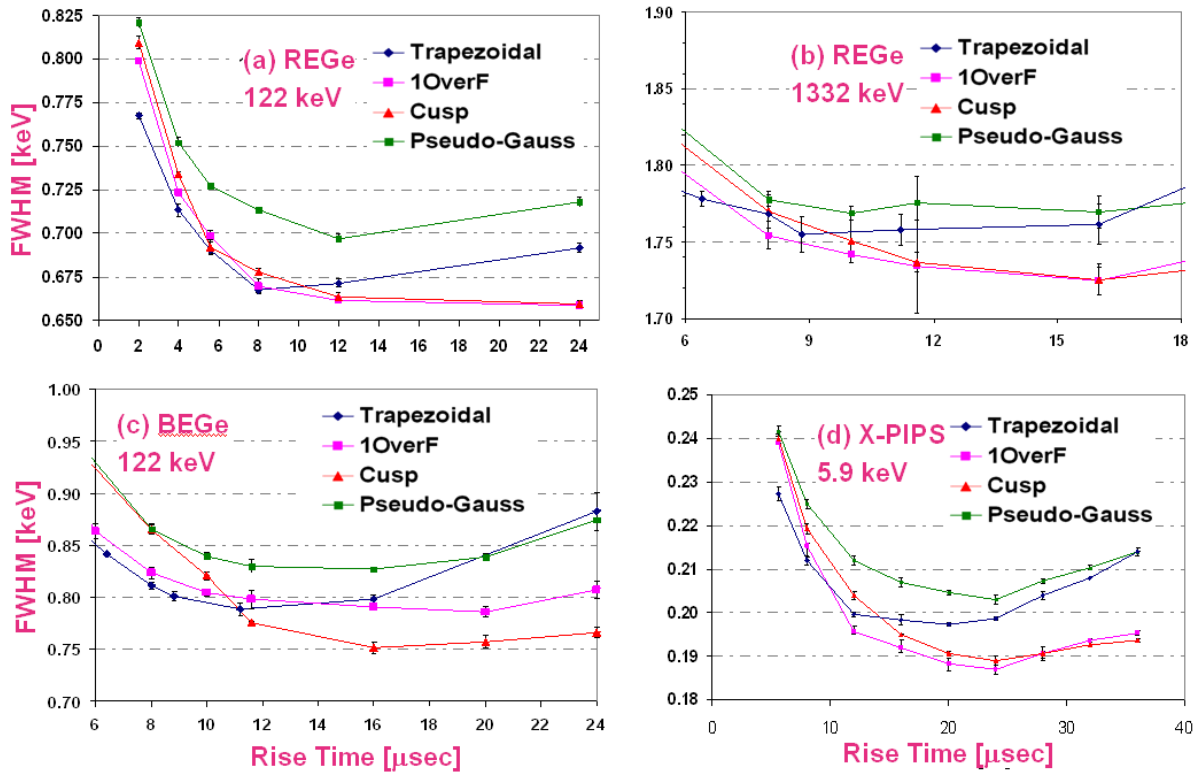

FIG. 2. Energy resolution measurements as a function of the rise time, (a) REGe detector at 122 keV, (b) REGe at 1332 keV, (c) BEGe at 122 keV and (d) X-PIPS at 5.9 keV. The 1-sigma uncertainties shown on the data points are extracted using repeat measurements of the same point and taking the standard error of the mean.

One can conclude that for the REGe and BEGe detectors, the cusp filter type is best for low noise Germanium applications where the system noise is comprised of mainly series (voltage) and parallel (current) white noises sources and the application allows the use of longer shaping times if allowed by throughput requirements. One notes that for the X-PIPS, the 1/f filter type is valuable for silicon X ray applications where the 1/f noise is a significant contributor to the total noise. This situation usually occurs when long shaping times are used to limit contributions from the series (voltage) noise sources, and the parallel (current) noise sources are not significant at this shaping. The medium coax detector showed similar trends as the REGe detector, and the LEGe results were also comparable to the BEGe conclusions.

4. CONCLUSIONS

Several types of filters were tested and proved to be able to improve the energy resolution and count rate performance of systems. From this study, we conclude that the trapezoidal filter is adequate for best energy resolution and high throughput general application. The cusp filter type is best for low noise Germanium applications where the system noise is comprised of mainly series (voltage) and parallel (current) white noises sources. This noise is typically dominated by the electronic (thermal and shot) noise of the preamplifier FET with little flicker (1/f) noise present. The 1/f filter type is valuable for silicon X ray applications where

the 1/f noise is a significant contributor to the total noise. This situation usually occurs when long shaping times are used to limit contributions from the series (voltage) noise sources, and the parallel (current) noise sources are not significant at this shaping. The pseudo Gaussian filter is useful in applications where throughput is not an issue and time constants can be short. Since the signal to noise ratio is not as good as the trapezoidal filter under typical noise conditions, the main value of this filter is the appeal to spectroscopy users that are still using analogue signal conditioning methods. Here, the user should get results comparable to analogue systems, but with much better temperature stability and better reproducibility.

These shapers are serious candidates for field usage and while one might be advantageous under some noise, charge collection and count rate conditions, another might be preferred under different situations. In selecting an appropriate filter to best suit a particular application, there is primarily a trade-off between energy resolution and signal throughput at high counting rates. The filters described in this paper are impractical to implement using analogue electronics, hence the need for digital signal processing which allows great flexibility and the ability to maintain high signal quality almost indefinitely.

REFERENCES

[1] OWENS, A., Spectral degradation effects in an 86 cm^3 Ge(HP) detector, Nucl. Instr. Meth. A238 (1985) 473.

[2] RADEKA, V., Sci., Low Noise Techniques in Detectors, Ann. Rev. Nucl. Part. 38 (1988) 217.

[3] JORDANOV, V.T., et al, Digital techniques for real time pulse shaping in radiation measurements, Nucl. Instr. Meth. A353 (1994) 261 and JORDANOV, V.T., Real time digital pulse shaper with variable weighting function, Vol 505, Issues 1–2; US Patent 6/844/791.

[4] RIPAMONTI, G., et al, Multiple delay line shaping: a new class of weighting functions suitable for digital signal processing, Nucl. Instr. Meth. A340 (1994) 584.

[5] RADEKA, V., Optimum Signal Processing for Pulse Amplitude Spectrometry in the Presence of High Rate Effects and Noise, IEEE Trans. Nucl. Sci., NS-15 (1968) 455.

[6] GOULDING, F.S., Pulse shaping in low noise nuclear amplifiers: A physical approach to noise analysis, Nucl. Instr. Meth. A100 (1972) 493.

[7] GATTI, E., SAMPEITRO, M., Optimum filters for detector charge measurements in presence of 1f noise, Nucl. Instr. Meth. A287 (1990) 513.

[8] GATTI, E., Geraci, A., Ripamonti, G., Optimum filter for 1f current noise smoothed-to-white at low frequency, Nucl. Instr. Meth. A394 (1997) 268.

VERSATILITY OF MODERN DIGITAL SIGNAL PROCESSING: LYNX® — A PLATFORM FOR GLOBAL SPECTROSCOPY APPLICATIONS

B. ZAKRZEWSKI
Canberra Industries Inc.,
Meriden, USA
Email: bzakrzewski@canberra.com

V.T. JORDANOV
Yantel LLC,
Los Alamos, USA

Abstract

The multichannel analyser (MSA) has been the workhorse of spectroscopic measurements since the 1940s. The MCA has evolved from a very simple device capably of the basic sorting (histogram) of the information into a complete signal processing platform. This presentation begins with a brief history of the MCA and then highlights what makes DSP based solutions better than the analogue based solutions of the past. Since the ADC is a key element of the DSP based instrument the advancements in high speed ADCs will be reviewed in regard to how their speed, number of bits and other performance factors impact the quality of the spectroscopic data. The additional benefits that digital processing brings to the user such as enhanced diagnostic capabilities will also be highlighted. A discussion of advanced data acquisition techniques will be provided to demonstrate the power and versatility of digital instruments such as the Canberra Lynx® Digital Signal Analyzer. Some real world examples are provided to highlight why DSP based instruments can provide the best resolution, count rate performance, spectrum stability and wider dynamic range than previous systems. Results from the Lynx under variable measurement conditions will be provided to enforce these concepts. The value of Loss Free Counting or measurement of short lived sampled or transient events will be reviewed. The value of Time Stamped List mode will be discussed and why this older technique is now being utilized once again within the scientific community. A review of benefits that Multi-Spectrum Scaling mode can bring to a wide variety of measurement applications requiring continuity of measurements will be provided.

1. MCA HISTORY

MCAs have been used for decades to record the energy distributions from radiation sensors of all types. The first MCAs were very low resolution devices based on vacuum tube technology. This existed in the 1940s to measure the pulse height of signals from proportional and scintillation detectors. Because of limited availability of memory, these MCAs were limited to just a few tens of channels resolution. Because of this, there were also electromechanical systems to record events such as the "kicksorter" design (Fig.1). The MCA as we know it today really began in the 1950s with the invention of the transistor and core memory. This allowed the development of MCAs with hundreds and even thousands of channels of resolution. Many of the first MCAs were actually created by stacking single channel analyser circuits together. Once the Wilkinson ADC method was developed, we had all the elements for the modern MCA. MCAs continued to offer more channels, become smaller, less expensive, and more reliable over the years to follow. Portable battery powered MCAs were developed in the 1980s. The real revolution in the industry came in the mid-1990s with the use of digital signal processing methods. These methods have almost completely replaced their analogue counterparts. Digital signal processing provides almost limitless potential to future radiation measurement systems due to its flexibility, stability, and continual decrease in overall cost. Below are major timeline events in the development of MCAs.

1930s: Vacuum tubes replace mechanics
1940s: Proportional and scintillation counters developed that need energy analysis
1944: 12-channel PHA built from SCAs (O. Frish et al Cambridge)
1947: 20-channel PHA (Fruendlich of Cambridge)
1950: Availability of transistors and core memory
1951: Mechanical kicksorter (30 channel, 100 counts/ch, 6 counts per second throughput) (Fig. 1)
1951: Wilkinson ADC method published
1953: First commercial MCA (ORNL design — Atomic Instruments) (Fig. 2)
1955: 200 channel MCA (core memory, Wilkinson ADC — RIDL) (Fig. 3)
1956: RIDL 256, 512, 1024, 2048 channel MCA
1959: First transistorized MCAs
1965: Standard NIM modules
1972: Semiconductor memory
1981: Battery powered MCAs
1993: Digital MCAs (complete digital signal analyser-DSA) (e.g. Fig. 4)

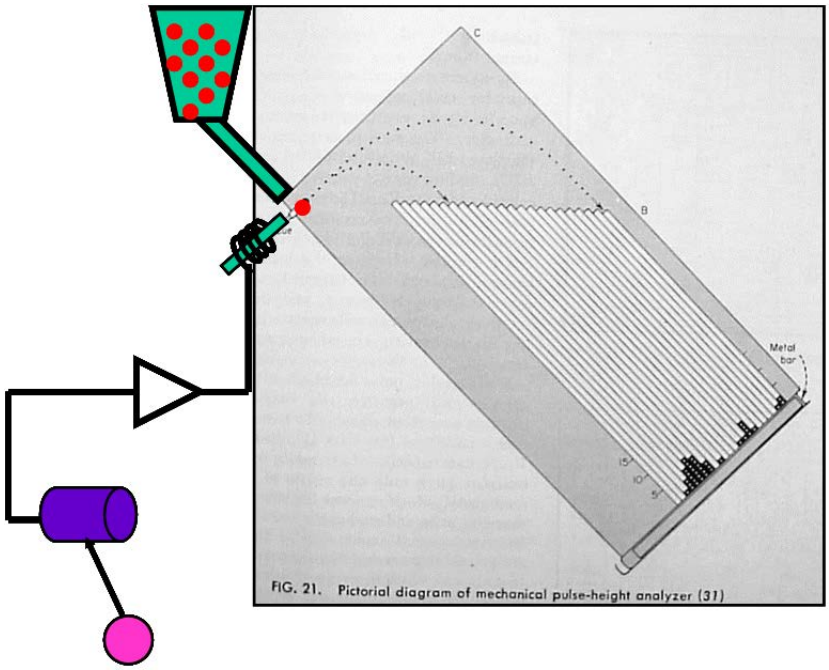

FIG. 1. Mechanical kicksorter (1950) – "When one sees a multichannel kicksorter in all its glory occupying two full-sized relay racks and containing several hundred tubes, one hopes for a simpler approach to the problem" JBH Kuper chair Inst &HP BNL.

2. DIGITAL VERSUS ANALOGUE SIGNAL PROCESSING

Analogue signal processing has served the industry very well over the past 50+ years but has suffered from the limitations of the passive components it is built upon. These components suffer from susceptibility to electric and magnetic fields and exhibit changes with age and temperature. The mainstay of analogue processing has been the ADC and the time invariant linear filter. Both these elements rely on a large number of passive components (resistors, capacitors, inductors) as their critical elements. The use of these components becomes a significant limitation on performance, especially as the complexity of the signal processing and as input rates is increased. Digital signal processing instead relies on digitizing the signal

as close to the sensor (detector) as possible and processing the signal entirely in the digital domain [1]. Once the signal is in the digital domain, it is immune to any external influences.

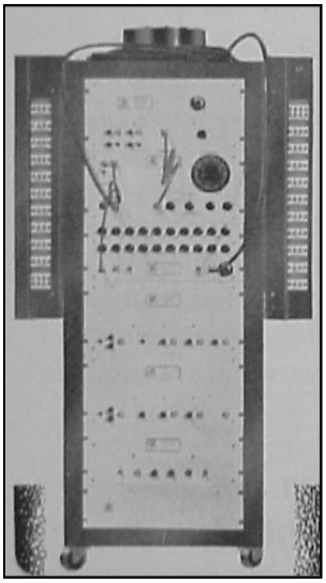

FIG. 2. Atomic Instruments Detector Lab MCA (1953.)

FIG. 3. RIDL 100 channel MCA (1955).

FIG. 4. Modern digital signal analyser (Lynx – Canberra).

Some of the benefits of digital processing are as follows:

- Stability – A digital system does not rely on passive components that can be affected by temperature changes and component aging.
- Noise Immunity – Digital systems have superior noise immunity so they are not affected by external noise sources.
- Complexity – Digital systems are not limited by external electronic component performance. They are not limited to just time invariant linear processing of the signal. With digital processing, one is able to implement processing algorithms that would be otherwise impossible to do so with analogue only systems. This opens up the possibility to utilize additional information contained within the signal such as the pulse shape.

3. DIGITAL MCA FEATURES

3.1. Filter settings

One of the most important functions on a modern DSA is to filter the detector signal using a signal transformation (shaping) that maximizes the signal to noise ratio (S/N). The advantages of digital processing are twofold. In the digital domain, almost any transformation function can be designed with the only limitations being the speed of execution and the desired complexity. The most common signal shape is the trapezoid which allows for very good S/N ratios and the ability to have an adjustable flat-top which can be set to mitigate problem with slow charge collection of the detector (i.e. ballistic deficit). The second DSA advantage is the large number of potential settings that can be used allowing better optimization to the measurement requirements. For example, the Canberra Lynx DSA has adjustable rise times from 0.4 μs up to 51 μs and flat-top times from 0–3.2 μs both in steps of 0.2 μs. The importance of this adjustability is shown in Fig. 5. The noise of a typical semiconductor detector is comprised of a number of different series (voltage) and parallel (current) noise sources that sum together in quadrature. The best resolution is obtain by operating at the minimum point on the noise curve. A DSA that has a large number of settings available can therefore best provide this optimum operating point.

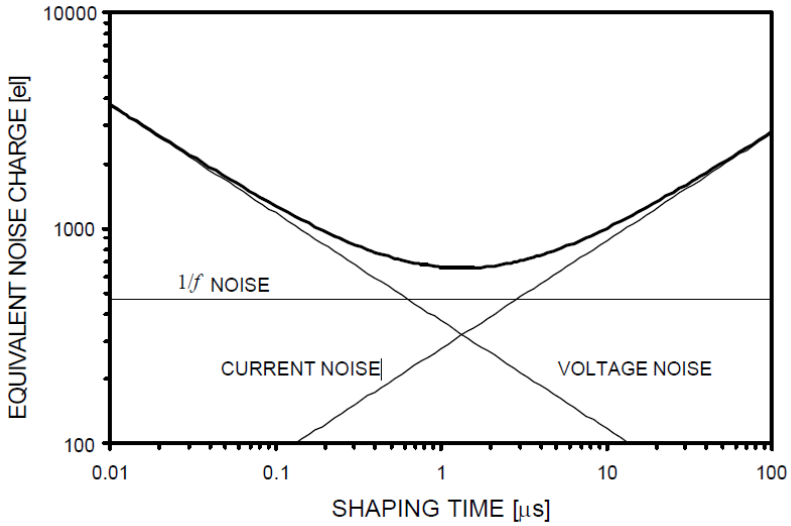

FIG. 5. Shaping versus noise for a typical detector.

3.2. Number of channels

The number of channels can be very important when a wide dynamic range is required. Detector technology continues to improve and the energy range available on these detectors has been extended. An example is a BEGe detector which can be used to make measurements from the 3 keV to 3 MeV with the energy resolutions of well under 1 keV (see Fig. 6). There are also some measurements requiring measurements up to and beyond 8 MeV. With the 32K channels that the Lynx DSA can provide, an 8 MeV measurement with better than 250 eV resolution on the peaks is possible (see Fig. 7).

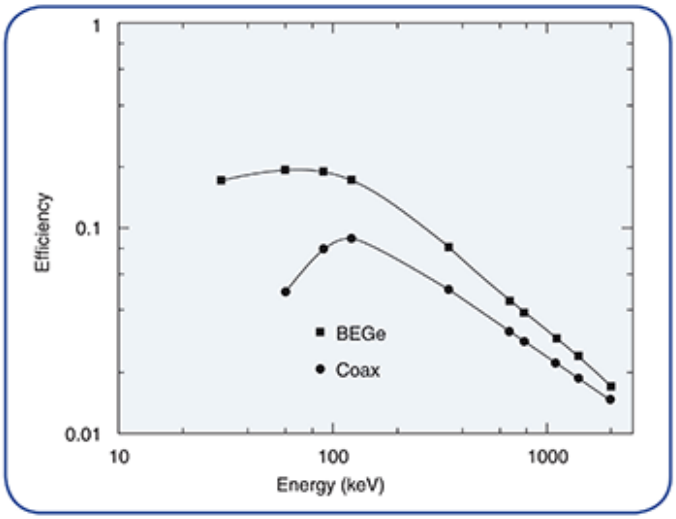

FIG. 6. BEGe versus standard coax efficiency.

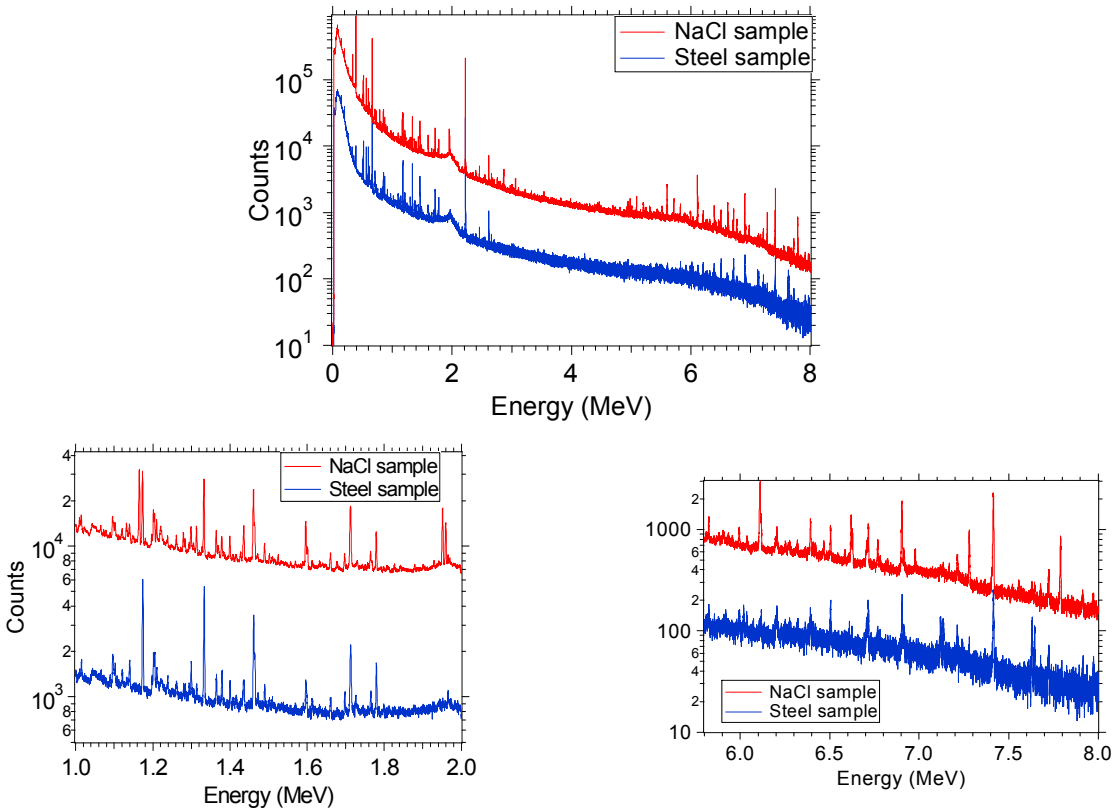

FIG. 7. Spectral measurement of 8 MeV with zoom of 1 to 2 MeV and 6 to 8 MeV.

3.3. Linearity

Just as important is to have both good integral and differential linearity. The former is important to determine the proper energy of the spectral peaks and the latter is important to maintain good peak shape and separation. This is why the number of bits the digitizer offers is important. The greater the number of bits, the lower both non-linearity's will be in the instrument.

3.4. Baseline (BLR – baseline restorer)

The need to maintain a stable baseline is just as important in a digital processor. This includes restoring the baseline between pulses. The real advantage of a digital pulse processor is that the restorer can be very sophisticated in comparison to what can be done in an analogue circuit. Restorers can be gated, asymmetrical, non-linear, and adjust themselves dynamically. They can be as complex or as simple as the application demands. The Lynx has an automatic BLR that dynamically adjusts the restoration based on the count rate. Features such as this can drastically simplify system set-up for the end user.

3.5. Sampling rate

The sampling rate of the digitizer used on the signal analyser is very important whenever both timing and energy information are of interest. For spectroscopic measurements, the digitizer must have enough bits to provide good resolution. If there is a desire to time discriminate, time stamp events, or analyse pulse shape, then sampling rates need to high enough to provide adequate timing information.

3.6. Data collection mode

Just as important as the quality of the spectral data is the method of data acquisition. Many systems need to synchronize acquisition to external equipment or analyse both timing and energy information. Modern DSAs can provide advanced acquisition modes of operation and lots of internal memory. Some of these modes are listed below:

3.6.1. Loss free counting (LFC)

Loss free counting uses a virtual pulser method to sample the system dead time at a high rate in order to determine and correct for counting losses. The virtual pulser method simulates pulses at the DSA stage of the pulse chain, counts these pulses while signal processing is free and busy, and calculates the correction factor to apply to the spectra due to pulse pile-up. Instead of extending the acquisition time based on this correction factor, the VPG operates at 5 MHz and applies this correction factor every tens of microseconds to the output counts in the spectra. LFC is a very useful technique when measuring samples with short decay times with respect to the measurement period. It can also be useful for other high count rate situations to reduce the measurement time. The Lynx offers dual loss free counting which is the ability to store both a corrected and uncorrected spectrum. Figure 10 shows an example of how much better LFC performs when transient sources are present.

3.6.2. Multichannel scaling

Multichannel scaling (MCS) is the ability to record a distribution of events versus time. The Lynx supports MCS with dwell periods down to 1μs.

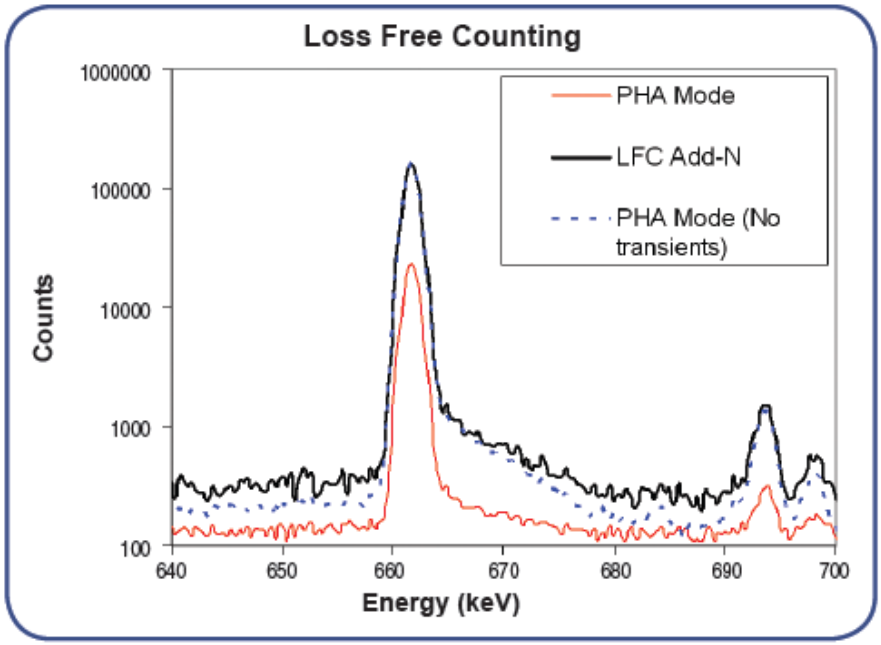

FIG. 8. Comparison between the live time corrected PHA mode (red) and the DLFC mode (black) spectra. Because the ^{137}Cs is introduced transiently for 20 seconds during the 5 min. count, the PHA mode cannot accommodate the rate loss by extending the real time. The dotted blue spectrum is separate count consisting of 20 seconds of live time with the ^{137}Cs source stationary in PHA mode. Note that the DLFC mode correctly accounts for the rate loss.

3.6.3. Time stamped list mode

Time stamped list mode can be used to retain both time of arrival and energy information. The correlation of this information is lost in the normal PHA or MCS histogram process (Fig. 8). List mode provides a record and playback type mechanism. The Lynx DSA can acquire list data at count rates over 300 kHz with time stamp resolutions of 100 ns. Some important reasons to use time stamp list mode include:

- To obtain a true event historical record
- Allows both time and amplitude to be stored
- Great tool for researchers to reanalyse data
- Multiparameter experiments possible when inputs are synchronized
- Ability to stream data to a host computer or server

3.6.4. Multispectral scaling (MSS)

Multispectral scaling is the ability to collect repeated PHA spectra with little to no dead time in between measurements. This feature is important when the user needs to measure samples in motion and have the data collection be synchronized with the motion. One application for MSS is the tomographic gamma scanner (see Fig. 9). The DSA in this case must be synchronized to the rotation of the barrel in order to properly create an image of the contents of the barrel.

FIG. 9. Tomographic Gamma Scanner system that makes use of MSS mode of the Lynx DSA.

4. CONCLUSIONS

Modern digital signal analysers such as the Lynx provide superior performance, stability, resolution and acquisition modes that would be impossible to accomplish with analogue processing methods alone. Some of the main advantages of digital signal processing are:

- Can readily optimize the measurement system for best resolution
- Can measure at high or varying counting rates
- Can provide excellent peak stability
- Can make high resolution measurements over a wide energy range

REFERENCE

[1] JORDANOV, V.T., et al, Digital techniques for real time pulse shaping in radiation measurements, Nucl. Instr. Meth. A353 (1994) 261 and JORDANOV, V.T., Real time digital pulse shaper with variable weighting function, 505 US Patent 6/844/791.

DIGITAL SIGNAL PROCESSING APPLICATION IN NUCLEAR FISSION

O. ZEYNALOVA, SH. ZEYNALOV,
Joint Institute for Nuclear Research,
Dubna, Russian Federation
Email: zeinal@nf.jinr.ru

F.-J. HAMBSCH, S. OBERSTEDT
Institute for Reference Materials and Measurements,
Joint Research Centre of European Commission, Belgium

Abstract

Digital signal processing algorithms for nuclear particle spectroscopy are described along with a digital pile-up elimination method applicable to equidistantly sampled detector signals preprocessed by a charge sensitive preamplifier. The signal processing algorithms are provided as recursive procedures that can be easily programmed using modern computer programming languages. The influence of the number of bits of the sampling analogue to digital converter to the final signal to noise ratio of the spectrometer is considered. The pile-up elimination method was originally developed for fission fragment spectroscopy using a Frisch-grid back-to-back double ionisation chamber and was mainly intended for pile-up elimination in case of high alpha-radioactivity of the fissile target. The influence of the pile-up elimination scheme on the final resolution of the spectrometer is investigated in terms of the distance between piled-up pulses using high a purity germanium detector. The efficiency of the developed algorithms is compared with other signal processing schemes published in literature.

1. INTRODUCTION

The basic element of a nuclear spectrometer is a detector combined with a charge sensitive preamplifier. The measurement of the kinetic energy of a radiation particle relies on the processing of the electric current pulse created by the motion of the free electrons/holes released during the ionization of the detector material. The time dependence of the detector current also conveys information on the ionization density along the ionizing particles' deceleration path. The total number of free electrons/holes is proportional to the particle kinetic energy, which can be evaluated as the integral of the current flown through the detector. The step-like pulse at the output of a charge sensitive preamplifier (CSPA) is the result of an integration of the detector current. The height of the pulse is proportional to the total charge produced during the deceleration of the charged particle. This pulse height can be measured as the difference between the baseline (before the particle hits the detector) and the peaking value (after total charge collection was done) of the pulse after filtering out the useless high frequency components with the help of a shaping filter amplifier (SFA).

This principle is implemented in commercially available nuclear electronic modules performing signal processing that can be represented as a sequence of mathematical procedures applied to the waveform of a continuous signal. Sometimes, when pulse shape information is needed, the analysis of the detector current signal can be more convenient. The current pulse can be converted into a step pulse by digital integration and vice versa. The output pulse of the SFA can have either a Gaussian or flat-top pulse shape that can be used as the input to a peak sensing analogue to digital converter (ADC) for pulse height analysis. From a mathematical point of view, one can consider the signal evolution from the detector to the ADC as a sequence of transformations that can be described by precisely defined mathematical expressions. For example, the CSPA integrates the input current pulse, the SFA convolutes the output signal of the preamplifier with a kernel function defined by the shaping parameters of the SFA and, the ADC converts the peak value of the shaped pulse to a digital output value. Recently, using waveform digitizer (WFD) the abovementioned mathematical transformations implemented in analogue electronic modules can be implemented software-wise using digital signal processing (DSP) algorithms. Some examples of the implementation

of DSP techniques to nuclear particle spectroscopy are reported in Refs. [1–5], where the analogue pulse processing modules with continuous time signals were replaced by direct calculations with sampled signals — discrete values taken from a continuous signal at equidistantly separated points.

2. HARDWARE AND SOFTWARE USED IN MEASUREMENT

Detector pulses were digitized using a TDS3054B digital storage oscilloscope from Tektronix Inc. as shown in Fig. 1. The TDS3054B allowed signal digitization with an accuracy of 8-bit and with a frequency of up to 5×10^9 samples/sec. Four waveforms of 10000 samples each can be simultaneously recorded in the local memory of the oscilloscope, controlled by a remote PC via Ethernet connection. Data exchange between the oscilloscope and the PC was facilitated by the TekVISA software library easily accessible from the Tektronix Inc. company web site. Both the data acquisition and the data analysis software were developed using Microsoft Visual C++ for Windows XP. Let us consider, for example, a high purity germanium (HPGe) detector irradiated by a ^{60}Co calibration source. Detector pulses after being processed by a CSPA (with -3 dB bandwidth of ~15 MHz) were digitized by the oscilloscope with 250 MHz and 8-bit (256 levels) accuracy.

According to Shannon's theorem [6], the digitization is a lossless procedure if the signal sampling frequency is more than 2*F, where F is the signal bandwidth. Let us consider Fig. 1 where the block diagram of the CSPA is presented to demonstrate the transformation of the detector signal. Let t being the time interval passed from the start of the measurement when the particle hits the detector and $I(t)$ is the instant value of the electric current flowing through the detector at time t. Assuming a particle entering the detector at $t=0$, the following relation between the detector current and the preamplifier output voltage $V(t)$ is valid:

$$V(t) = \int_0^\infty I(\tau)h(t-\tau)d\tau \qquad (1)$$

The measured output $V(t)$ can be used directly for the determination of the total charge created by the particle provided that $h(\tau)$ is known or determined in a separate measurement. Thanks to digitization, the solution of Eq. (1) with respect to $I(\tau)$ becomes possible allowing a direct evaluation of the detector current and the total charge.

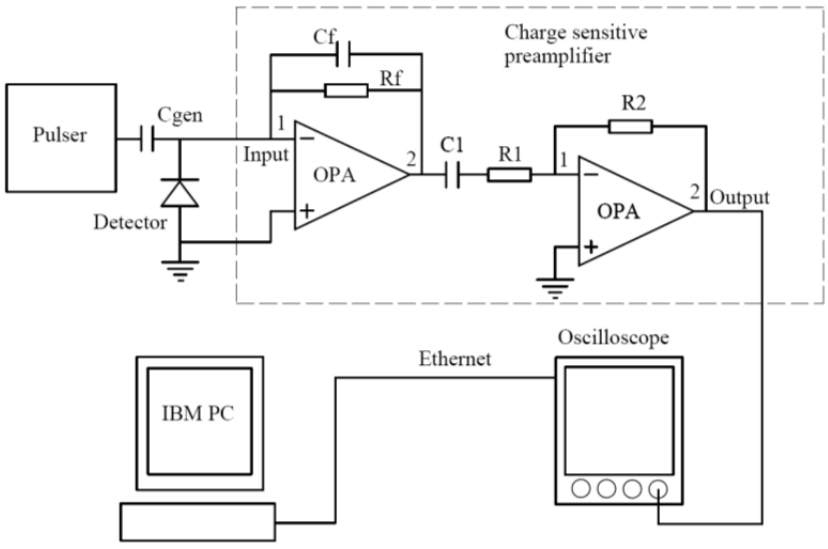

FIG. 1. Generalized block diagram of a charge sensitive preamplifier along with the data acquisition system.

3. IMPLEMENTATION OF THE DIGITAL PULSE SHAPING ALGORITHMS

Equation (1) provides the relation between the preamplifier output signal and the detector current caused by the ionizing particle, can be used as a starting point for the determination of the particle's kinetic energy. For the function $h(t-\tau)$ the approximation that can be represented analytically in Eq. (2) as is simpler, but it produces practically the same final result as the precise one.

$$h(t-\tau)=\begin{cases}\dfrac{1}{\alpha}\exp(-(t-\tau)/\alpha), t\geq\tau;\\ 0, t<\tau;\end{cases} \qquad (2)$$

The parameter α is the decay time of the preamplifier and is in the range of 50–100 μs. A δ-function like current pulse applied to a charge sensitive preamplifier input produces according to Eq. (1) a steplike output signal with fast rise time and exponential decay time α. The height of the pulse is proportional to the total charge composing the current pulse, hence to the kinetic energy of the ionizing particle. In the present measurement, the output signal of the preamplifier was digitized and stored for further off-line DSP analysis. An input function *i(t)* for the detector current can be found from Eq. (9) using the following recursive expression:

$$i_k=\lambda v_k - v_{k-1},\ k=0,1,2,\ .....N \qquad (3)$$

where $i_k=i(t_k)$, $v_k=v(t_k)$ are values taken at the sampling points t_k, $i_0=0$, and $\lambda=\exp(1/\alpha)$ is defined by the used preamplifier. The detector current pulses found with the help of Eq. (3) shown in Fig. 2 were used for pileup detection using the following criterion. If the distance between a two successive pulses was less than the predefined value, then the pile-up was flagged.

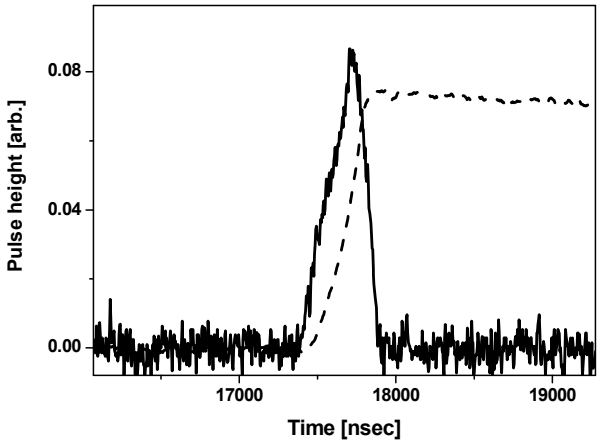

FIG. 2. The upscaled current pulse i(t) (solid line) found as the solution of Eq. (3) using the output pulse of the CSPA (dashed line) after smoothing.

In the optimal analogue signal processing procedure [8] the signal V*(t)* passed the C-R (circuit consisting of a serially linked capacitance – C and a resistance – R) differentiator with the transfer function as follows:

$$Df(\tau) = \delta(\tau) - \frac{1}{A}\exp(-\frac{\tau}{A}) \tag{4}$$

where δ(τ) is Dirac's delta-function and A is a shaping constant. The output of the differentiation circuit is a roughly estimated current pulse obtained above using Eq. (3). The differentiation is followed by 3-4 successive R-C (circuit consisting of a serially linked resistance – R and a capacitance – C) integrations with the following transfer function:

$$Int(\tau) = \frac{1}{A}\exp(-\frac{\tau}{A}) \tag{5}$$

After differentiation, the step-like function is transformed into an exponential decay function with the peak value proportional to the total charge value collected on the detector electrode. Successive integrations are needed to improve the signal to noise ratio resulting in an almost Gaussian shaped pulse. Historically, signal processing using Eqs. (4) and (6) was derived by optimization of the SNR using signal filtering after differentiation [7]. If the *W(t)* is casual filter then at *t* is chosen long enough the following equation describes the transformations in (4) and (6):

$$V^{Out}(t) = \int_0^t \frac{dV^{In}(\tau)}{d\tau} W(t-\tau)d\tau = -\int_0^t V^{In}(\tau)\frac{dW(t-\tau)}{d\tau}d\tau \tag{6}$$

It can easily be verified that the convolution of $\frac{dV^{In}(t)}{dt}$ with the weighting function:

$$W(\tau) = \frac{1}{A}\exp(-\frac{\tau}{A}) \tag{7}$$

is equivalent to the transformations given by Eqs. (4) and (5). The peak value of $V^{Out}(t)$, corresponding to the total measured charge of the ionizing particle, is proportional to the particle's kinetic energy. If Δ is the sampling period then, using substitutions

$V_k^{In} = V^{In}(k\Delta)$, $V_k^{Out} = V^{Out}(k\Delta)$ and $V_k^{Int} = \int_0^\infty V^{In}(\tau)\frac{dW(k\Delta-\tau)}{d\tau}d\tau$,

one can get the following relations from Eq. (6) and Eq. (7):

$$V_{k+1}^{Int} = V_k^{Int}A + V_k^{In},\ V_k^{Out} = V_k^{Int} - V_k^{In} \tag{8}$$

Applying N subsequent integrations using the relation $V_{k+1}^{Int} = V_k^{Int} \times A + V_k^{In}$, where at each next step the output signal from the previous step is treated as the input signal for the next step, is identical to passing the signal through a CR-RC^n – filter. Fig. 3 illustrates how a step-like pulse is transformed when passed through the CR-RC^4 filter. For a trapezoidal filter as shown in Fig. 4 the following recursive expression was obtained:

$$V_{k+1}^{Out} = V_k^{Out} - (V_{k-T+1}^{In} + V_{k-T-A}^{In} - V_{k-1}^{In} + V_{k-2T+1-A}^{In}) \tag{9}$$

The meaning of constants A and T is indicated in Fig. 4. For practical implementation, the following recursive formula for CR-RC^4 is more suitable:

$$
\begin{aligned}
&y(n) = a_0 \times x(n) + a_1 \times x(n-1) + \sum_{i=1}^{5} b_i \times y(n-i), \\
&a_0 = (1-x)^4 \times \frac{1+x}{2}, a_1 = -a_0, \\
&b_1 = 5 \times x, b_2 = -10 \times x^2, b_3 = 10 \times x^3, b_4 = -5 \times x^4, b_5 = x^5, \\
&x = \exp\left(-\frac{1}{T}\right).
\end{aligned}
\tag{10}
$$

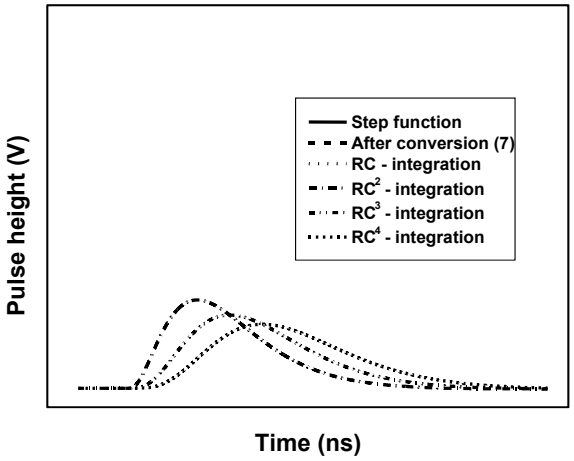

FIG. 3. Transformation of a step-like pulse passing through the stages of CR-RC^4 filter.

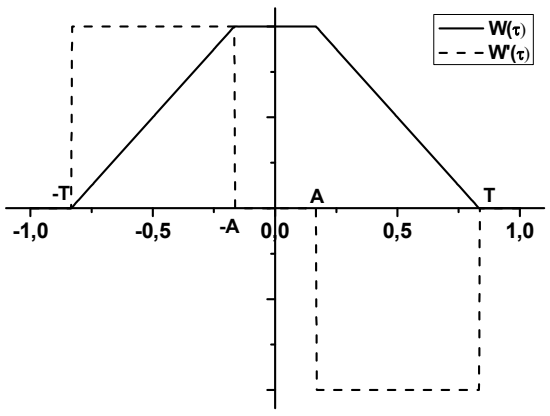

FIG. 4. The graph of the trapezoidal filter W(τ) and its derivative W'(τ).

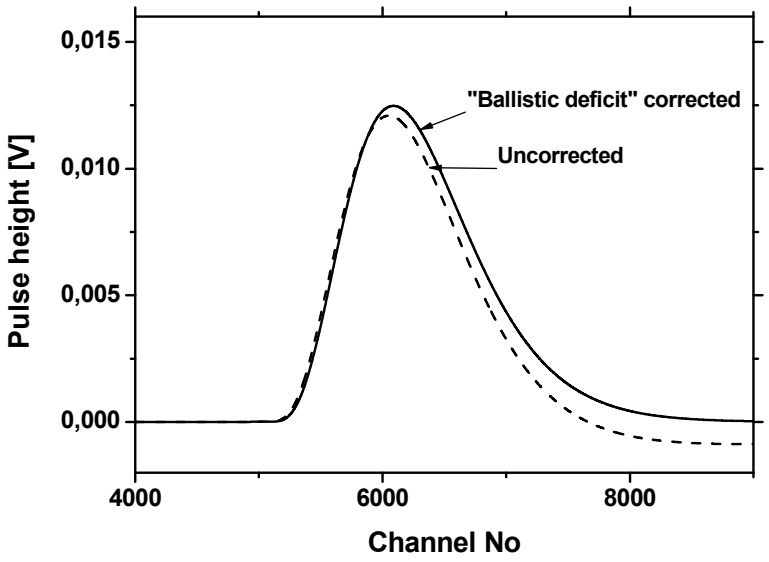

FIG. 5. Output pulse of the CR-RC^4 filter when a step-like pulse is applied to the input.

The output pulses of the CR-RC^4 (T = 2500 ns) and trapezoid filters (T = 1000 ns, A = 400 ns) are shown in Figs 5 and 6, respectively. As an example, a pulse height distribution for a ^{60}Co source using HPGe detector and the oscilloscope, presented in Fig. 7, is acquired using the CR-RC^4 shaping algorithm. The resolution was found to be 2.15 keV.

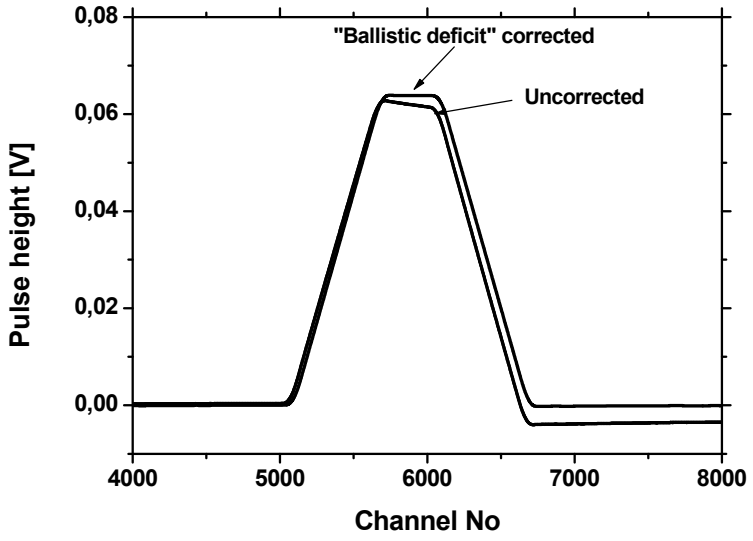

FIG. 6. Output pulse of the trapezoidal filter when a step-like pulse is applied to the input.

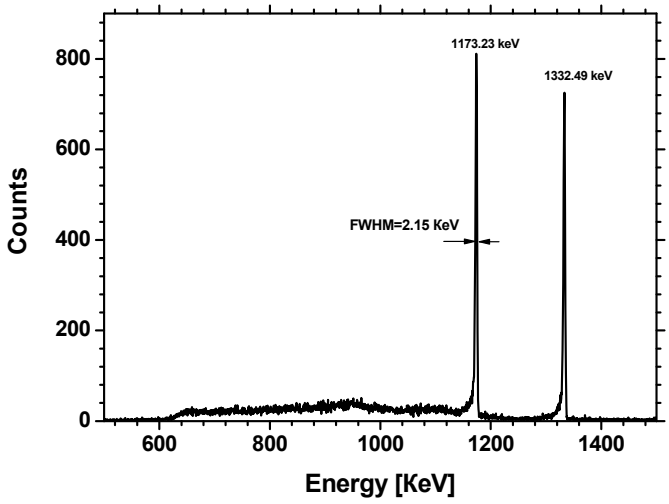

FIG. 7. Energy spectrum constructed from waveforms acquired during a measurement with a ^{60}Co calibration source.

4. FILTER DESIGN

Digital filter can be easily constructed using elementary filters RC (serial resistance–capacitance link) and CR (serial capacitance–resistance link) with the following procedure.

Let us consider one of the popular spectroscopy shaping amplifier, made up of single CR and 3–4 RC circuits. A RC circuit and its response to the step pulse functions are plotted in Fig. 8.

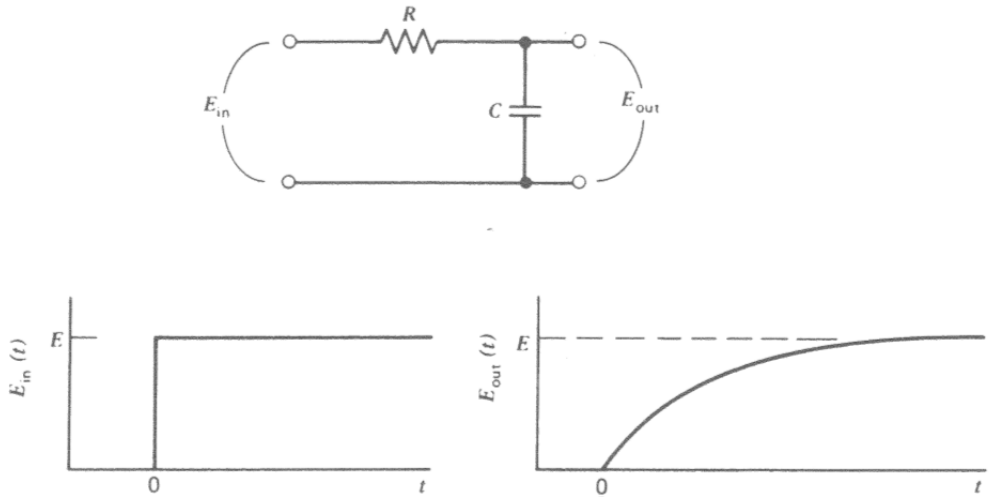

FIG. 8. RC circuits and response to the input step pulse.

Permutation of the resistor and capacitor transforms RC to CR circuit. Using the basic electricity laws (Ohm laws) one can get the following equation connecting the input and output signals:

$$E_{in}(t) = \frac{1}{C}\int i(t)dt + Ri(t) \rightarrow \frac{dE_{in}(t)}{dt} = \frac{i(t)}{C} + R\frac{di(t)}{dt} \qquad (11)$$

The solution of the equation provides the relation between input and output signal as follows:

$$E_{out}(t) = E_{in}(t) - \frac{1}{C}\int_0^{\infty} E_{in}(\tau) * \exp(-\frac{(t-\tau)}{RC})d\tau \qquad (12)$$

Similarly, the relation between input and output pulses for RC circuit can be found as:

$$E_{out}(t) = \frac{1}{C}\int_0^{\infty} E_{in}(\tau) * \exp(-\frac{(t-\tau)}{RC})d\tau \qquad (13)$$

It should be noticed that the output signal $E_{out}\ (t)$ is a convolution of the input signal $E_{in}\ (t)$ with the kernel function $h(t-\tau) = RC * \exp(-\frac{(t-\tau)}{RC})$, which is fully defined by the parameters of the RC circuit.

In DSP continuous function is converted into sampled form and all mathematical transformations is performed with sampled signal (one dimensional vector). The kernel $h(t-\tau)$ also is transformed to sampled form two dimensional matrix. Using discrete representation Eq. (13) can be converted into the following form:

$$\vec{E}_{out} = \vec{E}_{in} \times M_{\phi} \qquad (14)$$

where vectors $\vec{E}_{in}, \vec{E}_{out}$ are represent the sampled input and output signals respectively. The matrix M_{ϕ} represents the digital filter. Use of this representation simplifies a complex digital filter design. For example, to construct CR – filter one needs to define the matrix $M_{\phi}[i,j] = \exp(-\frac{(t_i - \tau_j)}{RC})$, bearing in mind that a physically feasible filter should satisfy the condition $t_i \geq \tau_j$. Then the output signal can be found as:

$$\vec{E}_{out} = \vec{E}_{in} - \vec{E}_{in} \times M_{\phi} \qquad (15)$$

The result of passage of the signal trough the four consecutive RC filters can be expressed as:

$$\vec{\vec{E}}_{out} = \vec{\vec{E}}_{in} \times M_{\phi} \times M_{\phi} \times M_{\phi} \times M_{\phi} \qquad (16)$$

Below, formulae are listed which are useful for interpolation of signal values between samples:

Parabolic interpolation

$$f(t_k+\Delta)=a(t_k+\Delta)^2+b(t_k+\Delta)+c$$
$$a=(f(t_{k+2})-2f(t_{k+1})+f(t_k))/2;\ b=f(t_{k+1})-f(t_k)-a(2k+1);\ \mathrm{c}=f(t_k)-bk-ak^2$$

Cubic parabolic interpolation

$$f(t_k+\Delta)=a(t_k+\Delta)^3+b(t_k+\Delta)^2+c(t_k+\Delta)+d$$
$$a=\frac{f(t_{k+2})-3f(t_{k+1})+3f(t_k)-f(t_{k-1})}{(k+2)^3-3(k+1)^2+3k^3-(k-1)^3},$$
$$b=\frac{f(t_{k+2})-2f(t_{k+1})+f(t_k)-a((k+2)^3-2(k+1)^3+k^3)}{2}$$
$$c=f(t_{k+2})-f(t_{k+1})-(2k+3)b-a((k+2)^3-(k+1)^3)$$
$$d=f(t_{k+2})-c(k+2)-b(k+2)^2-a(k+2)^3$$

RC^4 - filter in time domain

$RC^4(t,\tau)=\frac{1}{N}\frac{1}{\tau*3!}*(\frac{t}{\tau})^3*\exp(-\frac{t}{\tau})$, where N is normalization parameter τ is shaping parameter.

Butterworth filter of order 2n in frequency domain

$$B(\nu,\nu_0)=\frac{(2*\cos(\pi\nu))^{2n}}{(2*\cos(\pi\nu))^{2n}+(\frac{2}{\pi\nu_0}*\sin(\pi\nu))^{2n}}$$

where ν_0 is cut–off frequency.

5. INVESTIGATION OF PILEUP ELIMINATION SCHEME AND IMPLEMENTATION TO FISSION FRAGMENT SPECTROSCOPY

The pulse height measurement procedures, as described in the previous paragraph, is supposed to work with isolated pulses, i.e. pulses separated from each other by a time long enough to make influence of the pulses to each other negligible. In practice the distance between successive pulses, stimulated by nuclear particles, are random values having Poisson distribution. The pulse isolation method developed in present work, removes any additional pulse if one is detected at the time shorter than the double width of the shaping filter. The procedure influence the pulse height spectrum resolution, therefore the measurement procedure developed to investigate the spectrum degradation on the time between successive detector current pulses is illustrated in Fig. 9. The area occupied by the detected pileup pulse in the waveform (right hand part of Fig. 9) was forced to zero and then the target pulse height was calculated using pulse processing with the CR-RC^4 or the trapezoidal shaping as was described in the previous paragraph.

Unfortunately, even though forcing the area in the vicinity of the analysed pulse to zero does not affect the pulse itself, it influences the noise, eventually degrading the resolution of the spectrometer. Obviously, the scale of such an influence can be investigated by comparing the spectrometer resolution, when pileup flagged waveforms are completely excluded from the analysis, with the resolution, when the pileup elimination scheme was implemented. As was mentioned above at the available source intensity almost 100% of the acquired events were free of pileups. Therefore, pileup pulses were simulated by forcing of the average signal width time interval to zero and the resolution was compared with the resolution measured with undisturbed waveforms. The time between the analysed pulse and the simulated pileup was fixed to a certain value and the entire acquired data set was analysed to determine the resolution for the 1.173 MeV line of the ^{60}Co source. The procedure was repeated with different times between pulse and simulated pileup, and the dependence of the resolution on the time was measured and plotted in Figs 10 and 11 for the CR-RC^4 and for the trapezoidal filters, respectively.

In high resolution fission fragment spectroscopy with a double back to back Frisch gridded ionization chamber, usually the main cause of the pileup pulses is alpha radioactivity of the fissile sample, for example, the radioactivity of 0.5 mg ^{239}Pu target is 1 MBq. The measurement procedure at such high counting rates with use of CSPA (most common choice) usually can be arranged in the following way. The output signal of the preamplifier passes a differentiator with short time constant (~ 4 μs) in order to reduce the DC offset of the signal due to pile-up. Then the output pulse of the differentiator is sampled and using Eq. (3) is converted into the current pulse waveform. The pileup pulses are removed from the waveform as was described above and then the current pulse integrated using trapezoidal filter with ~ 1.5 μs width. For fission fragment mass spectroscopy a double back to back Frisch gridded ionization chamber has an energy resolution of ~ 600 keV [8]. The contribution of the electronic noise to this value measured with the help of a precision pulse generator was found to be less than 50 keV. Taking into account the results of the HPGe detector measurements, one can expect almost no degradation of the resolution for fission fragment spectroscopy when the pileup elimination scheme is implemented. This conclusion can open new perspectives for fission fragment mass and kinetic energy measurements from targets with high intrinsic alpha radioactivity such as ^{239}Pu, ^{241}Am, ^{245}Cm, because the pileup elimination scheme does not significantly influence the final energy resolution of the spectrometer.

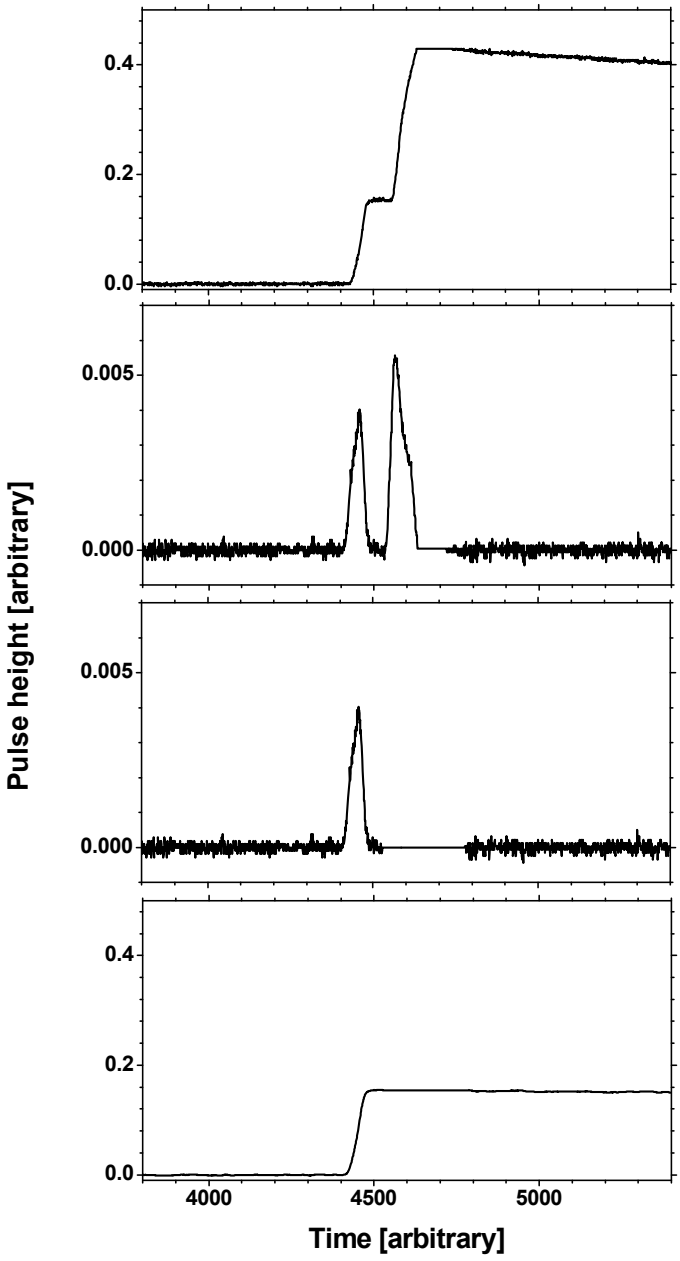

FIG. 9. The graphs demonstrate the sequence of pile-up elimination procedure.

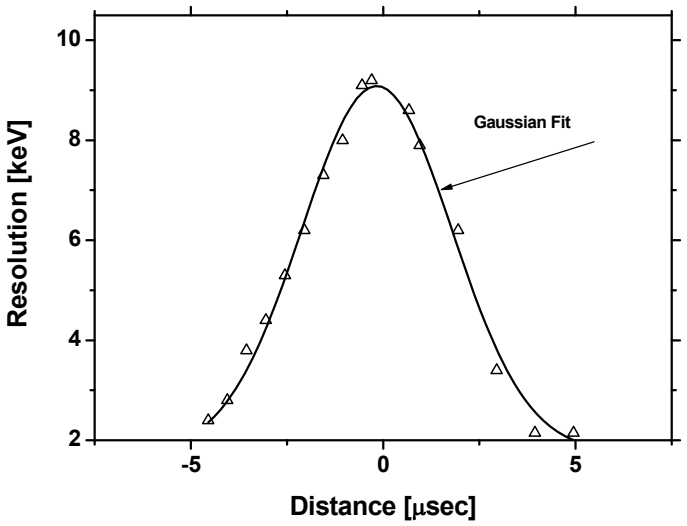

FIG. 10. Resolution as a function of the time between the original pulse and the simulated pile-up pulse for the CR-RC^4 filter.

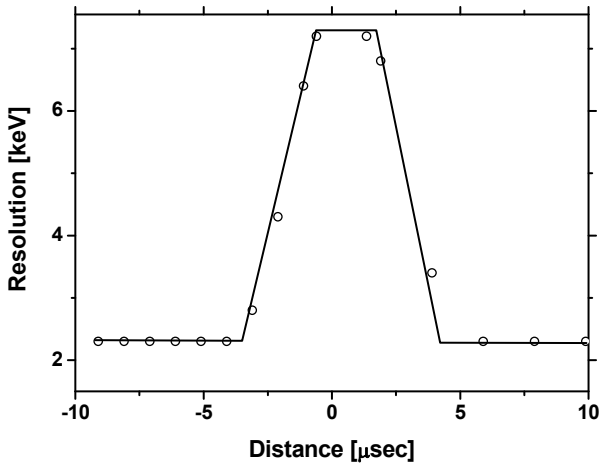

FIG. 11. Resolution as a function of the time between the original pulse and the simulated pile-up pulse for the trapezoid filter.

6. DIGITIZATION, SAMPLING NOISE AND NUMBER OF BITS

The measurement was performed using a HPGe detector and the TDS3054B oscilloscope (ENOB = 6.2 according to AnalogueDevices, Fundamentals of sampled data systems", AnalogueDevices, Application note AN-282.) as the waveform digitizer. The energy resolution determined from the spectrum being 2.15 keV FWHM for the 1.173 MeV line of the ^{60}Co source was achieved with an RC-CR^4 shaping. The parameter A = 4000 ns was chosen both for differentiator (Eq. 12) and integrator (Eq. 13). For comparison the procedure described in Ref. [9] was implemented for the analysis of the same data set, where the pulse height was calculated as the difference between values averaged in two windows of the same

width selected at the fixed position and symmetrically in respect to the step. From calculation point of view, the last procedure seems similar to the trapezoidal filtering considered above. The difference is that in the analysis with a trapezoidal filter the maximum value of the difference is selected between sequential values calculated for moving windows, but the procedure of Ref. [9] gives the difference at a predefined point, which cannot guarantee the maximum for arbitrary waveform.

Using widths of both windows of 10000 ns selected symmetrically in respect to the trigger position, a FWHM of 2.90 keV for the 1.173 MeV line of the ^{60}Co source was obtained, which is more than 40% worse than in the analysis with a trapezoidal filter. The first reason of degradation of the resolution is that the procedure described in Ref. [9] does not guarantee the best SNR value according to Ref. [7] (the best SNR can be achieved at the peak of the filtered signal). The second reason is that the present filtering procedure in contrary to the procedure with fixed positions of the windows, utilizes the full dynamic range of the signal including its rising edge. Apparently, a signal dynamic range limitation reduces the ENOB of the WFD increasing the sampling noise. Comparison of different signal processing results are summarized in Table 1, where the resolution is determined both for signals from the gamma source and for fixed pulse height signals from the precision pulse generator.

The energy resolution of the spectrometer with a HPGe detector depending on the analogue pulse processing electronic noise was investigated thoroughly in literature [7]. For the considered digital spectrometer, the sampling noise introduced by the WFD should be taken into account. Sampling and electronic noise are obviously uncorrelated and their effect on the detector resolution is additive, resulting the spectrometer resolution due to sampling and electronic noise of 1.4 keV (see Table 1). As it was mentioned above, the definition of ENOB according to Eq. (7) includes both sampling and the sampling ADC apparatus generated (differential nonlinearity, missing codes, temperature drift, etc.) noise. Assuming that only apparatus generated noise $s_x(t)$ applied to the input of the WFD and processed by the CR-RC^n or trapezoid algorithm, having impulse response function $w(t)$ one can determine the outputs $s_y(t)$, using the following well known formula:

$$\mathrm{s_y}(t) = \int_0^\infty w(t-\chi)s_x(\chi)d\chi \qquad (17)$$

The sampling noise improve factor (SNIF) after the signal passes through the filter with transfer function $w(t)$ can be calculated as the ratio $\sqrt{\overline{\mathrm{s_y^2}(t)}}\,/\,\sqrt{\overline{\mathrm{s_x^2}(t)}}$. To evaluate numerically the SNIF, the $s_x(t)$ was simulated considering sampling noise as a random discrete function homogenously distributed in the interval $[-1/2^{\mathrm{ENOB+1}}, 1/2^{\mathrm{ENOB+1}}]$ and sampled with the frequency of 250 MHz. The CR-RC^4 and the trapezoidal filters with response functions normalized to produce the unity height output pulse from the unity height input step function. Results of calculations are listed in Table 1 and can be compared with conventional analogue peak sense ADC, having N bits resolution. In this sense the sampling ADC used in our experiment is equivalent to the peak sense ADC having resolution ~11.8 bit.

TABLE 1. ENERGY RESOLUTION FOR DIFFERENT SFA MEASURED USING THE PULSE GENERATOR AND A ^{60}CO SOURCE

Filter	Pulser (keV)	1173.2 keV ^{60}Co line (keV)	SNIF
CR-RC^4	1.40	2.15	48
Trapezoidal	1.40	2.20	48
Ref. [11]	2.00	2.90	-

7. CONCLUSIONS

Signal processing algorithms described in this work were provided as recursive computational procedures that can be easily used for computation. From the sampled waveform of a detector signal amplified by a charge sensitive preamplifier, the detector current signal was first reconstructed and then used for pileup elimination and true ballistic deficit correction of the detector charge. The pileup elimination method can be effective for fission fragment spectroscopy as was demonstrated in this work using gamma ray spectroscopy as a simulation model.

REFERENCES

[1] GEORGIEV, A. GAST, W., Digital pulse processing in high resolution high throughput and gamma ray spectroscopy, IEEE Trans. Nucl. Sci. 40 (1993) 770–779.

[2] PULLIA, A., et al., Quasi-optimum γ and X spectroscopy based on real-time digital techniques, Nucl. Instr. Meth. A439 (2000) 378–384.

[3] BARDELLI, L., et al, Digital sampling systems in high resolution and wide dynamic-range energy measurements: Comparison with peak sensing ADCs, Nucl. Instr. Meth. A560 (2006) 517–523.

[4] KIHM, T., et al, A digital multi-channel spectroscopy system with 100 MHz flash ADC module for the GENIUS-TF and GENIUS projects, Nucl. Instr. Meth. A498 (2003) 334.

[5] KALININ, A.I., et al, Pulse shaping for Ge-spectrometers optimized for ballistic deficit and electronic noise, Nucl. Instr. Meth. A538 (2005) 718–722.

[6] MAX, J., Méthodes et techniques de traitement du signal et applications aux mesures physiques. Troisième Edition, MASSON (1981).

[7] RADEKA, V., Optimum signal processing for pulse-amplitude spectrometry in the in the presence of high-rate effects and noise, IEEE Trans. Nucl. Science 15 (1968) 455–470.

[8] BUDZ-JØRGENSON, C., KNITTER, H.H., STREADE, CH., HAMBSCH, F.J., VOGT, R., A twin ionization chamber for fission fragment detection, Nucl. Instr. Meth. A258 (1987) 209.

[9] KHRIACHKOV, V.A., et al, Low-background spectrometer for the study of fast neutron-induced (n,α) reactions, Nucl. Instr. Meth. A444 (2000) 614–621.

RECENT RESULTS FROM INVESTIGATION OF PROMPT FISSION NEUTRON EMISSION IN SPONTANEOUS FISSION OF ^{252}CF

SH. ZEYNALOV, O. ZEYNALOVA
Joint Institute for Nuclear Research,
Dubna, Russian Federation
Email: zeinal@nf.jinr.ru

F.-J. HAMBSCH, S. OBERSTEDT
Institute for Reference Materials and Measurements
Joint Research Centre of European Commission, Belgium

Abstract

The main motivation of the present work was investigation of the nature of anomalous (from the point of view of modern theory) dependence of the average prompt fission neutron number on the total kinetic energy of the fission fragments using modern digital signal processing approach. A twin Frisch-grid ionization chamber was used for fission fragment mass and kinetic energy spectroscopy. A fast neutron detector with NE213 (or analog) scintillation liquid was used for prompt fission neutron time of flight measurement. About 10^7 fission events, coinciding with prompt fission neutron detection was acquired in the experiment. Correlated fission fragment kinetic energies, their masses, an angle between fission axis and the prompt fission neutron, the prompt fission neutron velocity were measured with help of eight channel set-up of synchronized waveform digitizers, having 100 MHz sampling frequency and 12-bit pulse height resolution. Analysis of the acquired data revealed effects causing distortion of measured angular distribution of prompt fission neutron and the dependence of their average number on total kinetic energy of the fission fragment. Special modification of the experiment and respective modifications in the data analysis procedure brought to reasonable agreement between experimental results and theoretical calculations. In the first time the linear dependence of the average number of prompt fission neutron on total kinetic energy in the range of (140 – 220) MeV was demonstrated. The long time existing contradiction between experiment and theory was resolved and, a new measurement procedure allowing avoidance of above mentioned systematic errors in experiments with actinide targets like ^{235}U, ^{239}Pu, etc. was proposed.

1. INTRODUCTION

The experiment was basically adopted from Ref. [1] with the replacement of the traditional analogue signal processing instrumentation with digital signal processing hardware and associated software. The anode current caused by a fission fragment (FF) in the TGIC was amplified by a charge sensitive preamplifier and sampled with a 12-bit, 100 Ms/sec waveform digitizer (WFD). The step-like long anode signals were software-wise transformed into short current pulses, which allowed effective pulse pileup elimination. The anode current pulses were used to determine the fission fragment angle with respect to the cathode-plane normal. The prompt fission neutron (PFN) time of flight (TOF) spectroscopy was done after passing the neutron detector (ND) pulse, digitized with a 12-bit, 100 Ms/sec WFD, through a 12^{th} order digital low pass filter. The ND pulse shape discrimination was implemented using raw signal waveforms. The measurement of the FF characteristics, both in coincidence and non-coincidence with the PFN, was done without readjusting the apparatus. A ^{252}Cf source, deposited on a 100 μg/cm^2 thick Ni foil backing with an activity of ~ 500 fissions/sec, was mounted on the common cathode of a twin Frisch grid ionization chamber (TGIC), which operated under normal conditions with P-10 as working gas at a constant flow of ~ 50–100 ml/min. About 1.2×10^7 coincidences between FF and PFN signals were acquired in the measurement, which is comparable to the statistics mentioned in Ref. [1]. A scheme of the set-up is shown in Fig. 1.

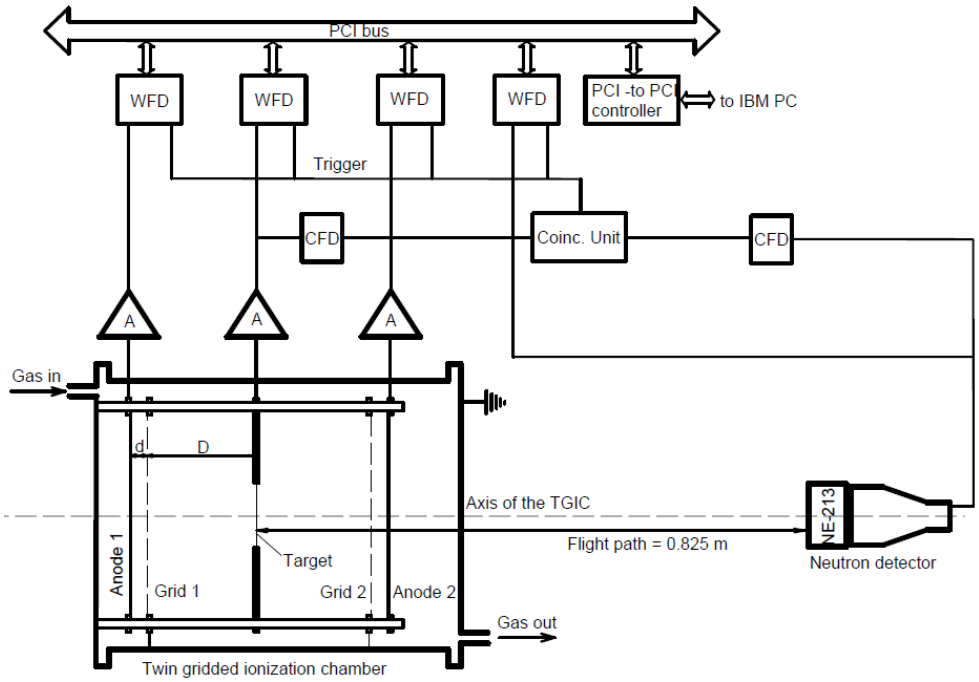

FIG.1. Experimental set-up.

2. EXPERIMENTAL METHOD AND RESULTS

The detailed information on PFN emission in fission is available from the measured dependence of average PFN multiplicity on the mass number A and the TKE of fissile nucleus-$\bar{\nu}(A,TKE)$. The late function allows obtaining of averaged characteristics on $\bar{\nu}(A)$ or $\bar{\nu}(TKE)$ by integrating over respective variable, if the mass yield matrix-*Y(A,TKE)* is known, for example:

$$\bar{\nu}(A) = \frac{\int_0^\infty \bar{\nu}(A,TKE)Y(A,TKE)dTKE}{\int_0^\infty Y(A,TKE)dTKE}, \qquad (1)$$

$$\bar{\nu} = \int_0^\infty \bar{\nu}(A,TKE)Y(A,TKE)dTKEdA, \quad 200 = \int_0^\infty Y(A,TKE)dTKEdA$$

A similar relation could be written for averaging over A:

$$\bar{\nu}(TKE) = \frac{\int_0^\infty \bar{\nu}(A,TKE)Y(A,TKE)dA}{\int_0^\infty Y(A,TKE)dA}, \qquad (2)$$

$$\bar{\nu} = \int_0^\infty \bar{\nu}(A,TKE)Y(A,TKE)dTKEdA, \quad 200 = \int_0^\infty Y(A,TKE)dTKEdA$$

Determination of $\nu(A),\nu(TKE)$ can be easily done if the measurement of $\nu(A,TKE)$ and $Y(A,TKE)$ could be arranged. In such an experiment in each fission event the FF and PFN kinetic energies, FF masses along with the angle between PFN and FF motion should be determined. All this information then could be used to reconstruct the PFN emission kinematics both in the laboratory (LF) and in the centre of mass (CMF) frames. We believe

that the possible explanations of the discrepancies in results of experiments from Refs. [2–6] might stem from a significant systematic error in measurements of kinematics parameters of FF. To verify our assumption a new method of FF mass and kinematics parameters spectroscopy was developed.

Two angular distributions of correlated FF, measured in LF using TGIC are presented in Fig. 2(a). The angle between the FF and the PFN was measured using the half of the TGIC from the layer side in one of the measurements and from the target backing side in the other measurement. Comparison of curves in Fig. 2(a) demonstrates a significant difference, increasing for the angles close to 90º. Apparently, the observed anisotropy in LF is due to the energy losses in the target backing. After transformation to the CMF during data analysis this effect will cause systematic errors, distorting the reaction kinematics.

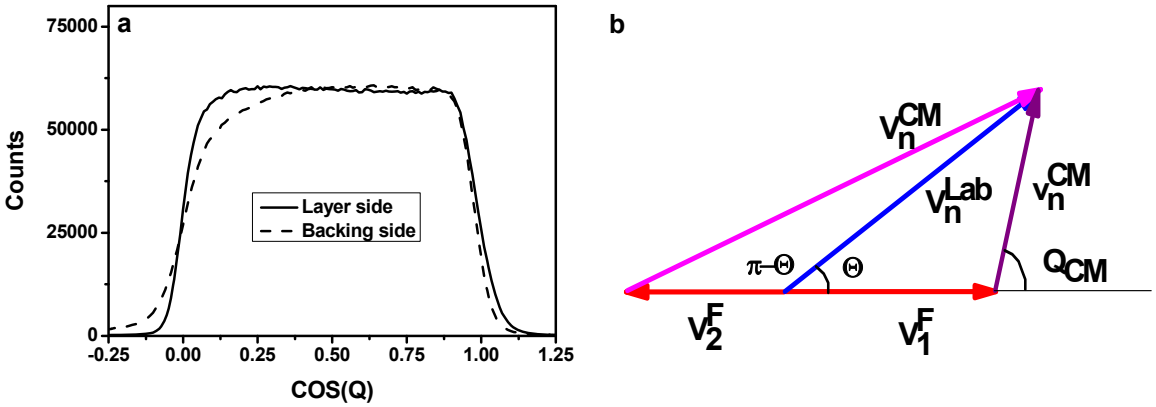

FIG. 2. (a) FF angular distribution measured for ^{252}Cf(sf) reaction with the half of TGIC from layer side (solid line) and from the backing side (dashed line), (b) ^{252}Cf(sf) reaction kinematics.

Another source of systematic error is the background created by the second FF, when the PFN emission of the first one is investigated. This kind of background could be taken into account using the following approach. According to the reaction kinematics depicted in Fig. 2b, kinetic energy of the second FF in CMF, must be much higher than the kinetic energy of the first FF. Bearing in the mind the exponential fall of the PFN energy spectrum in CMF [1], the contributions to the PFN from both FFs could be evaluated using the probabilities defined as:

$$W_+ = \frac{1}{N}\exp(\frac{-E_+}{N}),\ W_- = \frac{1}{N}\exp(\frac{-E_-}{N}),\ W_+ + W_- = 1 \qquad (3)$$

where W_+/W_--are probabilities of PFN emission and E_+/E_--are the kinetic energies of first and second FF respectively, the parameter N is a normalization factor. Comparison of mass distributions plotted using measured data and probabilities, defined by Eq. (3) are presented in Fig. 3. The results are in agreement with [1], where the background was found to be small. However, the neglect of background from the second FF could imitate anisotropy as it is demonstrated below. The angular distribution of PFN was plotted in Figs 4(a) and 4(b) using cos(Θ) values measured in the target layer side half of TGIC and the target backing side half of TGIC respectively. Transformation of measured in LF distributions to CMF was done using the following formula:

$$\Omega_{CM}(v_{CM},\Theta_{CM})dv_{CM}\,d\cos(\Theta_{CM}) = \frac{v_{CM}}{v_{lab}}\Omega_{lab}(\mathrm{v}_{\mathrm{lab}}(v_{CM},\Theta_{CM}),\Theta_{lab}(v_{CM},\Theta_{CM})) \qquad (4)$$

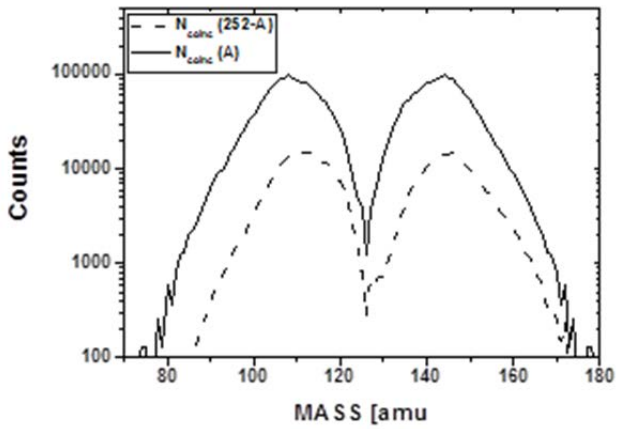

FIG.3. Relative contribution to PFN of investigated FF from the correlated FF as a function of the mass split.

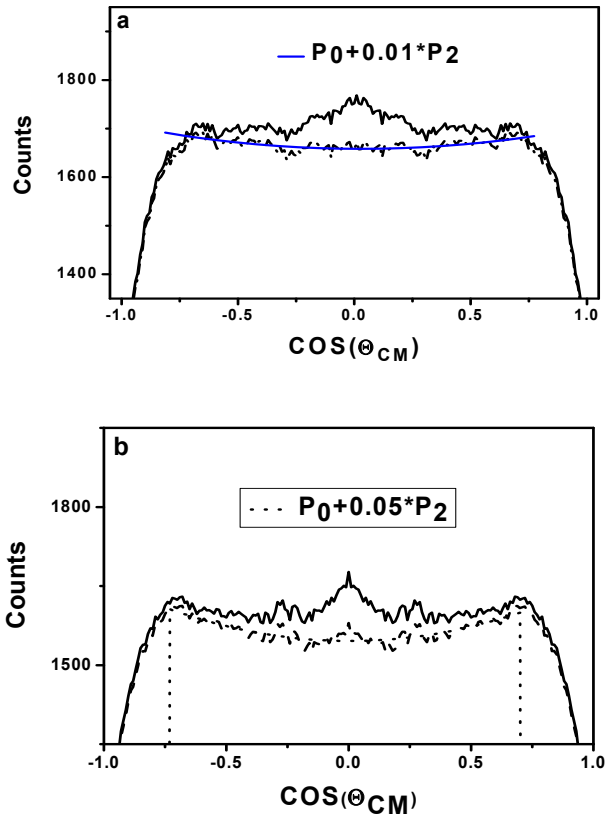

FIG. 4. Angular distribution of the PFN in CMF, when for evaluation of COS(Θ_{CM}) the COS(Θ_{lab}), measured in the half of the TGIC from the target layer side was used (left) and similar distribution, when for evaluation of COS(Θ_{CM}) the COS(Θ_{lab}), measured in the half of the TGIC from the target backing side was used (right).

Both distributions in Fig. 4 have peaks near $\Theta_{CM} \sim 90°$, disappearing after contribution from the second FF was subtracted. However, the anisotropy does not disappear completely due to energy losses distortion of FF angular distribution as shown in Fig. 2a. Angular distribution of FF in CMF, where the cos(Θ) was measured in the target layer side half of TGIC is plotted

in Fig. 5, proving the fact that more than 99% of PFN was emitted from the fully accelerated FFs.

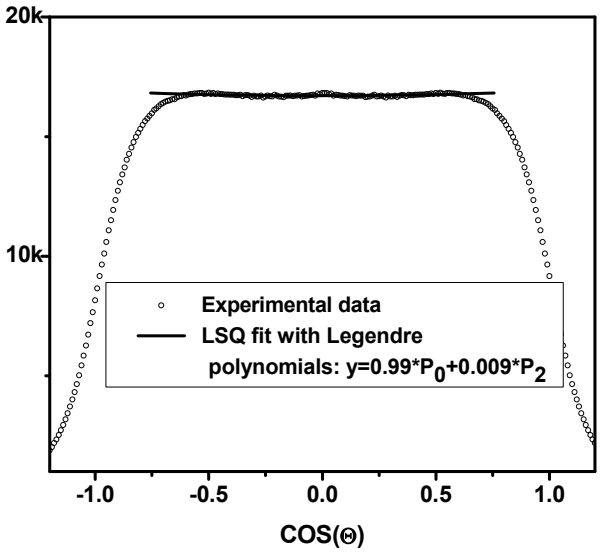

FIG. 5. PFN angular distribution after correction for background neutrons from the correlated FF along with the fit with Legendre polynomials.

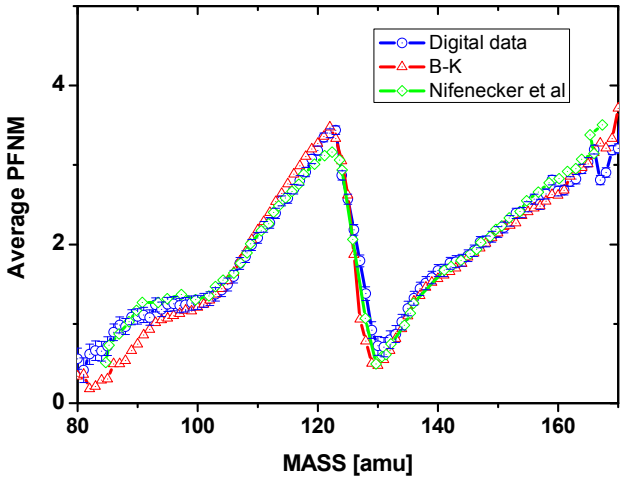

FIG. 6. Mass dependence of average PFN multiplicity on FF mass in comparison with literature and Ref [1].

The average PFN number emitted per fission event as a function of FF mass number, evaluated from the experiment with above described method presented in Fig. 6 in comparison with literature. The saw tooth shape of PFN distribution explained in model proposed by [7, 8] with use of two main assumptions: multimodal fission and random neck rupture (MM-RNR). The model provides the link between experimentally measured configuration, asymmetry and the neck shape of fissile nucleus. In addition, the function $\bar{\nu}(A,TKE)$ contains information on neck elasticity and excitation energy partition between FFs. Dependence of the average PFN number emitted per fission event as a function of TKE is presented in Fig. 7 in comparison with literature and with theoretical calculations.

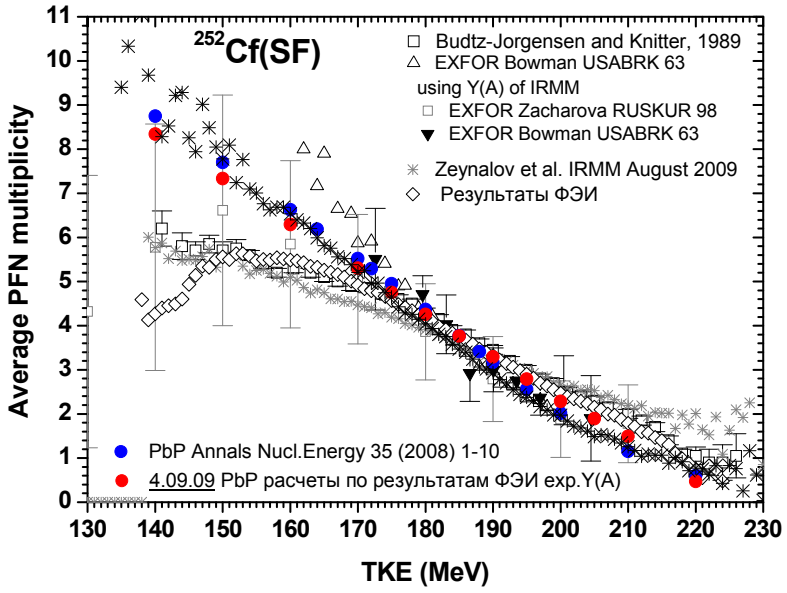

FIG. 7. Mass dependence of average PFN multiplicity on FF mass in comparison with literature and theoretical calculation [9].

3. OUTLOOK AND CONCLUSION

Two main sources of systematic error in PFN investigation were demonstrated, one of which is a background from the correlated FF. This background could be easily corrected using the procedure described above. However, the second systematic error source, caused due to energy loss in target is difficult to overpass in the considered experimental arrangement. Modification of the TGIC developed recently in our team gives some clue to resolve the problems. The anodes of TGIC in modified design are made position sensitive thanks to splitting them into two electrically isolated from each other parts as shown in the left part of Fig. 8 (backgammon method).

Motion of electrons in the grid anode space induces the electric current shared in two parts of the anode. The difference between instant currents is zero when the electrons are close to the line dividing the anode into two symmetric parts (ML-middle line). Deviation from this line to any direction perpendicular to the ML increases the current in the corresponding half of the electrode. This fact was implemented in the new design of TGIC, providing position sensitivity along the chosen direction. When anode of one half of TGIC is oriented along the X-axis of coordinate frame in the right side of Fig. 8 and anode of the other side is oriented along the Y-axis, the fission axis orientation in space can be measured. Let the Z-axis in Fig. 8 is stretched along the TGIC axis and the ionization chamber part of the experimental set-up was modified as shown in Fig. 9 leaving ND part unchanged. Two wideband current preamplifiers replaced the charge sensitive preamplifiers in each anode circuit. Considering drift of electrons created during FF deceleration inside the TGIC, the electric pulses at the preamplifier output can be used to evaluate the fission axis orientation in the coordinate frame of Fig. 8 using the following approach.

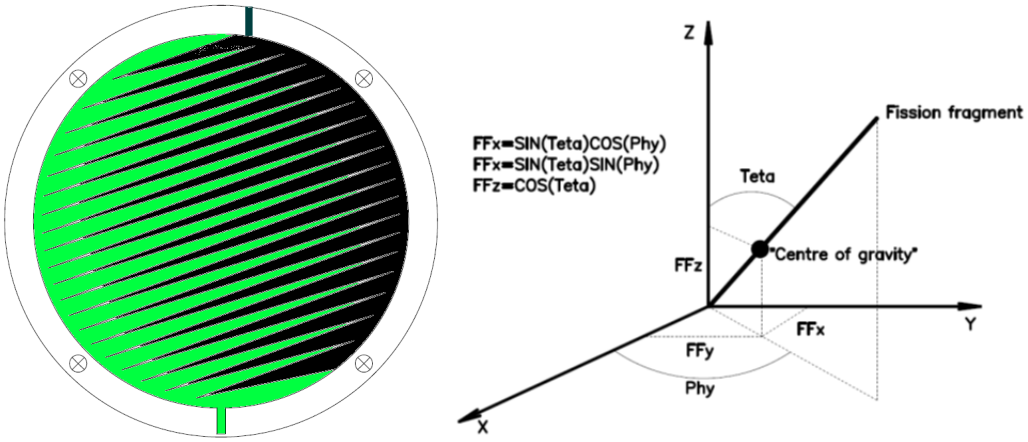

FIG. 8. The anode of position sensitive TGIC (left). Illustration of fission axis orientation evaluation in coordinate frame with z-axis directed along the TGIC axis (right).

To measure the cosine of the angle Θ between the FF and the TGIC's axis the drift time method, utilizing the drift time dependence on Θ of electrons released by the FF, was implemented:

$$T[L] = \frac{\sum_{k=Tg}^{Tg+L} k(I_1[k] + I_2[k])}{\sum_{k=Tg}^{Tg+L} (I_1[k] + I_2[k])} - T_g$$

where Tg is the trigger signal leading edge position, $I_1[k]$ and $I_2[k]$ are the sampled current pulses from the respective half of the anode. The trigger signal was obtained from the common cathode pulse and referred to as the time instant of the fission event. The dependence of cos(Θ) on the drift time can be found using the following formulae:

$$T_{90} = \frac{D + 0.5 * d}{W},\ T_{90} - T(E) = (T_{90} - T_0(\mathrm{E})) * \cos(\Theta),\ \ P^C = \frac{P^O * T_{90}}{T_{90} + \sigma * T}$$

where D and d are the cathode-grid and grid-anode distances, respectively, W is the free electron drift velocity, T_0, T_{90} are the drift times for FF having Θ equal to 0^o and 90^o, respectively, σ is the grid inefficiency, P^C, P^O are the grid inefficiency corrected and uncorrected total charges collected on the anodes and T is the drift time for the considered FF. The X_C coordinate of the FF "centre of gravity" was found using the following formula

$$X_C = \frac{\sum_{k=Tg}^{Tg+L} k * (I_1[k] - I_2[k])}{\sum_{k=Tg}^{Tg+L} (I_1[k] + I_2[k])}.$$

In the similar way the Y_C coordinate of the correlated FF, detected in another half of the TGIC, was found. The cosines between fission axis and the coordinate axis then were found using the following equations:

$$\begin{aligned} X_C &= R1 \times SIN(\Theta) \times COS(\Phi) \\ Y_C &= R2 \times SIN(Q) \times SIN(\Phi) \end{aligned} \qquad (5)$$

where R1, R2 are the average range of the FF, having known kinetic energies E1, E2 respectively. The ranges were supposed to be proportional to the maximum drift time known for the each half of the chamber from cos(Θ) calibration procedure similar to one used in [1]. Finally, the three cosines between FF axis and coordinate axis in fig. 8 were found:

$$COS(X) = SIN(Q) \times COS(\Phi) = \frac{X_C}{R1},\ COS(Y) = SIN(Q) \times SIN(\Phi) = \frac{Y_C}{R2},\ COS(Z) = COS(\Theta) \quad (6)$$

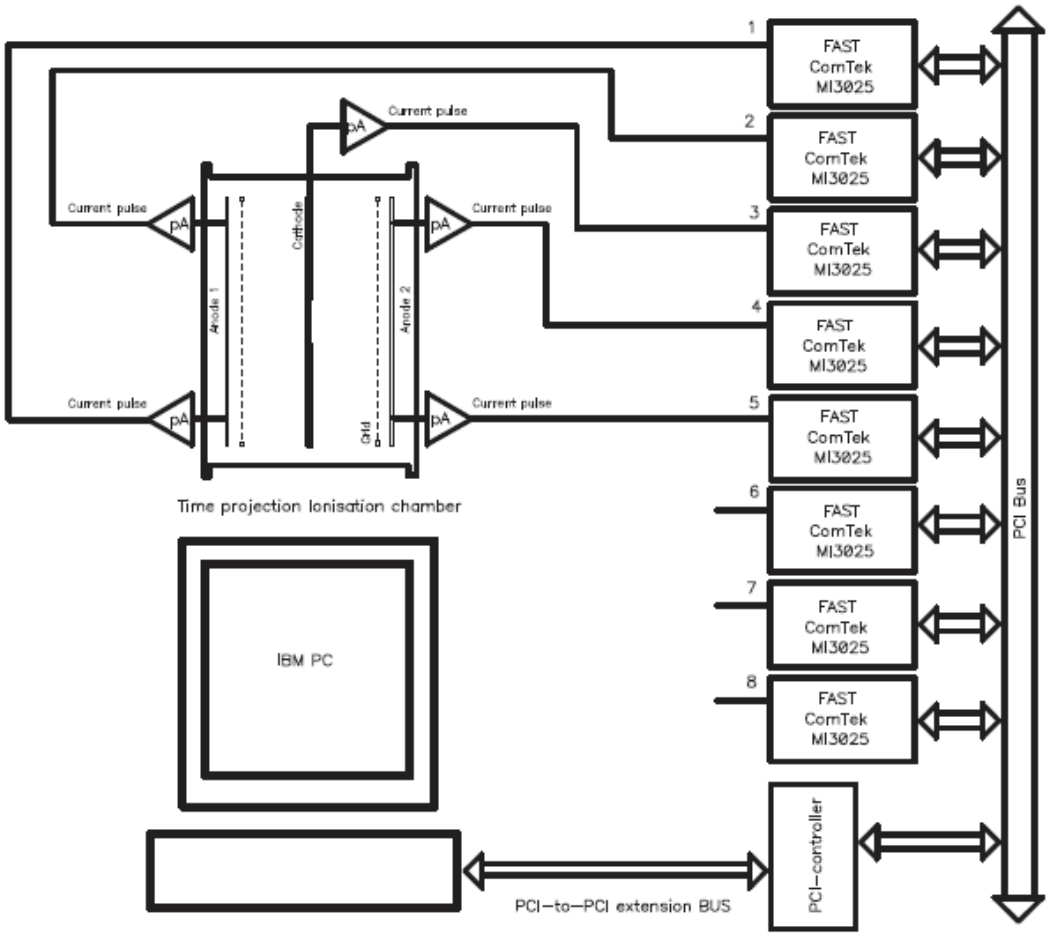

FIG. 9. Modified experimental set-up of time position sensitive TGIC.

The modified experimental set-up was used in measurement of spontaneous fission of ^{252}Cf to prove the claimed above properties of the TGIC. Angular distribution of FF measured for fixed intervals in COS(Z) are plotted in Fig. 10, demonstrating the angular sensitivity of the method.

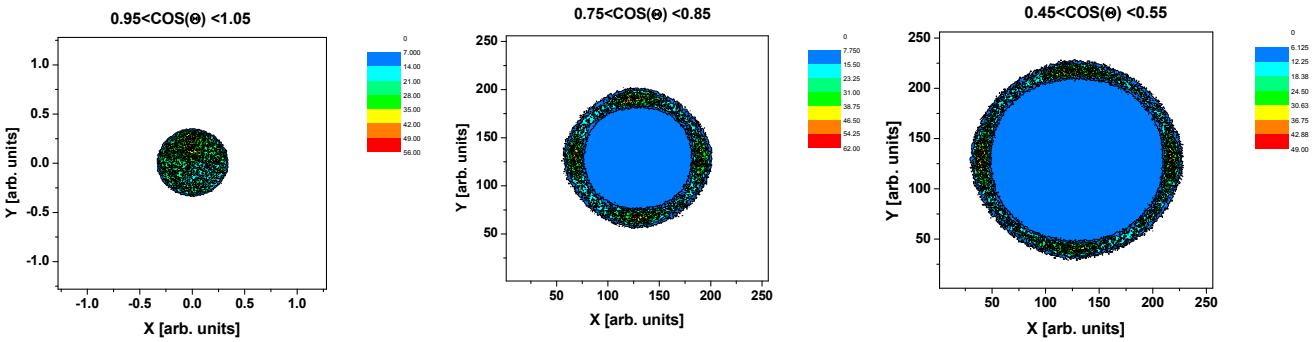

FIG. 10. FF angular distributions measured for different fixed intervals in COS(Z).

Preliminary evaluation of precision of the method is about 0.1 as averaged between three cosine values. A more detailed evaluation is underway and should be done in near future, but, nevertheless, the preliminary result is quite good too. Position sensitive TGIC developed in this work opens a new perspective in PFN investigation, especially for actinide targets like ^{236}U and ^{239}Pu. Apparently the target from these nuclei could not be made of negligible thickness, like in ^{252}Cf case from the one hand. The PFN investigation should be done in full solid angle from the other hand. Hence, allocation of ND at the TGICs axis to simplify measuring procedure does not work anymore. From this point of view position sensitive TGIC helps to solve this problem and additionally allows increase the number of ND, increasing the experiment efficiency at the same time.

REFERENCES

[1] BUDTZ-JORGENSEN, C., KNITTER, H.H., Simultaneous investigation of fission fragments and neutrons in ^{252}Cf (SF), Nucl. Phys. A490 (1988) 307.

[2] BOWMAN, H.R., THOMPSON, S.G., MILTON, J.C.D., SWIATECKI, W.J., Further Studies of the Prompt Neutrons from the Spontaneous Fission of ^{252} Cf, Phys. Rev. 129 (1963) 2133–2147.

[3] SKARSVAG, K., SINGSTAD, Angular correlation of fission fragments and prompt γ rays from spontaneous fission of ^{252}Cf, I., Nucl. Phys. 62 (1965) 103.

[4] VOROBYEV, A.S., SHERBAKOV, O.A., et al, Measurements of angular and energy distributions of prompt neutrons from thermal neutron induced fission, Nucl. Instr. Meth. A598 (2009) 795.

[5] KAPOOR, S.S., RAMANNA, R., RAMA RAO, P.N., Emission of prompt neutrons in the thermal neutron fission of ^{235}U, Phys. Rev. 131 (1963) 283–296.

[6] SAMANT, M.S., ANAND, R.P., et al., Pre-scission neutron emission in ^{235}U through fragment neutron angular correlation studies, Phys. Rev. C51 (1995) 3127–3135.

[7] NIFENECKER, H., SIGNARBIEUX, C., BABINET, R., POITOU, J., Symposium on Physics and Chemistry of Fission, 13–17 August, 1973, Rochester, N.Y., USA - Vienna: IAEA, 1974. -Vol. 2. - P. 117–178.

[8] BROSA, U., GROSSMANN, S., MÜLLER, A., Nuclear scission Physics, Phys. Rep. 197 (1990) 167–262.

[9] TUDORA, A., Multi-parametric prompt neutron and fission fragment experimental data described by the point by point model, Ann. Nucl. Energy 35 (2008) 1–10.

LIST OF PARTICIPANTS

Bogovac, M.	Bijenicka cesta 54 P.O. Box: 10000 Zagreb, Croatia Tel: +385 1 4561041 Email: bogovac@irb.hr
Bryndziar, P.	Atomove elektrarne Mochovce 935 39 Mochovce, Slovakia Tel: +421366363472 Fax: +421366391108 Email: pavol.bryndziar@enel.com
Dambach, M.	Albert-Ludwigs-University, Freiburg, Germany Email: markus.dambacher@fmf.uni-freiburg.de
El Tokhy, M.	Engineering Department, NRC, Atomic Energy Authority, Inshas, Cairo, Egypt P.O. Box 13759 Cairo 02, Egypt Tel: +0168395079 Fax: +0244620621 Email: engtokhy@gmail.com
Jidal, Z.	Residence Gendarmerie Royale, Cite des Oudayas, Temara Morocco Tel: +212537642351/53 Fax: +212537642504 Email: labgr@menera.ma
Jordanov, V. T	735 Camino Cereza Los Alamos 87544, USA Tel: +15059200045 Fax: +15056629040 Email: jordanov@ieee.org
Markowicz, A.	Department of Nuclear Sciences and Applications / Physics Section Wagramer str. 5, P.O.Box 100 1400 Vienna, Austria Tel.: +431 260028236 Fax.: +431 26007 Email: a.markowicz@iaea.org
Messai, A.	Ain Oussera, w de Djelfa P.O. Box B. P. 180 Ain Oussera 17200, Algeria Tel: +213 550886516 Fax: +213 27 87 42 80 Email: messai_adnane@yahoo.fr
Papp, T.	175 Elizabeth Street Guelph, N1E2X5 Ontario, Canada Tel: +15197801760 Email:tibpapp@cambridgescientific.net

Petriska, M.	Slovak University of Technology FEI, Ilkovicova 3, Bratislava 81219, Slovakia Tel: +421260291173 Email: martin.petriska@stuba.sk
Rashid, M.	Atomic Energy Research Establishment, Savar GPO Box 3787, Dhaka 1000, Bangladesh Tel: +88027701250 Fax: +88028613051 Email: mrashid@agni.com
Riede, J.	Bundesministerium für Landesverteidigung und Sport Platz der Eisenbahnpioniere 1 Korneuburg 2100, Austria Tel: +435020120320 Fax: +435020117210 Email: abcabws.physik@bmlvs.gv.at
Sghaier, H.	Institute Superieur d' Informatique et de Mathematiques de Monastir Avenue de la cornice B.P. 223 5000 Monastir, Tunisia Tel: 00216 98409267 Fax: 00216 73 350393 Email: H.Sghaier@isimm.rnu.tn
Stoehlker, U.	CTBTO Preparatory Commission Vienna International Centre 1400 Vienna, Austria IDC/SA/SM Tel: +43126030-6485 Email: ULRICH.STOEHLKER@CTBTO.ORG
Zakrzewski, R. A.	CANBERRA Industries Inc 800 Research Pkwy Meriden, 06450, USA Tel: 0012036392310 Fax: 0014343824789 Email: bzakrzewski@canberra.com
Zeman, A.	Department of Nuclear Sciences and Applications / Physics Section Wagramer str. 5, P.O.Box 100 1400 Vienna, Austria +431 260021705 +431 26007 Email: a.zeman@iaea.org
Zeynalov, S.	JINR Dubna Joliot-Curie 6, Dubna Moscow region, Russian Federation Tel: +73962163838 Fax: +74962165429 Email: zeinal@nf.jinr.ru

Zeynalova, Olga, V.

JINR Dubna
Joliot-Curie 6, Dubna
Moscow region, Russian Federation
Tel: +79263695202
Fax: +74962165429
Email: zeinalova@jinr.ru

Zwerger, A.

Albert-Ludwigs-University,
Freiburg, Germany
Physikalisches Institut
Hermann-Herder-Str. 3
79104 Freiburg, Germany
Tel: +49 761 203 5935
Email: Andreas.Zwerger@physik.uni-freiburg.de

CONTRIBUTORS TO DRAFTING AND REVIEW

Bogovac, M.	Ruđer Bošković Institute Zagreb, Croatia
Bryndziar, P.	Slovenské elektrárne,a.s. Nuclear Power Plant Mochovce Mochovce, Slovakia
El Tokhy, M.S.	Engineering Department Atomic Energy Authority Inshas, Cairo, Egypt
Jidal, Z.	Residence Gendarmerie Royale Cite des Oudayas Temara, Morocco
Jordanov, V.T.	Yantel LLC Los Alamos, USA
Messai, A.	Centre de Recherche Nucléaire de Birine CRNB –COMENA, Algeria
Papp, T.	Cambridge Scientific Guelph, Ontario, Canada
Petriska, M.	Slovak University of Technology Faculty of Electrotechnical Engineering Bratislava, Slovakia
Rashid, M.M.	Institute of Nuclear Science and Technology Atomic Energy Research Establishment Savar Dhaka, Bangladesh
Sghaier, H.	Institute Superieur d' Informatique et de Mathematiques de Monastir Avenue de la corniche Monastir, Tunisia
Zakrzewski, B.	CANBERRA Industries Inc Meriden, USA
Zeynalova, O.,	Joint Institute for Nuclear Research Dubna, Russian Federation
Zeynalov, SH.	Joint Institute for Nuclear Research Dubna, Russian Federation

IAEA
International Atomic Energy Agency

Where to order IAEA publications

In the following countries IAEA publications may be purchased from the sources listed below, or from major local booksellers. Payment may be made in local currency or with UNESCO coupons.

AUSTRALIA
DA Information Services, 648 Whitehorse Road, MITCHAM 3132
Telephone: +61 3 9210 7777 • Fax: +61 3 9210 7788
Email: service@dadirect.com.au • Web site: http://www.dadirect.com.au

BELGIUM
Jean de Lannoy, avenue du Roi 202, B-1190 Brussels
Telephone: +32 2 538 43 08 • Fax: +32 2 538 08 41
Email: jean.de.lannoy@infoboard.be • Web site: http://www.jean-de-lannoy.be

CANADA
Bernan Associates, 4501 Forbes Blvd, Suite 200, Lanham, MD 20706-4346, USA
Telephone: 1-800-865-3457 • Fax: 1-800-865-3450
Email: customercare@bernan.com • Web site: http://www.bernan.com

Renouf Publishing Company Ltd., 1-5369 Canotek Rd., Ottawa, Ontario, K1J 9J3
Telephone: +613 745 2665 • Fax: +613 745 7660
Email: order.dept@renoufbooks.com • Web site: http://www.renoufbooks.com

CHINA
IAEA Publications in Chinese: China Nuclear Energy Industry Corporation, Translation Section, P.O. Box 2103, Beijing

CZECH REPUBLIC
Suweco CZ, S.R.O., Klecakova 347, 180 21 Praha 9
Telephone: +420 26603 5364 • Fax: +420 28482 1646
Email: nakup@suweco.cz • Web site: http://www.suweco.cz

FINLAND
Akateeminen Kirjakauppa, PO BOX 128 (Keskuskatu 1), FIN-00101 Helsinki
Telephone: +358 9 121 41 • Fax: +358 9 121 4450
Email: akatilaus@akateeminen.com • Web site: http://www.akateeminen.com

FRANCE
Form-Edit, 5, rue Janssen, P.O. Box 25, F-75921 Paris Cedex 19
Telephone: +33 1 42 01 49 49 • Fax: +33 1 42 01 90 90
Email: formedit@formedit.fr • Web site: http://www. formedit.fr

Lavoisier SAS, 145 rue de Provigny, 94236 Cachan Cedex
Telephone: + 33 1 47 40 67 02 • Fax +33 1 47 40 67 02
Email: romuald.verrier@lavoisier.fr • Web site: http://www.lavoisier.fr

GERMANY
UNO-Verlag, Vertriebs- und Verlags GmbH, Am Hofgarten 10, D-53113 Bonn
Telephone: + 49 228 94 90 20 • Fax: +49 228 94 90 20 or +49 228 94 90 222
Email: bestellung@uno-verlag.de • Web site: http://www.uno-verlag.de

HUNGARY
Librotrade Ltd., Book Import, P.O. Box 126, H-1656 Budapest
Telephone: +36 1 257 7777 • Fax: +36 1 257 7472 • Email: books@librotrade.hu

INDIA
Allied Publishers Group, 1st Floor, Dubash House, 15, J. N. Heredia Marg, Ballard Estate, Mumbai 400 001,
Telephone: +91 22 22617926/27 • Fax: +91 22 22617928
Email: alliedpl@vsnl.com • Web site: http://www.alliedpublishers.com

Bookwell, 2/72, Nirankari Colony, Delhi 110009
Telephone: +91 11 23268786, +91 11 23257264 • Fax: +91 11 23281315
Email: bookwell@vsnl.net

ITALY
Libreria Scientifica Dott. Lucio di Biasio “AEIOU”, Via Coronelli 6, I-20146 Milan
Telephone: +39 02 48 95 45 52 or 48 95 45 62 • Fax: +39 02 48 95 45 48
Email: info@libreriaaeiou.eu • Website: www.libreriaaeiou.eu

JAPAN
Maruzen Company Ltd, 1-9-18, Kaigan, Minato-ku, Tokyo, 105-0022
Telephone: +81 3 6367 6079 • Fax: +81 3 6367 6207
Email: journal@maruzen.co.jp • Web site: http://www.maruzen.co.jp

REPUBLIC OF KOREA
KINS Inc., Information Business Dept. Samho Bldg. 2nd Floor, 275-1 Yang Jae-dong SeoCho-G, Seoul 137-130
Telephone: +02 589 1740 • Fax: +02 589 1746 • Web site: http://www.kins.re.kr

NETHERLANDS
De Lindeboom Internationale Publicaties B.V., M.A. de Ruyterstraat 20A, NL-7482 BZ Haaksbergen
Telephone: +31 (0) 53 5740004 • Fax: +31 (0) 53 5729296
Email: books@delindeboom.com • Web site: http://www.delindeboom.com

Martinus Nijhoff International, Koraalrood 50, P.O. Box 1853, 2700 CZ Zoetermeer
Telephone: +31 793 684 400 • Fax: +31 793 615 698
Email: info@nijhoff.nl • Web site: http://www.nijhoff.nl

Swets and Zeitlinger b.v., P.O. Box 830, 2160 SZ Lisse
Telephone: +31 252 435 111 • Fax: +31 252 415 888
Email: infoho@swets.nl • Web site: http://www.swets.nl

NEW ZEALAND
DA Information Services, 648 Whitehorse Road, MITCHAM 3132, Australia
Telephone: +61 3 9210 7777 • Fax: +61 3 9210 7788
Email: service@dadirect.com.au • Web site: http://www.dadirect.com.au

SLOVENIA
Cankarjeva Zalozba d.d., Kopitarjeva 2, SI-1512 Ljubljana
Telephone: +386 1 432 31 44 • Fax: +386 1 230 14 35
Email: import.books@cankarjeva-z.si • Web site: http://www.cankarjeva-z.si/uvoz

SPAIN
Díaz de Santos, S.A., c/ Juan Bravo, 3A, E-28006 Madrid
Telephone: +34 91 781 94 80 • Fax: +34 91 575 55 63
Email: compras@diazdesantos.es, carmela@diazdesantos.es, barcelona@diazdesantos.es, julio@diazdesantos.es
Web site: http://www.diazdesantos.es

UNITED KINGDOM
The Stationery Office Ltd, International Sales Agency, PO Box 29, Norwich, NR3 1 GN
Telephone (orders): +44 870 600 5552 • (enquiries): +44 207 873 8372 • Fax: +44 207 873 8203
Email (orders): book.orders@tso.co.uk • (enquiries): book.enquiries@tso.co.uk • Web site: http://www.tso.co.uk

On-line orders
DELTA Int. Book Wholesalers Ltd., 39 Alexandra Road, Addlestone, Surrey, KT15 2PQ
Email: info@profbooks.com • Web site: http://www.profbooks.com

Books on the Environment
Earthprint Ltd., P.O. Box 119, Stevenage SG1 4TP
Telephone: +44 1438748111 • Fax: +44 1438748844
Email: orders@earthprint.com • Web site: http://www.earthprint.com

UNITED NATIONS
Dept. I004, Room DC2-0853, First Avenue at 46th Street, New York, N.Y. 10017, USA
(UN) Telephone: +800 253-9646 or +212 963-8302 • Fax: +212 963-3489
Email: publications@un.org • Web site: http://www.un.org

UNITED STATES OF AMERICA
Bernan Associates, 4501 Forbes Blvd., Suite 200, Lanham, MD 20706-4346
Telephone: 1-800-865-3457 • Fax: 1-800-865-3450
Email: customercare@bernan.com · Web site: http://www.bernan.com

Renouf Publishing Company Ltd., 812 Proctor Ave., Ogdensburg, NY, 13669
Telephone: +888 551 7470 (toll-free) • Fax: +888 568 8546 (toll-free)
Email: order.dept@renoufbooks.com • Web site: http://www.renoufbooks.com

Orders and requests for information may also be addressed directly to:

Marketing and Sales Unit, International Atomic Energy Agency
Vienna International Centre, PO Box 100, 1400 Vienna, Austria
Telephone: +43 1 2600 22529 (or 22530) • Fax: +43 1 2600 29302
Email: sales.publications@iaea.org • Web site: http://www.iaea.org/books

INTERNATIONAL ATOMIC ENERGY AGENCY
VIENNA
ISBN 978–92–0–141310–9
ISSN 1011–4289